5-2012

Finite Element Modeling and Design of Honeycomb Sandwich Panels for Acoustic Performance

David Griese
Clemson University, d.c.griese@gmail.com

Follow this and additional works at: https://tigerprints.clemson.edu/all_theses

Part of the Mechanical Engineering Commons

FINITE ELEMENT MODELING AND DESIGN OF HONEYCOMB SANDWICH
PANELS FOR ACOUSTIC PERFORMANCE

A Thesis
Presented to
the Graduate School of
Clemson University

In Partial Fulfillment
of the Requirements for the Degree
Master of Science
Mechanical Engineering

by
David Christopher Griese
May 2012

Accepted by:
Dr. Joshua D. Summers, Committee Chair
Dr. Lonny L. Thompson
Dr. Gregory M. Mocko

ABSTRACT

Honeycomb cellular metamaterial structures offer many distinct advantages over homogenous materials because their effective material properties depend on both their constituent material properties and their geometric cell configuration. From this, a wide range of targeted effective material properties can be achieved thus supporting forward design by tailoring the honeycomb cellular materials and properties for specific applications. One area that has not been fully explored is the set of acoustic properties of honeycomb materials and how these can offer increased design flexibility when targeting acoustic performance. Understanding these relations, the designer can effectively tune designs to perform better in specific acoustic applications. One such example is the insulation of target sound frequencies to prevent sound transmission through a panel.

This work explores how certain geometric and effective structural properties of in-plane honeycomb cores in sandwich panels affect the sound transmission loss properties of the panel. The two acoustic responses of interest in this work are the general level of sound transmission loss of the panel and the location of the frequencies related to the natural frequencies that exhibit high levels of sound transmission, or low sound transmission loss. Two different studies comparing constant mass sandwich panels and constant core shear modulus sandwich panels are conducted to determine the effects of varying properties. The results of these studies are used to formalize a design method, which is then used on a test case design application.

DEDICATION

This thesis work is dedicated to friends and family, especially my parents, Jim and Nancy Griese, my brother, Bill Griese, and my fiancé, Megan for their continued love and support throughout my graduate school experience and in all of the work that has led up to it.

ACKNOWLEDGMENTS

TABLE OF CONTENTS

LIST OF TABLES

LIST OF FIGURES

CHAPTER 1: MOTIVATION AND BACKGROUND

The selection of material is an important aspect in design and the type of material is typically chosen based on its mechanical properties [1]. These material properties directly affect the performance and form of the final design for a variety of applications. If homogenous materials are used, then the designer is limited to a fixed set of material properties. Honeycomb meso-structures, part of a broader class of cellular metamaterials, are advantageous in that their effective material properties depend on both the fixed constituent material properties and the geometry of the structure [2,3,4]. In varying the geometry of the structure, a wide range of material properties are possible without changing the constituent material, thus offering the designer more flexibility. As such, they make it possible to satisfy multiple requirements simultaneously that may have been previously conflicting. Because of this, honeycomb metamaterials have been used in many different applications and design methods have been developed that revolve around them. One area in honeycomb metamaterial design that has not been fully explored is how they can be designed to have desired acoustic responses in addition to satisfying other mechanical constraints. Potential applications could include the tuning of vehicle and building noise to isolate problematic sound frequencies.

The objectives of this thesis are to (1) develop a general finite element model using commercially available software to study the acoustic properties of honeycomb sandwich panels, (2) show in detail how varying the mechanical and geometric properties of the honeycomb core affects the acoustic responses, (3) identify key responses that can

be changed and the main factors that control them, and (4) explain how this can be used in forward design for acoustic applications.

1.1   Cellular Materials in Design

Cellular materials have become increasingly popular in research and design due to their ability to have macro material properties that are substantially different from their micro, or host material properties [2,3,4,5,6,7,8]. This field of engineered materials is referred to as metamaterials. One specific group of cellular meta-materials, hexagonal honeycomb meso-structures, are frequently used in applications where a high out-of-plane stiffness to weight ratio is desirable [5,9]. In these applications, they are commonly used as a lightweight core material of a sandwich construction in which the core separates two stiff face sheets. In addition to their generally good lightweight stiffness properties, they have also been shown to be advantageous in other areas such as impact absorption [4,10], low energy loss elastomeric materials [11,2,12,3], and thermal management [13].

In addition to offering these desirable properties, cellular honeycomb meta-materials offer a major advantage in that they can be tailored to have specific material properties depending on the application. If conventional homogenous materials are used, then the designer is limited to a specific set of fixed material properties. However, since cellular materials depend on both the fixed constituent material properties (micro-) and the geometry of the structure (meso-), a broad range of effective properties (meta-) can be attained by modifying the geometry of the cells. These prefixes are further explained in Figure 1.1. This allows for materials to be designed for certain applications where

previously conflicting mechanical properties are desired and, due to their varying set of geometric parameters, they can also provide a good platform for optimization [10,14].
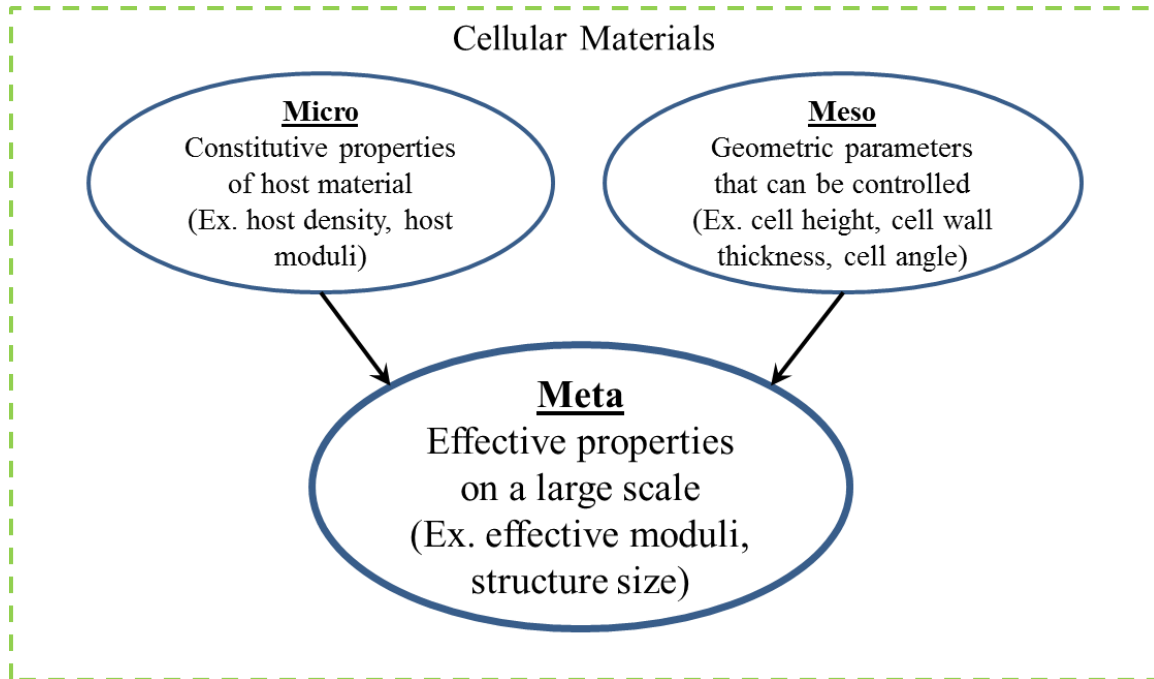
Figure 1.1: Properties that make up cellular materials

This design flexibility, meaning the capability to vary and target specific material properties, makes honeycomb cellular material a prime candidate for many different applications. Work has been done within the Clemson Engineering Design Applications and Research (CEDAR) lab to use honeycomb cellular materials for innovative design approaches to some of these applications. One such application was the use of metal honeycombs as low energy loss compliant structures for the shear band of the Michelin Tweel [11,2,12]. Due to the low energy loss properties of the constituent metal material and the ability to modify shear and strain parameters, target values could be achieved that mimic the same shear flexure properties of rubber without the negative side effect of high

energy loss. The control of these target properties through changes in local geometric parameters was validated through analytical work, finite element simulations, and physical experimentation [15]. This work was formalized into an automated design tool that used newly defined geometric parameters to generate designs that targeted these shear compliant properties [3].

Another area studied was the use of honeycombs as impact energy absorption material to better understand and generalize their dynamic behavior for use in forward design [4]. Applications of this concept include lightweight alternatives for absorbing impact and improving crashworthiness in automotive, aerospace, and military applications. This work was also automated into a tool that could quickly analyze the energy absorption of different model geometries and find an optimum design [10].

In addition to these previous applications, there may also be acoustic applications, where this same type of design flexibility and tailoring of properties would be desirable. One such application, which served as the motivation for this work, is in the design of military vehicles to attain targeted acoustic signatures. This target acoustic signature is the level of sound transmission across a range of frequencies through a partition, also known as the sound transmission loss curve which will be described in later sections of this thesis report. In general, it may be possible to control which driving frequencies are blocked resulting in reduced magnitudes of sound transmission (high sound transmission loss) and which ones, related to the natural frequencies, induce more vibrations and have high magnitudes of sound transmission (low sound transmission loss).

This signature of high and low levels of sound transmission loss is determined by the mechanical properties of the partition's material, which are usually fixed. However, with honeycomb cellular materials, it is possible to vary these mechanical properties through the control of meso-properties and achieve differing target acoustic signatures. An example of this is shown in Figure 1.2, where the sound transmission loss curve of a solid aluminum panels is compared to two different aluminum honeycomb panels. This can be done without compromising mechanical constraints, thus giving the designer more flexibility. Changing the acoustic signature would give the designer control over which frequencies of sound have reduced transmission and which frequencies cause high transmission levels. This concept could then aid in building noise isolation and potentially the acoustic disguising of military defense vehicles.
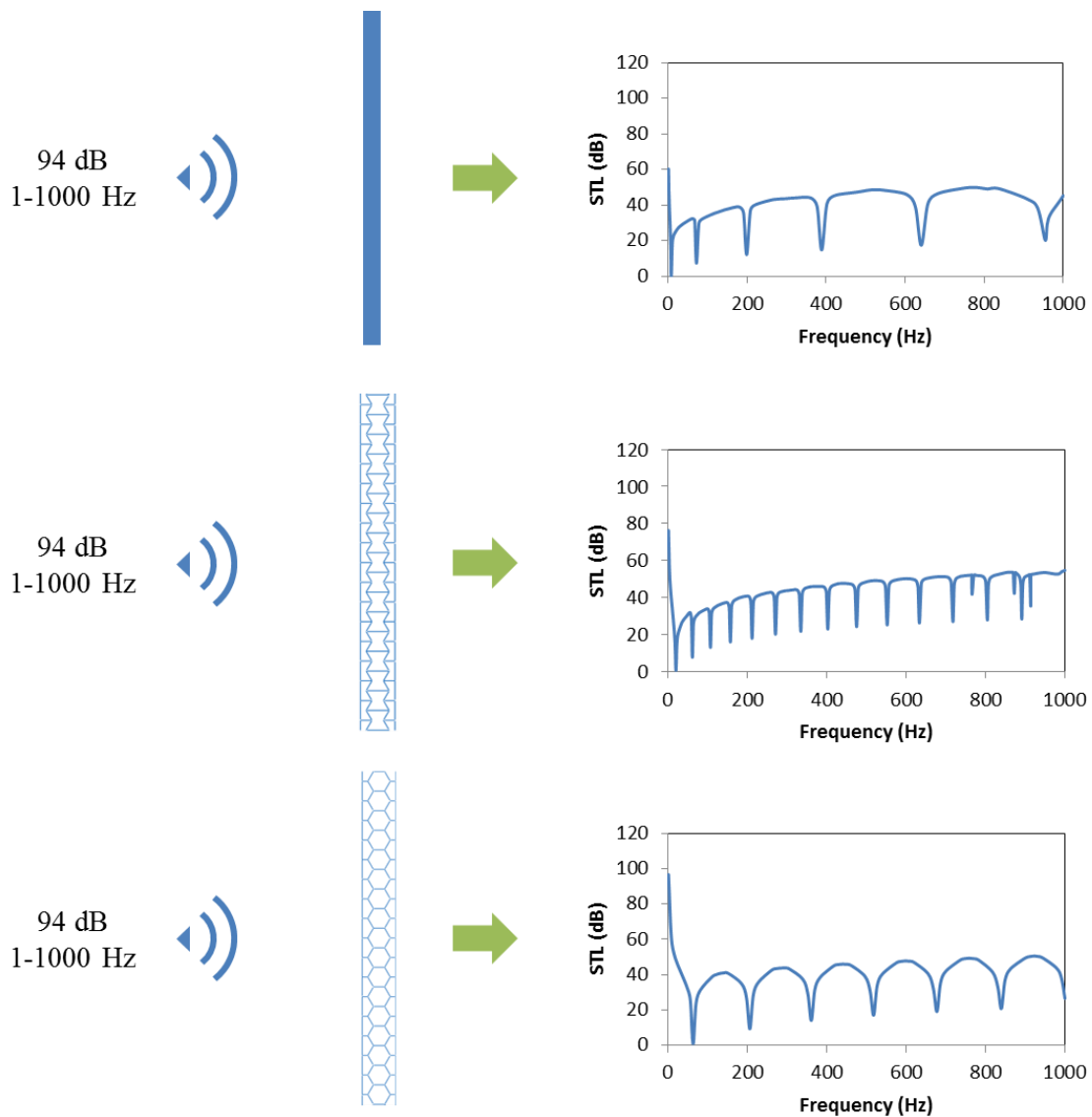
Figure 1.2: Changeability of acoustic response through variation of core geometry

The static mechanical properties of honeycomb cores are generally understood and can be defined by Gibson and Ashby's cellular materials theory (CMT) [5]. This work will try to relate these mechanical properties to the acoustic response of the panel. Understanding which responses can be changed and which properties change the response will allow the designer to tailor the panels to achieve specific acoustic

responses. This work will show this through a systematic design method in the later sections of this report.

1.2   Sound Transmission Characteristics of Partitions

Before discussing the details of this research, it is important to make a clear distinction between two different concepts. Often times in acoustic work, the terms sound insulation and sound absorption are used interchangeably. However, there is a difference between the two. Sound absorption is the conversion of sound energy into heat energy [16]. The most common metric for absorption is the absorption coefficient (α), which describes the ratio of *absorbed* to incident sound energy. It is on a scale of 0 to 1 with 0 signifying a reflection of all incident sound and 1 being absorption of all incident sound. Adding materials with high absorption coefficients can help to dampen the vibrations in a partition. It is a useful concept for reducing the level of sound within a space but not for reducing the sound between adjacent spaces.

Alternatively, sound insulation refers to the "blocking" of sound by a partition between a sound source and the listener [16]. It is described by the transmission coefficient (τ), which is the ratio of *transmitted* to incident sound energy. It is also on a scale of 0 to 1, where 0 signifies no sound transmission and 1 signifies complete sound transmission of all sound energy. It is important to note that, unlike sound absorption, a coefficient of 0 is not practical since all partitions will transmit some sound [16]. The descriptor for sound insulation is a decibel level calculated from the transmission coefficient, which will be described in later sections. Sound insulation is useful for reducing the sound between adjacent spaces. While sound absorption can sometimes

affect the sound insulation of partition, there are other more significant factors involved and they are two different concepts. This work mostly focuses on sound insulation and not sound absorption.

The most common performance metric for sound insulation of a material is the sound pressure transmission loss (STL), also known as sound reduction index [9,16,17]. The details for the calculation will be described in later sections, but in general it describes the difference between the transmitted and incident sound pressure. The sound transmission loss of a panel is frequency dependent and can be influenced by the material and geometry of the panel [9,16]. The main controlling factor for the sound transmission loss depends on the specific frequency range being analyzed and the general curve for the sound transmission loss can be divided into four distinct regions based on this concept. These four regions are shown in Figure 1.3 below.
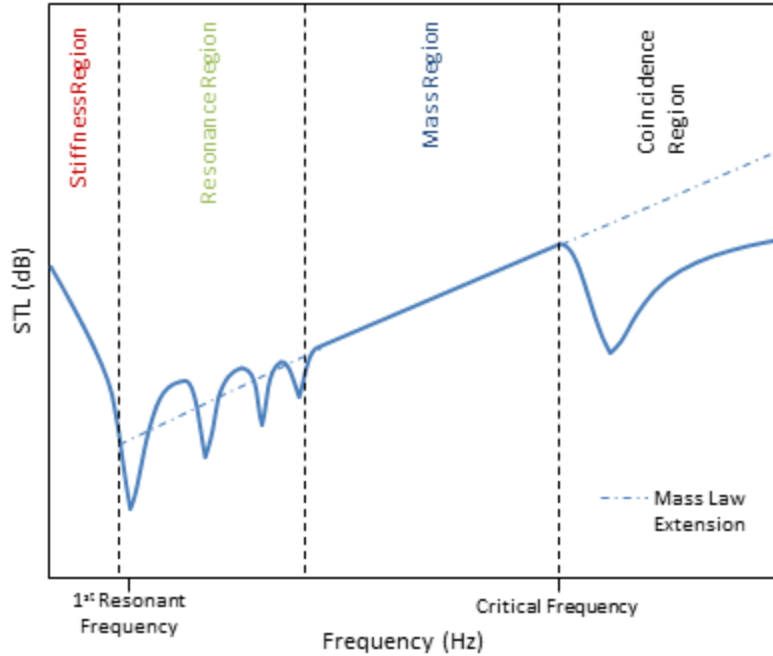
Figure 1.3: Frequency dependent sound transmission regions of a panel

At low frequencies, the sound transmission loss is controlled by the panel's stiffness [9,17]. Other factors such as damping and mass have little effect here. For constant frequency, the STL in this region increases with a higher first resonance frequency. This range ends with the appearance of the first resonance frequency [18].

At slightly higher frequencies, the STL is controlled by the natural resonance of the panel. The resonant frequencies are the frequencies at which the panel vibrates at higher levels. The resonant frequencies depend on the material, size, shape, and mounting parameters of the panel. At these driving frequencies, due to the high level of vibration of the panel, high amounts of sound energy are transferred to the transmitted side and there are noticeable dips in the STL [9,16].

After the resonance range, the sound pressure transmission loss of the panel is governed by its mass in what is known as the mass controlled region. For many typical sound insulation applications, this is a particularly important range [9]. In this range the STL can be accurately predicted by the mass law:

$$STL = 10\log\left[1 + \left(\frac{m\omega\cos\theta}{2\rho c}\right)^2\right]$$ [1.1]

where m is the mass per unit area, ω is the angular frequency, θ is the angle of incidence, ρ is the density of the acoustic medium, and c is the speed of sound in the acoustic medium.

For normally incident waves, the incidence angle is 0°. By substituting this into the equation and changing the angular frequency to cyclic frequency ($\omega/2\pi = f$), and assuming $m\omega/(2\rho c) \gg 1$, the mass law can be simplified into the normal incidence mass law:

$$STL = 20\log(fm) - 42dB$$ [1.2]

where f is the cyclic frequency in Hertz and m is the mass per unit area. While Eq. 1.2 is an empiric law, it can accurately describe the sound transmission in the mass region and it can give a rough estimate for the sound transmission in the resonance region [16,17,19].

At even higher frequencies, bending waves can result in what is known as the coincidence effect. The coincidence effect first occurs at the critical frequency (f_c) of the panel, which is given by:

$$f_c = \frac{c^2}{1.8h} \sqrt{\frac{\rho}{E}} \qquad \textbf{[1.3]}$$

where c is the speed of sound in the material, ρ is the density of material, and E is the elastic modulus of the material. The coincidence effect occurs when the bending waves in the partition match the wavelength of the incident sound waves. This causes the bending displacement to be in phase with the surface of the panel [16]. The resulting effect is an efficient transfer of acoustic energy from the incident sound waves to the transmitted side of the panel and a noticeable drop in STL, known as the coincidence dip, starting at the critical frequency [9]. This region is referred to as the coincidence region.

1.3   Advantages of Using Honeycomb Cellular Materials in Partitions

The major components that affect the sound transmission capabilities of a panel are its stiffness, weight, damping, and resonant properties.   Honeycomb cellular materials, if used as the core material in a three layer sandwich construction, offer many different possibilities because these properties can be manipulated. Due to the variable range of effective properties possible with honeycomb cellular materials, these governing properties can be changed while keeping other crucial properties constant.

The three regions where the use of honeycomb cellular materials can be advantageous are in the stiffness, resonance, and coincidence controlled regions [9]. The stiffness controlled region offers opportunities due to the fact that honeycomb cellular

materials have a stiffness that can be adjusted [9]. Therefore, varying levels of stiffness panels could be produced and changed without affecting the weight of the panel. Because of this variability, the range of this region could be increased or decreased to generate a larger or smaller stiffness controlled region. The resonance region also offers opportunities due to the fact that the natural resonances are largely dictated by the shape and mechanical properties of the panel. Since there are many configurations for the honeycomb core, differing locations of resonant frequencies, quantity of frequencies, and size of the resonance controlled region can be manipulated. In addition, cellular materials often have better damping properties [9]. They can also be used to shift the coincidence region, but that will not be discussed in this work.

The mass controlled region is the one area where honeycomb cellular materials would not be advantageous. The only way to improve this region is by increasing the mass of the panel. Honeycomb cellular materials in general have a low mass and therefore would not be as desirable here [9]. Therefore, this work focuses on the design of varying transmission loss panels using honeycomb cores at low to mid frequencies (below 1000 Hz). Given size or weight constraints, many different acoustic responses can be generated and these responses can be tuned using a few important key geometric parameters.

1.4   Previous Work in Sound Transmission of Honeycomb Panels

There has been much work done in the field of studying the acoustic properties of sandwich panels. Many researchers have studied sandwich panels analytically, with some of the earlier works using energy expressions to study the behavior of sandwich

structures. Kurtze and Watters [20] were some of the first to look into the sound transmission loss of sandwich panels, suggesting that they may have distinct advantages over single layer panels. Their analytical model consisted of elastic skins that sandwiched an incompressible core, transmitting shear waves. However, the incompressible core model, which employed panel impedances, only accounts for flexural motions in the panel. Ford, *et al.* [21] improved upon their model by incorporating a compressible core that allowed for both flexural and dilatational motions. They used this model to study different sandwich panel properties focusing on polyurethane foam core panels. They used the kinetic and strain energies in bending at each natural frequency to describe the effects of sound transmission through the panel. Their work was also validated with experimental studies.

The energy expressions by Ford, *et al.* were later refined and modified by Smolenski and Krokosky [22] and presented in greater detail by including relative displacements. They gave particular attention to the influence of core properties on the dilatational natural frequencies. They also completed experimental random incidence sound transmission tests to compare and validate their theoretical results. Since then, other researchers have continued to make modifications and improvements to the model [23,24,25].

The study of multi-layer sandwich panels eventually led into the study of the effects of alternative anisotropic core materials. Moore and Lyon studied the effects of using orthotropic cores on the panel's performance [26] using both analytical expressions and experimental validation. Other researchers would eventually expand upon this work

of using orthotropic cores [27]. In addition, the effects of the previously discussed factors, stiffness, mass, damping, and also thickness, have been studied for other types of anisotropic core panels [28,29].

One of the most common orthotropic core materials used in these studies is the honeycomb core. The general effects of honeycomb cores have been studied recently [8,30,31,14] as well as other similar truss-like periodic panels [32,33]. In one study by Ruzzene, a spectral finite element model is employed to study the response of honeycomb truss core panels over a broad range of frequencies [8]. The spectral finite element method uses a reduced number of elements and is a powerful tool for describing the dynamic response over a broad range of frequencies [34]. In most cases for the spectral element method, researchers must develop their own code and commercial software is not readily available.

The finite element method is also capable of predicting the dynamic vibratory behavior of panels accurately, but performance of the method does drop off as frequency increases due to element sizing and other factors compared to the spectral element method [34]. Over a large range of frequencies, the special techniques such as the spectral formulation are needed. However, if the frequency range being studied is low, then the finite element method can be used to predict the vibratory behavior with a high level of accuracy. In addition, commercial software is readily available for the finite element method and can be easy for the designer to use, but only if the software is well understood. That is why the finite element model is used in this work. Effort was made to include a detailed description for the setup of the model so that the model could be

easily recreated, which would otherwise be tedious for those not familiar with the software [33].

In most of the previous works of studying the effects of honeycomb cores, only certain core configurations have been tested and the responses have not been correlated directly to the geometric properties. While this is helpful in understanding the behavior of the panels, it is not as helpful to the designer as knowing the effects of changing controllable parameters. It has not fully been explored how the geometric configurations of honeycomb cores can generate differing acoustic responses and offer greater design flexibility. These geometric factors need to be further explored so that they can be used to effectively design structures to achieve targeted acoustic properties in addition to satisfying other mechanical properties. This work aims to study these factors using a method that can be easily used and recreated to design honeycomb sandwich panels for varying acoustic performance properties.

1.5   Thesis Overview

This thesis report is organized in a format and order summarized by the flow chart seen below in Figure 1.4.
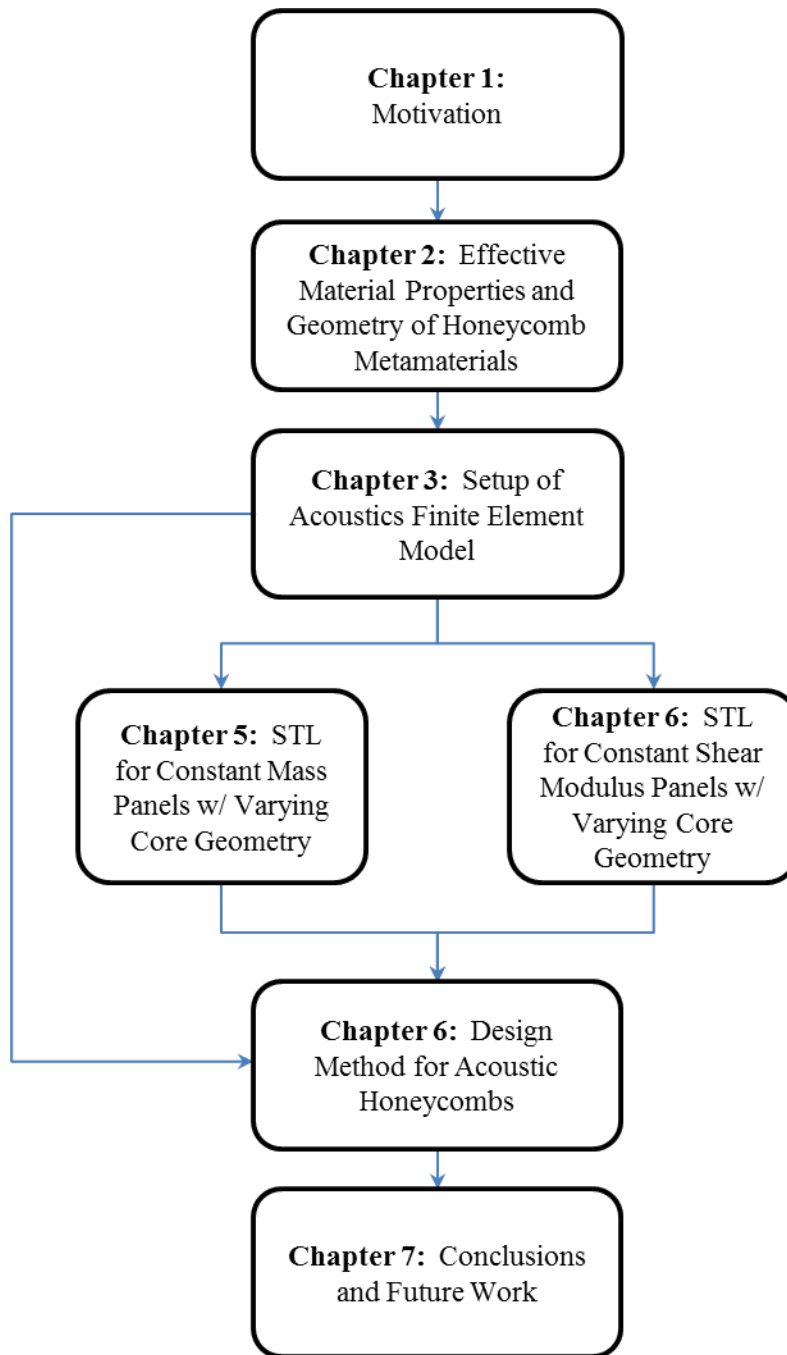
Figure 1.4: Overview of thesis flowchart

Chapter 1 covers the motivation for this work, discussing how honeycomb cellular materials are used in design and how this can be applied to acoustic applications.

It summarizes the previous applications of honeycomb cellular material design and discusses briefly a motivating application for this work. A gap is identified in the need to understand the acoustic behavior of honeycomb panels and what acoustic properties can be controlled. This ability to control the acoustic properties would allow for use in forward design.

Chapter 2 discusses the mechanical effective properties of honeycombs as defined by Gibson and Ashby. The effective properties used include effective Young's modulus (in the x and y directions), shear modulus, and density. It also discusses how the size of honeycomb meso-structures can be controlled through core geometry parameters. The controlled structure size allows for structures to be designed that adhere to limiting size constraints.

Chapter 3 discusses in detail the modeling parameters necessary to set up the finite element model in ABAQUS 6.10. This model was developed through an iterative trial and error process due to the fact that no other model with commercial software was found to use from literature. The model is validated by comparing its results with those from a spectral element model that was found in literature. It is used to gather the results for the later chapters in this thesis.

Chapters 4 and 5 discuss the results and outcomes of two different studies that employ the finite element model to examine the effects of various properties on the acoustic response of honeycomb panels. In Chapter 4, eighteen different models with constant mass are studied with internal cell angles ranging from -45° to 45° in 5°

increments. In Chapter 5, eighteen models with constant core shear modulus are studied with the same internal cell angle range as the constant mass study.

Chapter 6 describes a systematic and formalized method for designing honeycomb sandwich panels for acoustic applications. The process is described step by step and employs the finite element model and the outcomes of the previous property effects studies. The systematic method is applied to a hypothetical test design problem to show how it can generate multiple designs solutions that satisfy given requirements. Guidelines for selection of the final design solution are also discussed.

Chapter 7 summarizes the work in its entirety and highlights the main conclusions from this research. In addition, future work in this field is described to attain an even better understanding of the acoustic behavior. Other areas related to this work that can be explored are also discussed.

CHAPTER 2: EFFECTIVE MATERIAL PROPERTIES AND GEOMETRY OF
HONEYCOMB METAMATERIALS

The sandwich panels studied in this work are of a three layer construction, with two face sheets and a honeycomb core in between them. The static mechanical properties of the honeycomb core are generally understood and can be defined by Gibson and Ashby's cellular materials theory (CMT) [5], which is described in this section. It is important to note that this study uses honeycomb cores that are in-plane with the loading, which is a deviation from most works that study out-of-plane honeycomb cores. The difference between the two is illustrated in Figure 2.1. The material for both the face sheets and the core is aluminum. All panels have a core height of 8.66 cm and face sheet thicknesses of 2.5 mm. The thickness of the core cell walls varies based on the model.
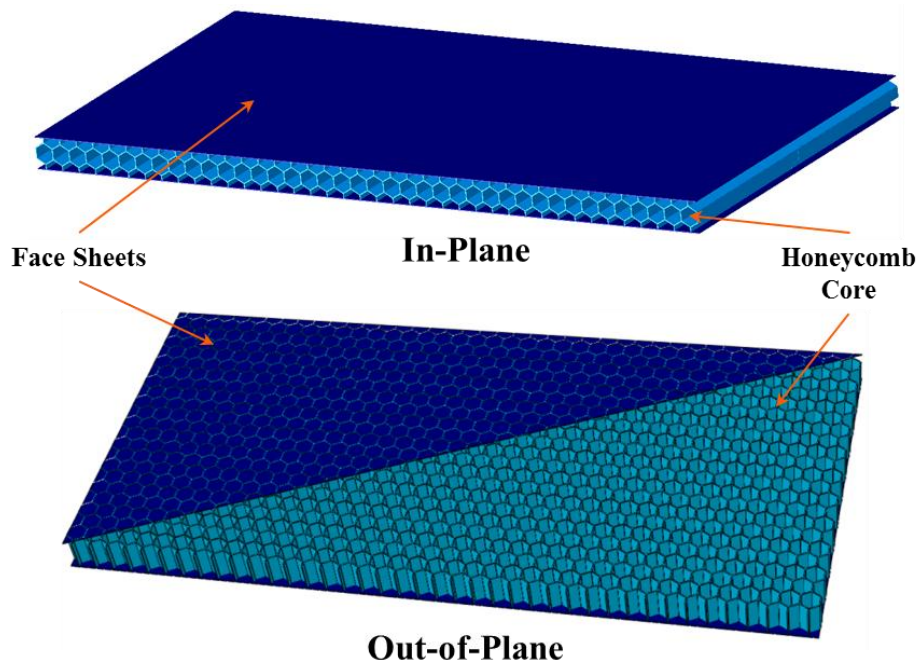
Figure 2.1: In-plane honeycomb cores vs. out-of-plane cores

19

2.1 Geometric Modeling Parameters

The unit cell is highlighted for two honeycomb panels in Figure 2.2. In the design of honeycomb materials, the conventional unit cell geometric parameters used, shown in Figure 2.3, are cell angle (θ), vertical member height (h), angled member length (l), and cell wall thickness (t). These parameters can be used to find the effective properties of the overall honeycomb structure. The unit cells in the figure shown are of a standard hexagonal model ($\theta = 30°$, $h = l$) and a frequently used auxetic model with similar mechanical properties ($\theta = -30°$, $h = 2l$). In this work, the cell angle will be varied from -45° to +45° in 5° increments, and the h, l, and t values will be adjusted to maintain a specific unit cell size and effective property.
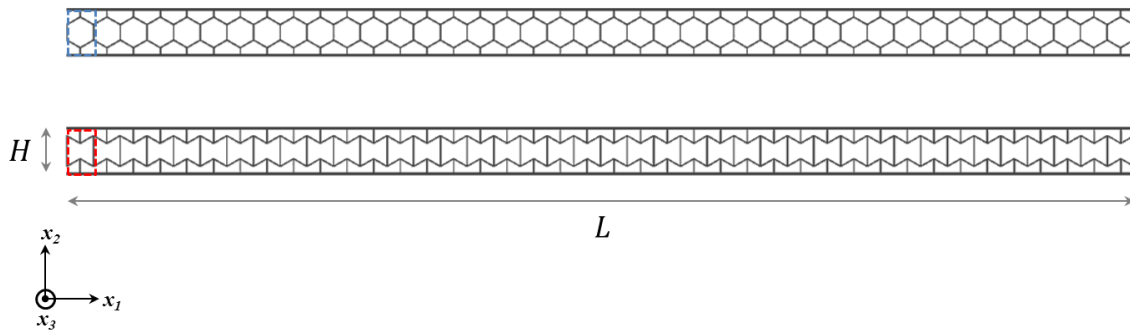
Figure 2.2: Sandwich panels with standard and auxetic cores and unit cell parameters
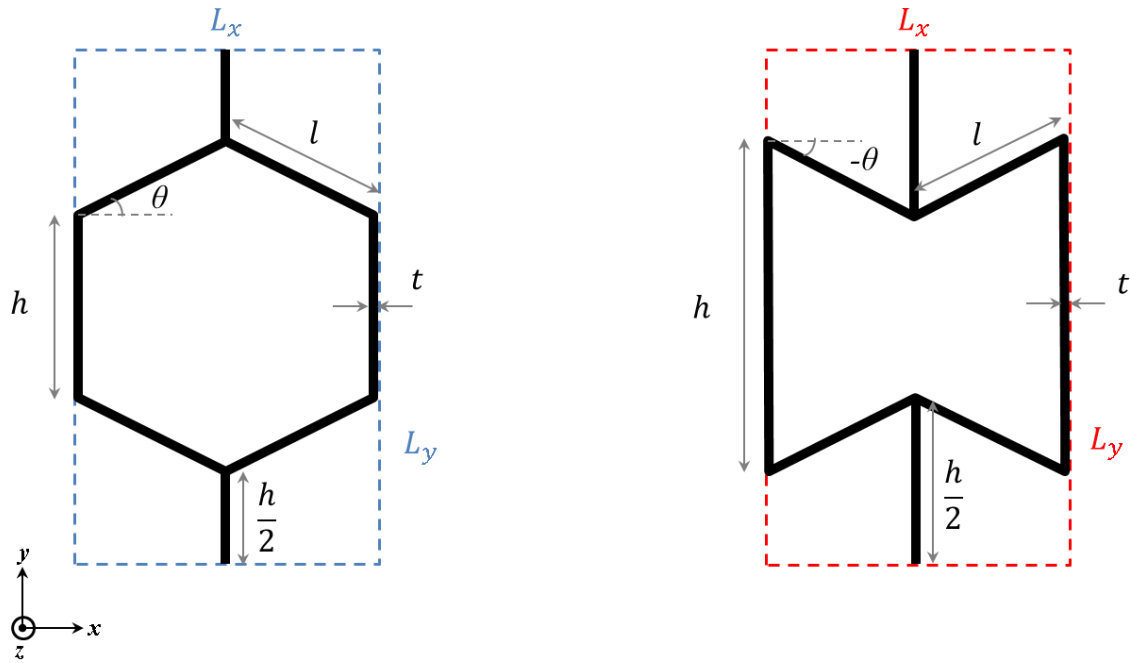
Figure 2.3: Local goemetric unit cell sizing parameters

2.2 Controlling Overall Panel Structure Size

The sizing of honeycomb structures presents a unique challenge when designing the material. If there are constraints on the overall size of the structure, which is the case with this work and many other design problems, then a change in one of the conventional geometric parameters must be accompanied by a modification of the other parameters in order to adhere to the design size constraints.

To address this issue, previous studies [3] have developed new parameters to adjust the size of the cell relative to the overall structure size, but those will not be used in this study. Instead, another method is developed which ensures the maintenance of a constant unit cell size. If the number of vertical and horizontal unit cells is kept constant, then the result is a constant overall structure size between different models. The length

along the x-direction of the unit cell is determined by the parameters θ and l. Using basic geometric principles, the x-direction length can be calculated. In this study, a specific x-direction length is specified to fit either 40 or 80 cells horizontally along a panel length of 2 m. The parameter θ is varied and an l is calculated to accompany this change. The length of the unit cell along the y-direction is determined by the parameters θ, h, and l. Again, this length can also be calculated using geometric principles. For this study, a specific y-direction length is specified to fit either 1 or 2 cells vertically along a panel height of 8.66 cm. Having already determined θ and l, an h is calculated to accompany this. The unit cell sizing equations used are given by Equations 2.1 and 2.2.

$$L_x = 2l\cos\theta \qquad \text{[2.1]}$$

$$L_y = 2(h + l\sin\theta) \qquad \text{[2.2]}$$

As can be seen by Figure 2.4, the results of using these equations are different panels of cellular configurations that all have the same overall structure size.
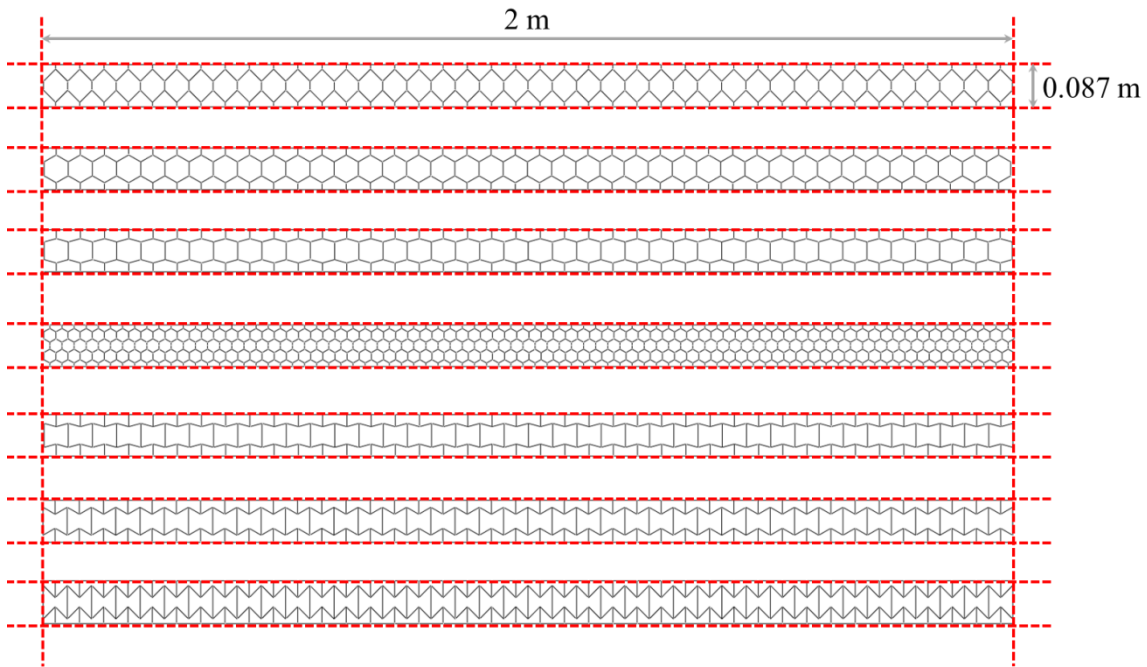
Figure 2.4: Overall structure sizing of various models

2.3   Effective Properties

The unique advantage that honeycomb cellular materials offer is that the conventional geometric parameters discussed can be changed in order to achieve varying overall macro parameters that the host material does not have. For low deformation, before a critical stress is reached, the main mechanism of deformation in honeycombs is the bending of the cell walls and the honeycomb behaves linear elastically. Gibson and Ashby's cellular material theory (CMT) [5] quantifies these effective elastic properties for honeycomb structures in the form of equations, derived from Bernoulli-Euler beam theory, that use the aforementioned geometric cellular parameters as input variables. The effective elastic properties studied here include in-plane elastic modulus in the x and y directions and in-plane shear modulus:

$$E_{11}^* = E\left(\frac{t}{l}\right)^3 \frac{\cos\theta}{\left(\frac{h}{l}+\sin\theta\right)\sin^2\theta} \qquad \text{[2.3]}$$

$$E_{22}^* = E\left(\frac{t}{l}\right)^2 \frac{\left(\frac{h}{l}+\sin\theta\right)}{\cos^3\theta} \qquad \text{[2.4]}$$

$$G_{12}^* = E\left(\frac{t}{l}\right)^3 \frac{\left(\frac{h}{l}+\sin\theta\right)}{\cos^3\theta} \qquad \text{[2.5]}$$

where E is the elastic modulus of the constituent material, and h, l, t, and θ are the geometric unit cell parameters. Also, studied is the effective density of the honeycomb structure:

$$\rho^* = \rho\frac{\frac{t}{l}\left(\frac{h}{l}+2\right)}{2\cos\theta\left(\frac{h}{l}+\sin\theta\right)} \qquad \text{[2.6]}$$

where ρ is the density of the constituent material. This equation is derived from simple geometric relations.

In this study, either the effective density or effective shear modulus of all the models is kept constant. Constant effective density ensures that all models have the same volume of material and consequently the same overall mass. Constant mass is selected as this as this is generally the property that governs the overall magnitude of the sound transmission response, with some deviations, such as in the stiffness region. Constant

24

shear modulus is kept constant in another study because it ensures that some degree of structure stiffness is kept constant between the models. While this is not the only property that governs the panel stiffness, other works in literature have identified the shear parameters as a significant one [35].

CHAPTER 3: SETUP OF ACOUSTIC FINITE ELEMENT MODEL USING
COMMERCIAL SOFTWARE

To provide consistent results between different panels studied, it is necessary to develop a standard finite element analysis (FEA) model. Due to the fact that there is little literature found that makes use of commercial finite element analysis software, a model is created with ABAQUS v6.10 from scratch that resembles many of the features seen in published studies, which use custom analysis codes. The model developed is cross checked with results from those studies to ensure that it provides consistent results. The same model can be replicated and used in future studies so that future results can be accurately compared.

The FEA model developed, shown in Figure 3.1, consists of a honeycomb sandwich panel and a fluid domain, which is effectively attached to the top of the panel. The panel is loaded on the bottom side to mimic an incoming sound pressure wave of controlled frequency. The vibration in the panel caused by the sound wave is then allowed to propagate through the panel into the acoustic fluid domain, where results can be required both numerically and visually. Details on the specific modeling and response collection parameters are also discussed in this chapter.
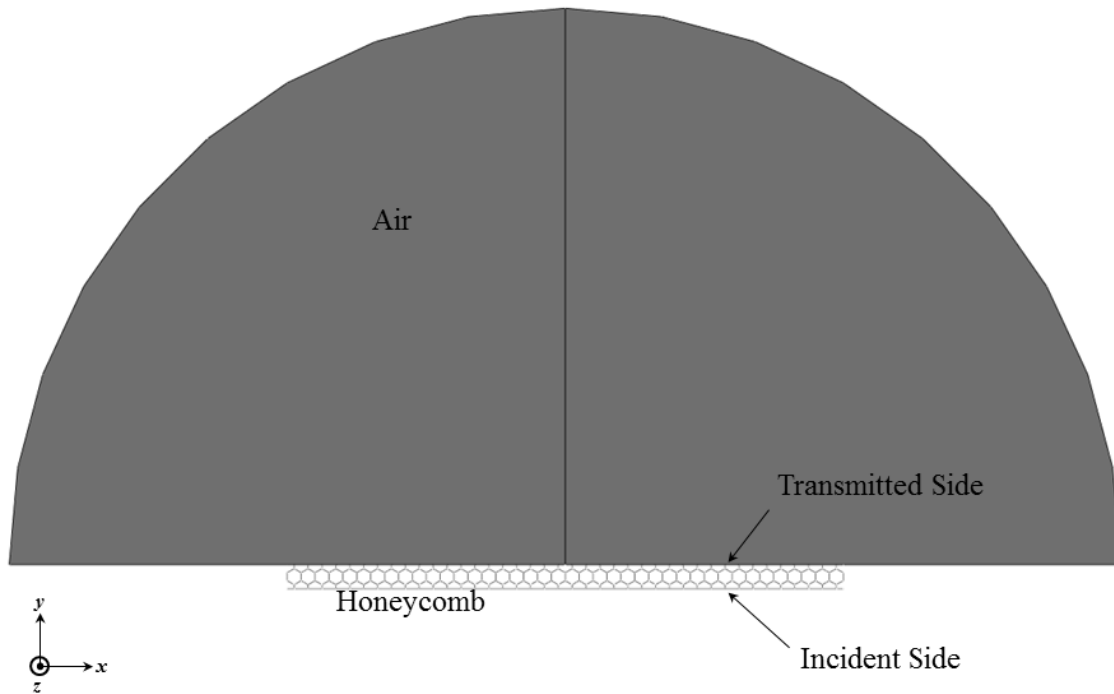
Figure 3.1: Physical setup of acoustic model

3.1 Justification for a Two Dimensional Model

Due to the fact that the loading is in the same plane as the geometry of the core and face sheets, the problem can be set up as a two dimensional (2D) model. Using a 2D analysis helps to significantly reduce the analysis time and also makes the sketch for the parts easier to generate. If the loading is out of the plane of the core geometry, as is the case with out-of-plane honeycomb core sandwich panels, a three dimensional model would have been necessary. In the case of the 2D analysis, an assumption is made that the out of plane thickness is large enough that the corresponding out of plane boundary effects can be ignored.

3.2   Analysis Components and Material Properties

There are only two parts used in the analyses of this work. These include the honeycomb sandwich panel being studied and the air fluid on the transmitted (top) side of the honeycomb structure. For the natural frequency analysis, only the honeycomb sandwich panel is needed.

The honeycomb sandwich panel is modeled as a single part. Modeling the core and face sheets separately is also an option but is not done in this study for simplicity and to avoid the need to include extra tie constraints at the connection points. Moreover, the currently envisioned manufacturing process to create these panels is through layered manufacturing or machining from monolithic workpieces. The component is modeled as a 2D planar deformable part with a wire profile. The core section of all models consists of either 20 cells in the x-direction and 1 cell in the y-direction or 40 cells in the x-direction and 2 cells in the y-direction. The angle of the core unit cells varies from -45° to +45°. The thickness of the face skins and each cellular wall is controlled using rectangular profiles that are assigned as beam sections. The "a" dimension of the profile corresponds to the thickness in the xy-plane and is varied to achieve the desired effective properties. The "b" dimension of the profile corresponds to the out-of-plane length and is set to unity for the sake of simplicity. All sections of the honeycomb panel are assigned the material properties of aluminum, which are summarized in Table 3.1.

Table 3.1: Material Properties of aluminum used in finite element model

Density – ρ (kg/m³)	Young's Modulus – E (GPa)	Poisson's Ratio - v
2700	71.9	0.3

The second part, the air fluid, is modeled as a semi-circular domain to mimic the effects of air on the surface of the honeycomb structure. This part is necessary to determine the transmission of the sound from the structure to the air and to simulate any damping effects that the air may have on the structure. The air is modeled also as a 2D planar deformable part, but with a shell profile. A solid, homogenous section is applied to the part with an out-of-plane thickness set to unity like the honeycomb. The part is given the material and acoustic properties of air, which are summarized below in Table 3.2. The impact of different fluid region properties is out of scope for this research and is reserved for future investigation.

Table 3.2: Material/acoustic properties of air used finite element model

Density – ρ (kg/m³)	Speed of Sound in Air – c (m/s)	Bulk Modulus – κ (Pa)
1.2	343	141179

3.3   Element Justification and Mesh Setup

For the honeycomb sandwich panels, B-22 beam elements are used for both the face skins and the core section. B-22 elements consist of three nodes and are planar beam elements of quadratic geometric order. These quadratic order elements are chosen in order to reduce computational effort while still keeping a high level of accuracy compared to linear beam elements. These beam elements are commonly used in static, quasi-static, and some dynamic honeycomb analyses [11,3,6,36]. In dynamic analyses

where there is large deformation, beam elements have problems handling contact and can often result in the piercing of one element by another. Some researchers have used shell elements, which are better at handling contact, to account for this [4]. However, since the deformation in this work is small, beam elements are sufficient. The elements are sized to have at least four elements per the smallest edge in the core, as recommended by previous works [37,4,7]. Therefore, the mesh size changes for each model according to the geometric properties of the core.

The air domain is modeled using AC2D3 elements, which are 3-node 2-D acoustic triangles commonly used to model acoustic mediums [38,39]. The mesh seed size of these elements in close proximity of the honeycomb structure is 0.012 m. By using a mesh bias from the center of the semicircular domain to the edge, the element size gradually increases to 0.08 m at the edge of the fluid domain (Figure 3.2). The reason for the changing mesh size is that only the air directly in contact with the honeycomb panel is of concern for the data post-processing accuracy and therefore must be fine. The rest of the air fluid domain only serves for visualization purposes and is not of as much importance. The ABAQUS user manual recommends that there should be at least 6-8 elements per wavelength of the highest analyzed frequency for acoustic radiation analyses [38,40]. The mesh size selected in this work well exceeds this recommendation to avoid any error associated with having too coarse of a mesh. It is important to note that, due to the shape of the domain, use of triangular elements, and random nature of the mesh generation, the mesh is not perfectly symmetric and therefore

the visual results for the pressure distributions will not be completely symmetric. This is seen in the acoustic pressure field results presented later in this work.
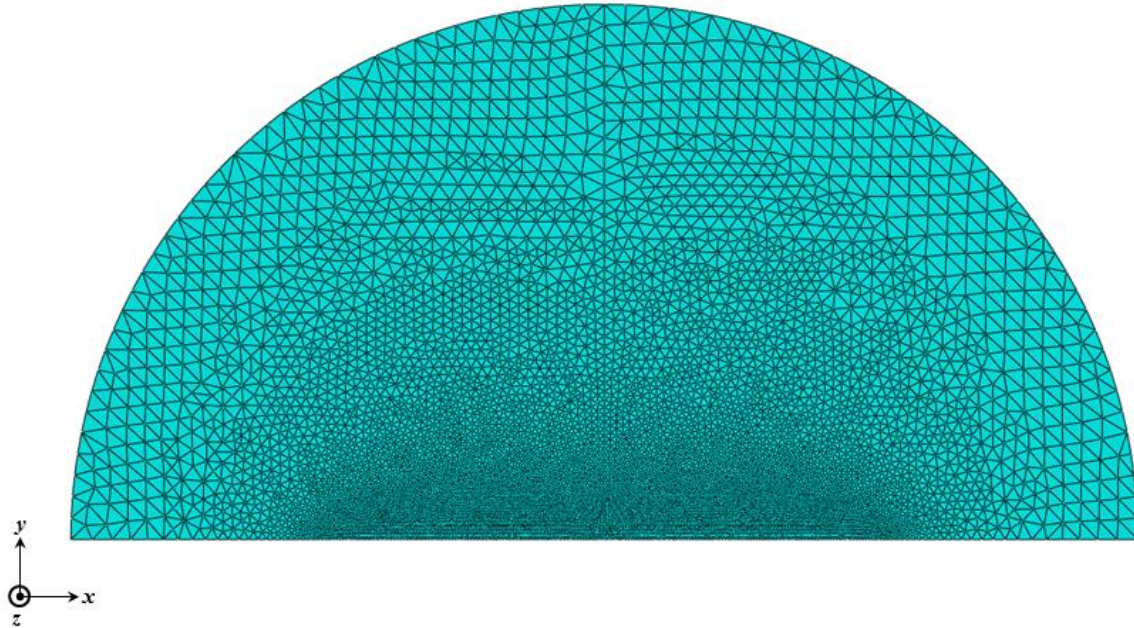
Figure 3.2: Mesh of the air domain showing bias towards edge in contact with the sandwich panel

3.4 Boundary Conditions and Loads

For the boundary conditions, the ends of the structure are pinned to simulate being connected to a rigid insulator. The displacement of all the nodes along the two edges, including both the face sheets and the core are constrained to zero in both the x and y directions (Figure 3.3). The rotation along the out-plane-axis is not constrained. Pinned boundary conditions are consistent with other work found in literature [8]. These boundary conditions are used for both the natural frequency and steady state analyses. No boundary conditions are specified for the air domain, allowing it to move freely.
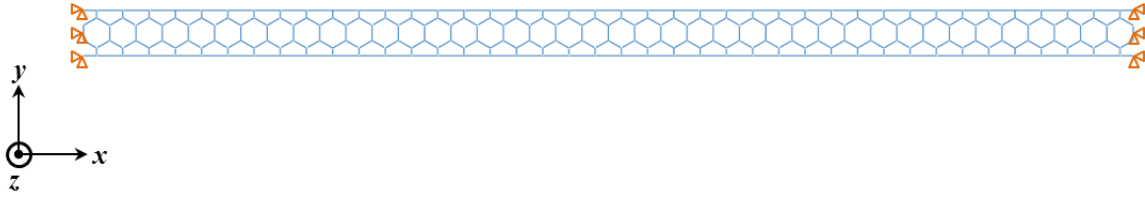
Figure 3.3: Pin boundary conditions along the ends of the honeycomb structure

For the steady-state analyses only, a uniformly distributed pressure load of unit amplitude, which varies sinusoidally with the frequency of the step, is applied to the bottom face sheet (Figure 3.4) of the structure to simulate the effects of an incoming sound wave. The underside of the bottom face sheet is specified as a surface to make the loading face selection easier. In this work, direct incidence ($\alpha = 0°$) is specified for simplicity. For the natural frequency analysis, this load is not necessary and thus no load is applied to the structure.

Unit amplitude
pressure load
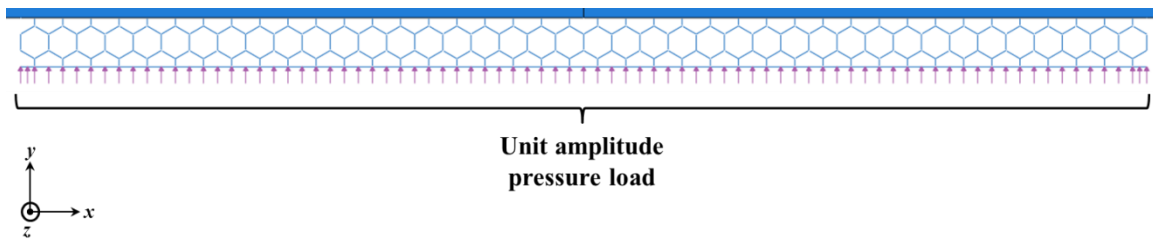
Figure 3.4: Sinusoidally varying unit pressure load

3.5 Constraints

To ensure that the honeycomb panel and the air do not lose contact, a surface based tie constraint is used. This constraint couples the structural field with the acoustic field and ensures that the two deform together as one component at the interface. For the surface based tie constraint, a master surface and a slave surface must be defined. The

master surface is typically the stiffer of the two components [38,37]. Therefore, the top skin of the honeycomb sandwich panel is defined as the master surface and the bottom surface of the air fluid is defined as the slave surface. After the user defines the surfaces to be "tied," ABAQUS automatically generates the fluid-solid coupling necessary for the analysis [40].
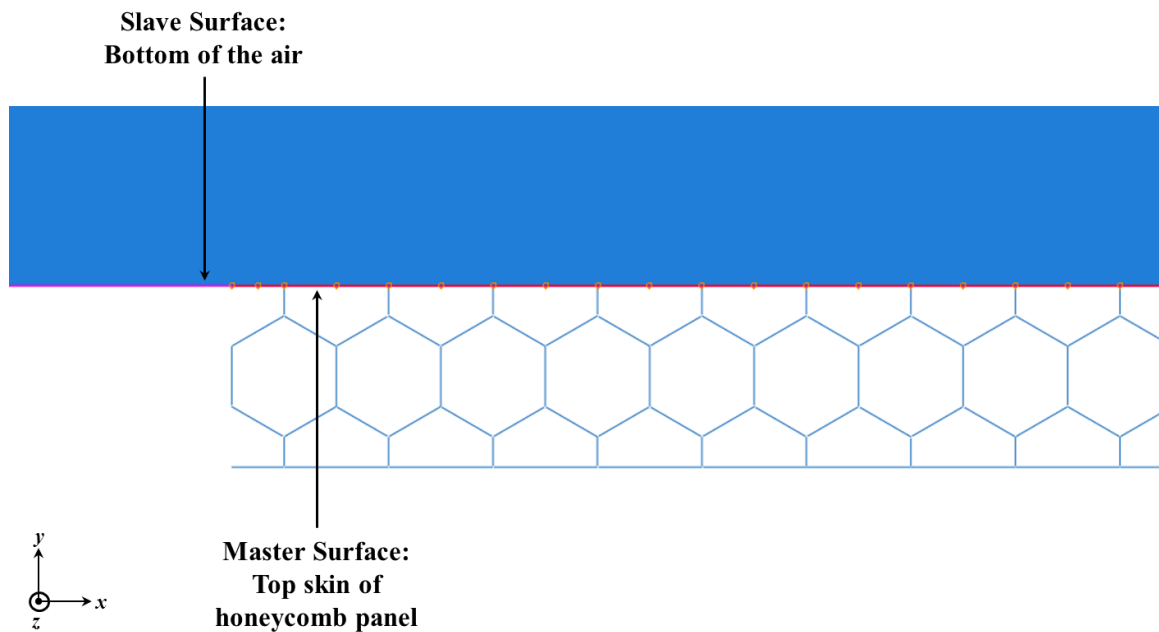
Figure 3.5: Tie Constraint

It is also important to make sure that the sound waves do not reflect off of the top surface of the fluid region back into the area of data collection. The fluid must be modeled to simulate an infinite amount of surrounding air. Even though many real world applications will have some constraining boundary, such as building rooms, modeling an infinite amount of air provides a good starting point for comparison and is commonly done in acoustic analyses [39,40]. To achieve this, an absorbing interaction via surface

impedance is defined along the top surface of the fluid region. The absorption definition for this model is specified as non-reflecting. The geometry is specified as circular with a radius of 2, based on the semi-circular geometry of the air fluid.

The effect of modeling an infinite amount of air can also be achieved using ABAQUS's acoustic infinite elements [40,38]. This feature offers the same ability to model a non-reflecting surface while also being capable of interpolating in the infinite direction, allowing for the visualization of the acoustic far field in steady-state dynamic analyses. It is helpful for reducing large domains, while still recording far-field results. However, since the acoustic pressures in the distant outer fluid are not of importance for this analysis, the absorbing interaction is chosen due to its simplicity.

All of these modeling and analysis parameters are summarized in the diagram shown below in Figure 3.6
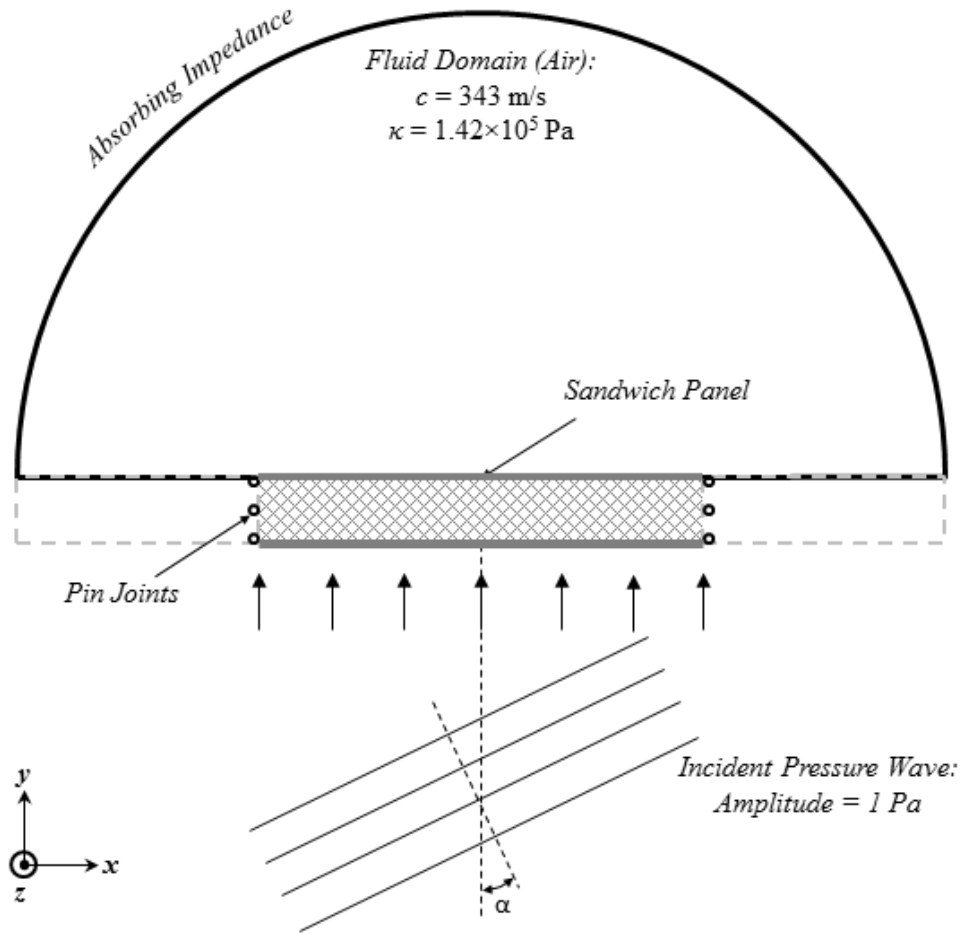
Figure 3.6: Model setup diagram with loading conditions

3.6   Natural Frequency Extraction Procedure

In order to understand the vibratory properties of the honeycomb sandwich panels and to focus the transmission loss study, a natural frequency extraction is first run on each of the panel models. The undamped modal frequencies and mode shapes of the sandwich panels are gathered using the natural frequency extraction analysis procedure in ABAQUS/CAE 6.10. These modal frequencies, when damping is small, correlate to the

resonating frequencies of the structure and can describe where there will be higher levels of vibration [17].

During the analysis, only the honeycomb sandwich structure is analyzed and the air is not included. Since the damping effects of the air are small, it is excluded in order to save analysis time. The analysis procedure in ABAQUS consists of two steps:

1. <u>Initial Step</u> – Default initial conditions are defined automatically by ABAQUS; these are not modified

2. <u>Linear Perturbation, Frequency Step</u> – Modal frequencies are extracted using Lanczos eigensolver

The frequency step is carried out over a specified range of 1-1000 Hz, which is the frequency range of interest for this study and represents a low to mid-frequency range. This performs the analysis in the stiffness region and well into the resonance region.

3.7   Steady State Dynamics, Direct Procedure

Since the loading is a constant sinusoidal sound wave, this analysis can be simulated using a steady state dynamics procedure. A steady-state procedure allows for the levels of sound transmission of the honeycomb sandwich panels to be measured. The dynamic steady state, direct procedure in ABAQUS is used for this. The analysis consists of two steps:

1. <u>Initial Step</u> - Default initial conditions are defined automatically by ABAQUS; these are not modified

2. <u>Steady State Dynamics, Direct</u> – Frequency sweep over specified range with frequency specific load is performed, extracting pressure data at each step

The procedure is carried out over the range of 1-1000 Hz, the same as the natural frequency extraction analysis. The natural frequencies from the previous analysis are input into this range as analysis points. Each interval between natural frequencies contains six or seven points with a bias parameter of two towards the natural frequencies. This is done so that there would be a refined response around the natural frequencies, which are the points of interests.

3.8   Response Collection/Post-processing

One of the most common metrics for describing the acoustic performance of a panel is the sound transmission loss (STL) of the panel over a range of frequencies. A measure of sound pressure transmission loss is the difference between the incident and transmitted acoustic pressure through the panel:

$$STL = 10\log_{10}\left|\frac{p_i^2}{p_t^2}\right|$$

[3.1]

where,

$$p_i^2 = \boldsymbol{p_i} \cdot \boldsymbol{p_i}$$

$$p_i^2 = \boldsymbol{p_t} \cdot \boldsymbol{p_t}$$

and

$$\boldsymbol{p} = \langle p_1, p_2, ..., p_n \rangle$$

is a vector of the pressure values at the nodes along the face sheets of the honeycomb.

During the steady state analysis, a history output is specified for the acoustic pressure (POR) of all the air nodes in direct contact with the top panel of the sandwich panel, or the transmitted side. The acoustic pressure results are in the form of complex numbers and therefore the magnitude of these complex numbers is recorded. Since the loading is specified as a unit pressure wave, the incident pressure on all the nodes on the bottom, or incident, side of the panel is one. The norm of each of these acoustic pressure output vectors is calculated and squared. Together, these results are used to calculate the sound transmission loss of each of the panels using Equation 3.1.

3.9   Analysis Time

Each of the analyses is run on a Dell Precision T7400 computer with dual quad core 2.00 GHz Intel Xeon processors, allotting six of the cores for use. The natural frequency analysis for all the models takes only a small amount of time to complete, with all analyses taking under a minute to complete. The steady state analyses takes longer, ranging anywhere from approximately two to eleven minutes to complete. In general, the negative angle models take longer for both the natural frequency analysis and the steady state analysis to complete due to the higher number of vibration modes. For the steady state analysis, this means that there are more points of analysis to evaluate. The mesh size also plays a factor in the analysis time, though not as significant as the number of

vibration modes. This is why the 2 x 80 models take longer to complete due to the finer meshes. As a general reference for the time variation, the analysis times for the -30° and +30° models are shown in Table 3.3, which includes both the 1 x 40 and 2 x 80 unit cell configurations of the models.

Table 3.3: Analysis times for the +30° and -30° models

	Natural Frequency Analysis Time	Steady State Analysis Time
+30° (1 x 40)	0m 22s	2m 02s
+30° (2 x 80)	0m 25s	3m 41s
-30° (1 x 40)	0m 31s	5m 15s
-30° (2 x 80)	0m 45s	10m 48s

3.10 Model Validation

To verify that the model presented shows consistent trends, the results are compared to previous results found in literature [8], which uses a spectral element formulation. The sound transmission loss results in the 1-1000 Hz frequency range for a square truss core sandwich panel are shown in Figure 3.7. These results are normalized to account for scaling differences. The square truss core model is used only for comparison purposes but is not studied further in this work. It can be seen that the finite element model used does follow the same trends as found in previous literature, especially for the first group of resonant frequencies. At about 900 Hz, the results for the square truss core do begin to deviate some. However, the agreement between the results is more than sufficient for this work.
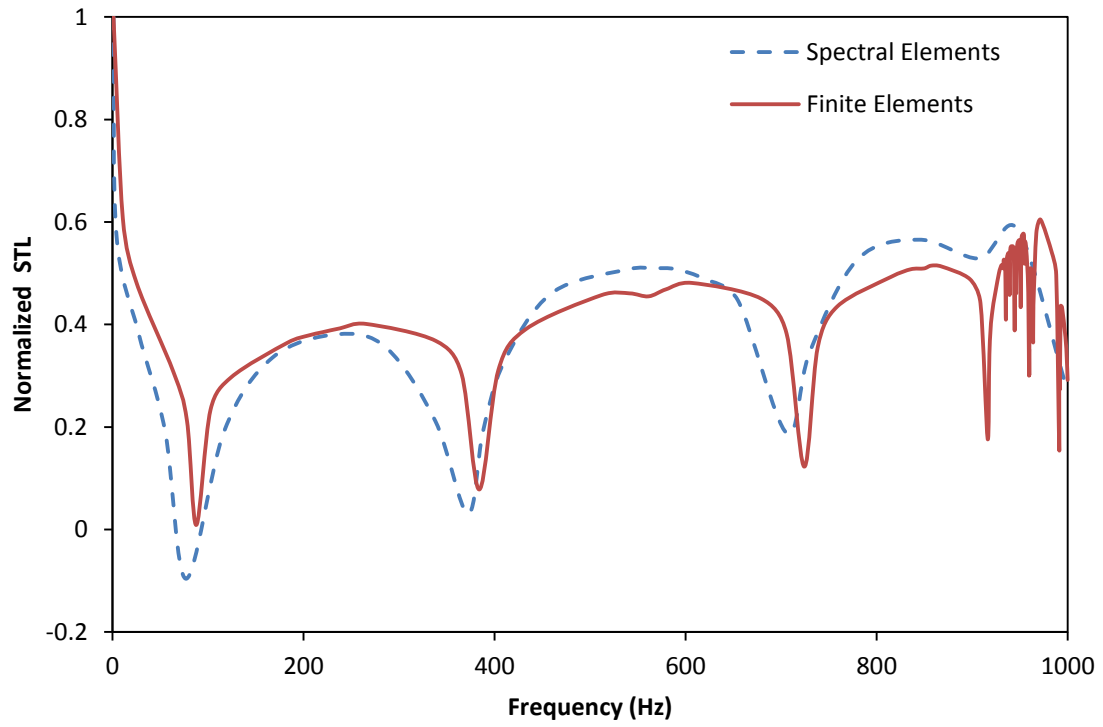
Figure 3.7: Comparison of the normalized sound transmission loss between spectral element results [8] and finite element model proposed in this paper

CHAPTER 4: SOUND TRANSMISSION LOSS FOR CONSTANT MASS AND
STRUCTURE SIZE PANELS WITH VARYING CORE GEOMETRY

The first scenario studied is of panels with constant mass and overall structure size. Structure size is kept constant due to the fact that most design problems have fixed size constraints. The overall mass is of particular interest due to its believed effect on the general magnitude of the sound transmission loss. As previously discussed, the mass almost solely dictates the level of sound transmission in the mass region and influences the general magnitude in the resonance controlled region. This idea is tested and confirmed.

While mass and structure size are kept constant, the core geometry is varied by changing the local geometric parameters. Varying the geometry changes the effective stiffness and resonant properties of the panel. While it is understood that these do have effects on the acoustic responses, it is not known to what degree each of the properties affects the response in this specific application. By studying varying model configurations of constant size and mass, one can begin to highlight the key global effective properties and even potentially the local parameters that are significant in changing the shape of the sound transmission loss response, without necessarily changing the magnitude of the response.

4.1 Honeycomb Models

The honeycomb models tested consist of cores that contain either one cell in the vertical direction and 40 cells in the horizontal direction (1 x 40) or two cells in the vertical direction and 80 cells in the horizontal direction (2 x 80). The varying dimension

size is to test for boundary effects, which are discussed later in this chapter. The models range from -45° to +45°, changing in 5° increments. Between each of the models, the *l* and *h* are varied in order to keep the overall size of the unit cells the same within the 1 x 40 or 2 x 80 arrangement using the guidelines specified in Chapter 2. The thickness of the cell walls is also varied to ensure that an effective density of 270.0 kg/m^3 is kept constant. Since the structures all have the same overall dimensions, constant effective density ensures constant mass between the models. The geometric properties of all the models tested are summarized in Table 4.1 and Table 4.2 below. For all of the models, a face sheet thickness of 2.5 mm is used. Figures 4.1, 4.2, and 4.3 are shown to illustrate how each of the geometric parameters changes in relation to changes in internal cell angle under the constant unit cell size constraints. This is shown for both the 1 x 40 and 2 x 80 models. It can be observed that, under constant mass constraints, the thickness increases as cell angle increases up to the positive 30° model and then begins to decrease. The *h* and *l* parameter charts illustrate the geometric relations for the constant unit cell size approach used. The inverse relationship between vertical height member and cell angle can also be observed. For all of the parameters, the 2 x 80 models exhibit the same trend as the 1 x 40, but at exactly half the magnitude.

Table 4.1: Geometric and effective properties of 1 x 40 constant mass honeycomb cores
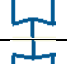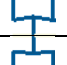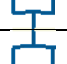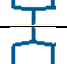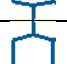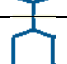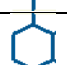
Cell Angle		Unit Cells	l (mm)	h (mm)	t (mm)	$G_{12}*$ (MPa)	$\rho*$ (kg/m^3)	$E_{11}*$ (MPa)	$E_{22}*$ (MPa)
-45°		1 x 40	35.36	68.30	1.56	0.579	270	7.01	21.0
-40°		1 x 40	32.64	64.28	1.67	0.862	270	13.3	28.1
-35°		1 x 40	30.52	60.81	1.78	1.23	270	24.6	36.2
-30°		1 x 40	28.87	57.73	1.88	1.68	270	44.9	44.9
-25°		1 x 40	27.58	54.97	1.97	2.25	270	83.1	54.2
-20°		1 x 40	26.60	52.40	2.05	2.94	270	160	63.7
-15°		1 x 40	25.88	50.00	2.13	3.76	270	340	73.2
-10°		1 x 40	25.39	47.71	2.20	4.75	270	883	82.4
-5°		1 x 40	25.10	45.49	2.26	5.93	270	3960	90.8
5°		1 x 40	25.10	41.11	2.37	9.04	270	4550	105
10°		1 x 40	25.39	38.89	2.41	11.1	270	1170	109
15°		1 x 40	25.88	36.60	2.45	13.6	270	519	112
20°		1 x 40	26.60	34.20	2.48	16.8	270	283	112
25°		1 x 40	27.58	31.64	2.49	21.0	270	170	111
30°		1 x 40	28.87	28.87	2.50	26.6	270	107	107
35°		1 x 40	30.52	25.80	2.49	34.9	270	67.9	99.9
40°		1 x 40	32.64	22.32	2.47	48.2	270	43.1	91.0
45°		1 x 40	35.36	18.30	2.43	73.4	270	26.7	80.1

Table 4.2: Geometric and effective properties of 2 x 80 constant mass honeycomb cores

Cell Angle		Unit Cells	l (mm)	h (mm)	t (mm)	$G_{12}*$ (MPa)	$\rho*$ (kg/m³)	$E_{11}*$ (MPa)	$E_{22}*$ (MPa)
-45°		2 x 80	17.68	34.15	0.78	0.579	270	7.01	21.0
-30°		2 x 80	14.43	28.87	0.94	1.68	270	44.9	44.9
-15°		2 x 80	12.94	25.00	1.06	3.76	270	340	73.2
15°		2 x 80	12.94	18.30	1.22	13.6	270	519	112
30°		2 x 80	14.43	14.43	1.25	26.6	270	107	107
45°		2 x 80	17.68	9.151	1.22	73.4	270	26.7	80.1
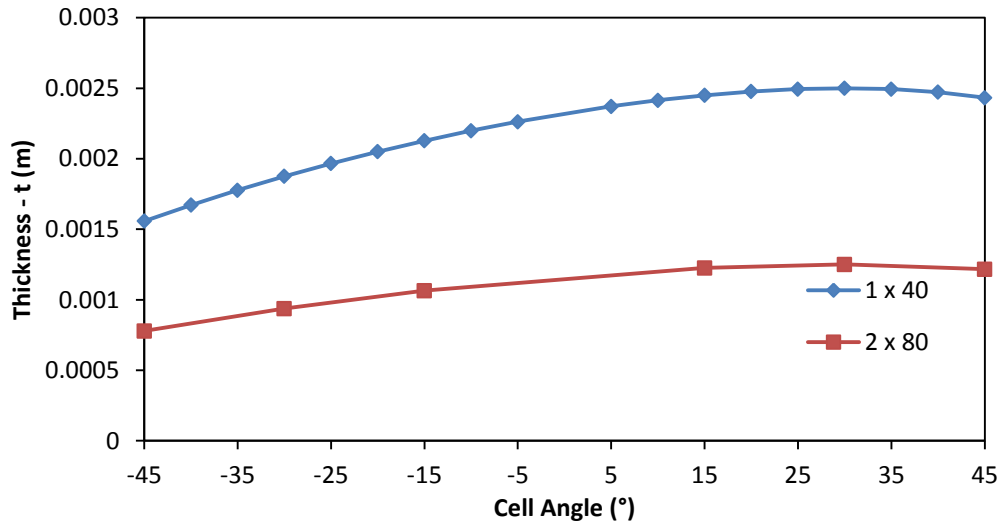
Figure 4.1: Cell wall thickness at varying cell angles for constant mass
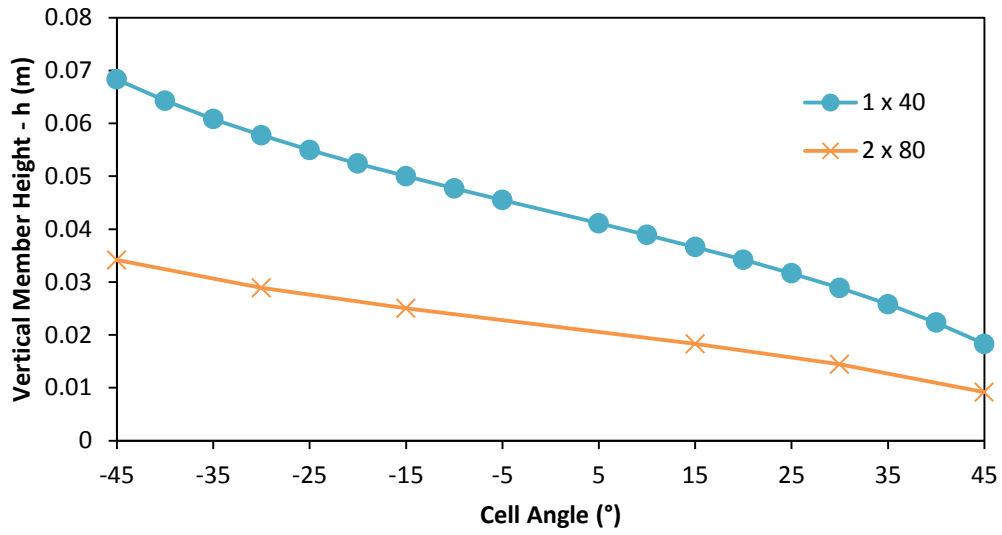
Figure 4.2: Vertical member height at varying cell angles for constant mass
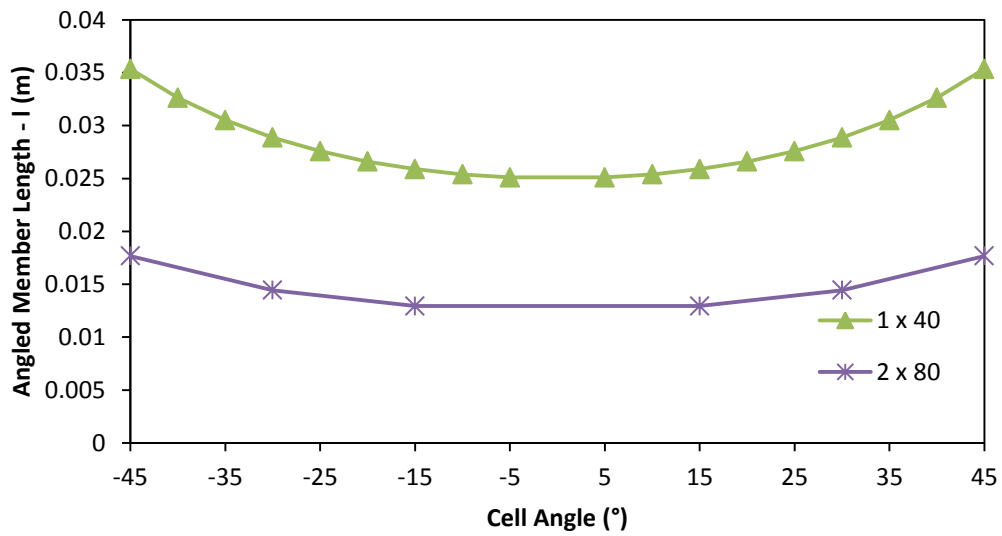
Figure 4.3: Angled member length at varying cell angles for constant mass

4.2   Natural Frequencies

The natural frequency extraction is performed on all of the models shown. The results are broken up into the results from the 1 x 40 models and the 2 x 80 models. All the results are recorded for use in the steady state analysis, but only the first ten are reported here for analysis. The reason for this is that the later modes in a natural frequency extraction tend to be less accurate and it is determined that the modes past the tenth would not be as meaningful.

4.2.1   Natural Frequencies for 1 x 40 Models

The first ten modes and their corresponding frequencies are shown below in Table 4.3 (positive angles) and Table 4.4 (negative angles). It should be noted that the +45° model only has nine modes within the specified range.

Table 4.3: Natural frequencies of positive angle constant mass honeycomb core sandwich panels
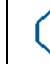
Mode #	5°	10°	15°	20°	25°	30°	35°	40°	45°
1	43.0	46.1	49.3	53.5	57.9	62.8	68.5	75.3	83.8
2	88.2	94.4	100.7	109.4	118.7	129.7	143.2	160.3	183.6
3	138.3	148.3	158.4	172.3	187.6	205.9	228.6	258.1	299.5
4	189.5	203.3	217.0	236.0	257.2	283.0	315.5	358.6	420.5
5	241.4	259.3	276.8	301.0	327.8	360.8	403.0	459.9	542.9
6	293.6	316.0	337.4	366.7	399.0	439.0	490.5	560.8	664.8
7	346.2	373.2	398.8	433.3	471.0	517.8	578.4	661.6	762.8
8	399.2	430.8	460.8	500.6	543.8	597.2	666.5	761.2	786.0
9	452.7	488.9	523.4	568.6	617.4	677.3	755.2	762.2	906.2
10	506.7	547.6	586.6	637.4	691.7	758.2	760.3	862.9	------

Table 4.4: Natural frequencies of negative angle (auxetic) constant mass core sandwich panels

Mode #	-45°	-40°	-35°	-30°	-25°	-20°	-15°	-10°	-5°
1	11.7	14.2	16.8	19.6	22.6	25.7	29.0	33.4	36.3
2	23.6	28.7	34.0	39.7	45.7	52.0	59.0	68.1	74.2
3	36.3	43.9	52.2	61.0	70.5	80.6	91.7	106.4	116.2
4	49.8	60.0	71.2	83.3	96.3	110.3	125.6	145.8	159.0
5	64.3	77.1	91.3	106.7	123.3	141.2	160.8	186.2	202.5
6	79.9	95.4	112.5	131.2	151.5	173.2	196.7	227.2	246.4
7	96.8	114.8	134.9	156.9	180.7	206.2	233.5	268.7	290.7
8	114.9	135.5	158.4	183.7	210.9	240.1	270.9	310.8	335.4
9	134.4	157.4	183.2	211.6	242.2	274.8	309.1	353.5	380.7
10	155.2	180.6	209.2	240.6	274.4	310.4	348.0	396.7	426.6

The lowest first modal frequency for the regular honeycomb core sandwich panels occurs at 43.0 Hz, which is for the +5° mode. After that, the first natural frequency increases as the cell angle increases (becomes more positive) for each of the positive angle models. The lowest first modal frequency for the auxetic core sandwich panels occurs at 11.7 Hz, which is for the -45° model. The first natural frequencies again occur later for each auxetic core after that as the cell angle increases (becomes less negative). In general, it can be observed that the lower angle models, meaning less positive for the regular honeycombs and more negative for the auxetics, have lower overall natural frequencies at each of the mode numbers. That is, as the cell angle increases, the first natural frequency increases. In addition, those models that have lower first natural frequencies have subsequent natural frequencies that are lower and the spacing between modes is smaller. This is not necessarily stating that the cell angle is responsible for

dictating the behavior of the natural frequency since the geometric parameters are interrelated. It is simply stating the trend between the two with these particular models.

4.2.2 Mode Shapes

The mode shapes for the first ten natural frequencies of the positive 30° model are also provided for visualization purposes in Figure 4.4. Other examples of model vibration modes can be viewed in the Appendix, but all the models exhibit similar mode shapes due to the similar overall structure of the panel. The first ten modes observed for each model are all flexural vibrations, meaning that the two face sheets bend in the same direction. Dilatational vibrations (Figure 4.5), which occur when the face sheets bend in opposite directions, are not seen until higher frequencies.

1st Mode

2nd Mode

3rd Mode

4th Mode

5th Mode

6th Mode

7th Mode

8th Mode

9th Mode

10th Mode
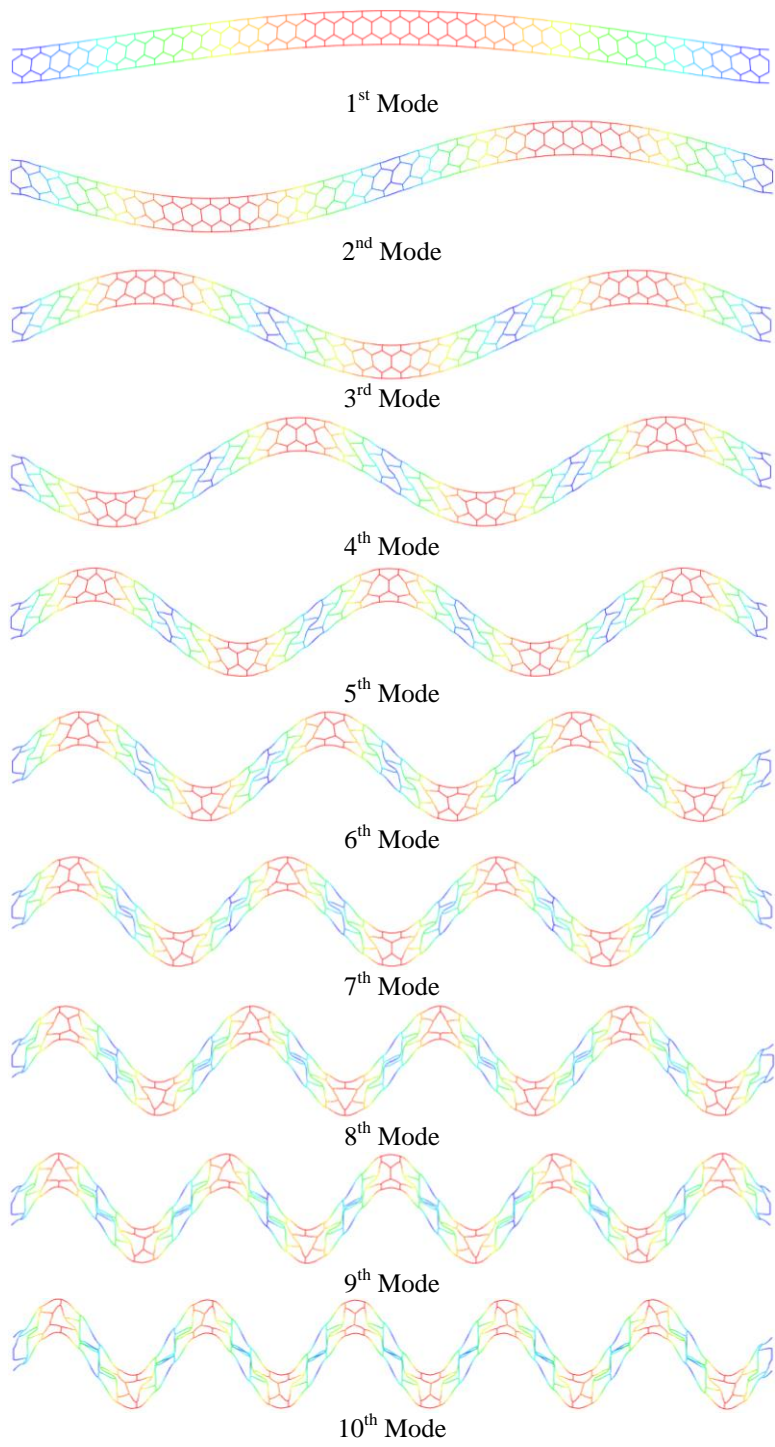
Figure 4.4: Vibration modes for a 30° standard honeycomb core
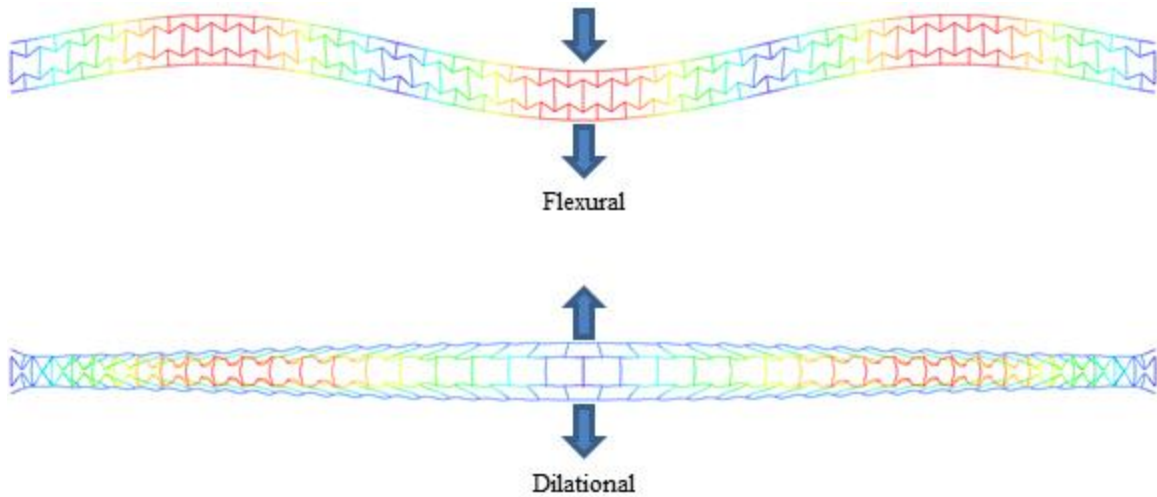
Figure 4.5: Example of flexural vs. dilatational modes of vibration

4.2.3 Trends/Observations

The natural frequency (vibrational mode) of a structure depends on its general mass and stiffness properties. Also, since all of the modes are directly related to the first mode, the location and trend of the natural frequencies can be understood by studying the occurrence of the first natural frequency of each of the models. In addition to describing the behavior of the subsequent vibrational modes, the first natural frequency also describes the extent of the stiffness region in the sound transmission curve, which applies to frequencies before the first natural frequency. Even though the overall stiffness of a complex structure depends on several interrelated parameters, an attempt is made to determine if any single property in particular stands out as being more significant. Scatter plots are created in to visualize the potential effects that each of the effective global stiffness properties, which includes effective shear modulus (G_{12}*) and effective Young's modulus in the x (E_{11}*) and y (E_{22}*) directions, have on the first natural frequency value. The plots are shown in Figure 4.6 through 4.8.
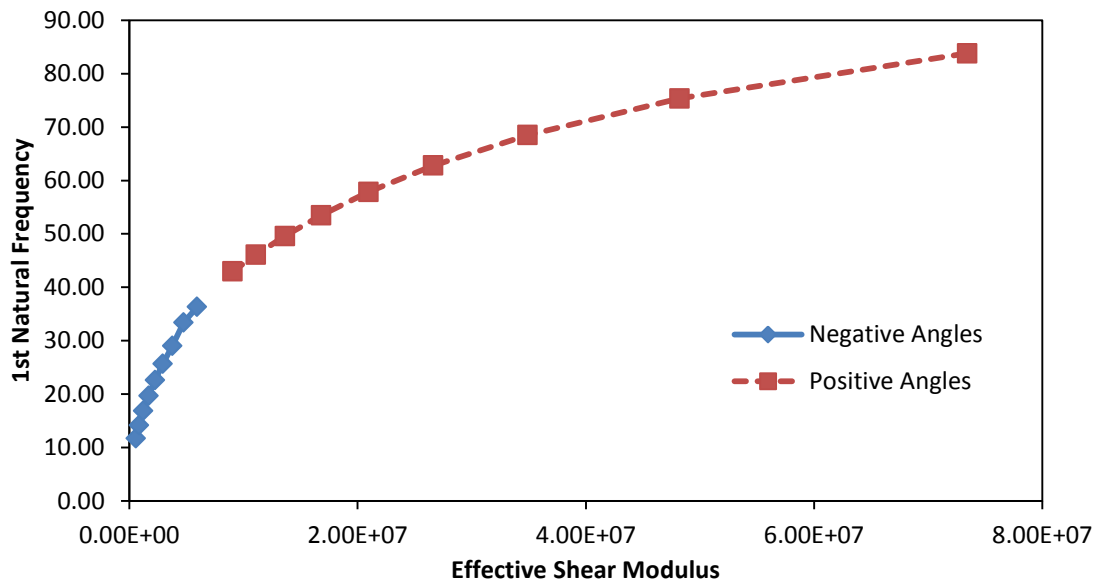
Figure 4.6: First natural frequency compared with effective shear modulus
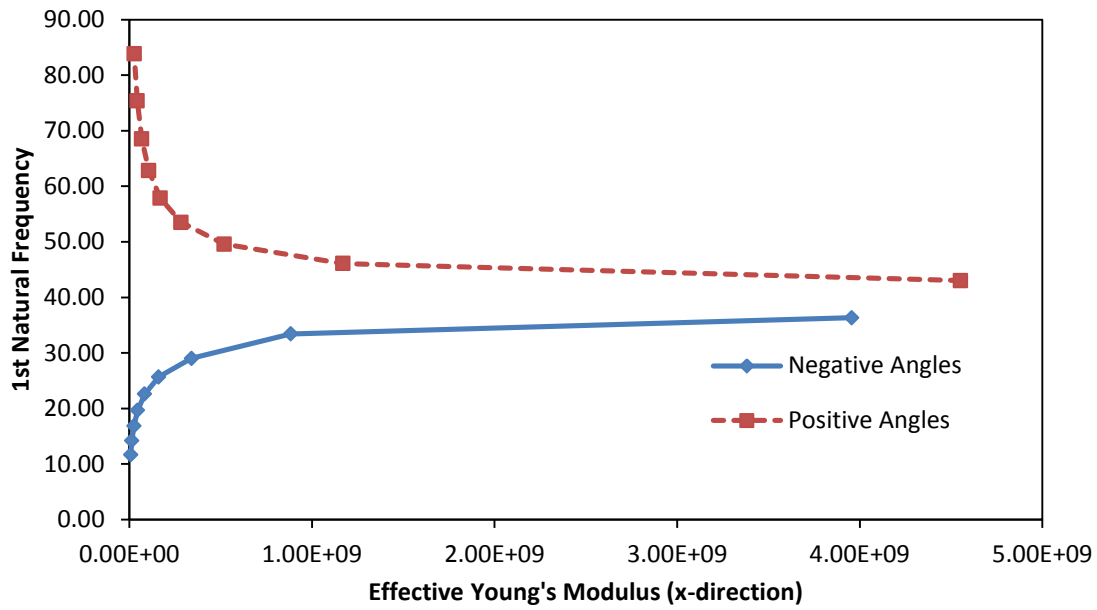
Figure 4.7: First natural frequency compared with effective Young's modulus (x-direction)
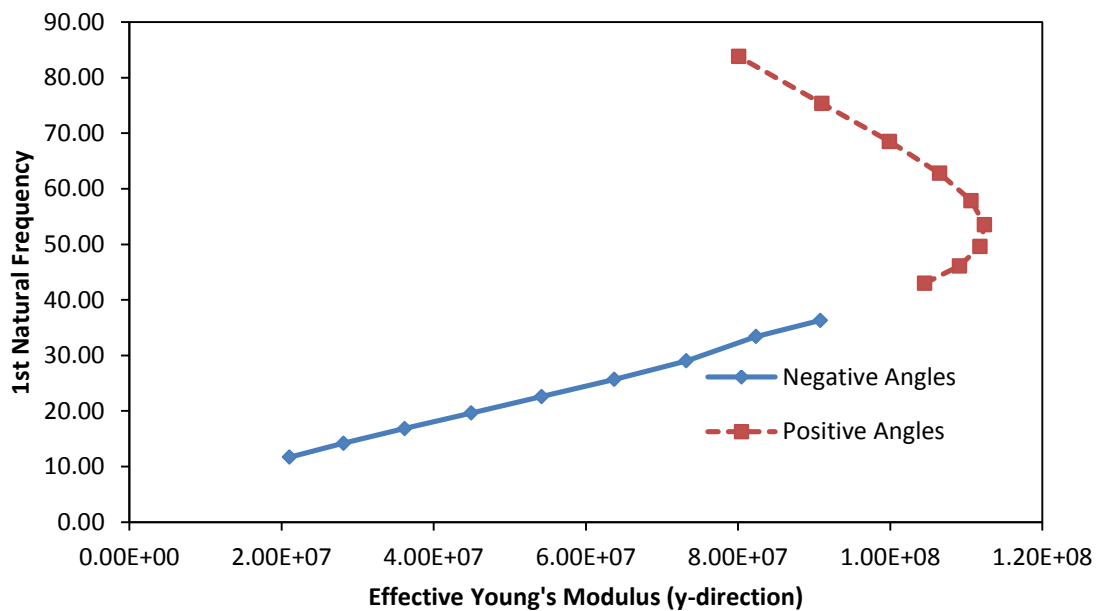
Figure 4.8: First natural frequency compared with Young's modulus (y-direction)

In viewing the results, the shear modulus and Young's modulus in the x-direction appear to show logarithmic relationships with the first natural frequency. For the Young's modulus in the x and y directions, the positive angle models behave differently than the negative angled ones. In fact, for the $E_{11}*$, the negative and positive angled models mirror each other in their behavior. A sensitivity analysis is performed to study the influence that the global effective stiffness properties have on the first natural frequency and determine if any can be eliminated from future evaluations. However, all properties seem to have a significant influence and none can be omitted from consideration. This is a result of all the properties being highly interrelated in their effect on the overall stiffness of the structure. However, the shear modulus does show the most promise for potentially predicting the behavior based off of a single parameter. An attempt is also made to determine the effects that the geometric parameters, or local stiffness properties, have on the response. However, again due to the interrelated nature of the parameters on the global stiffness properties, no generalizations on one single property can be made and this area should be explored further.
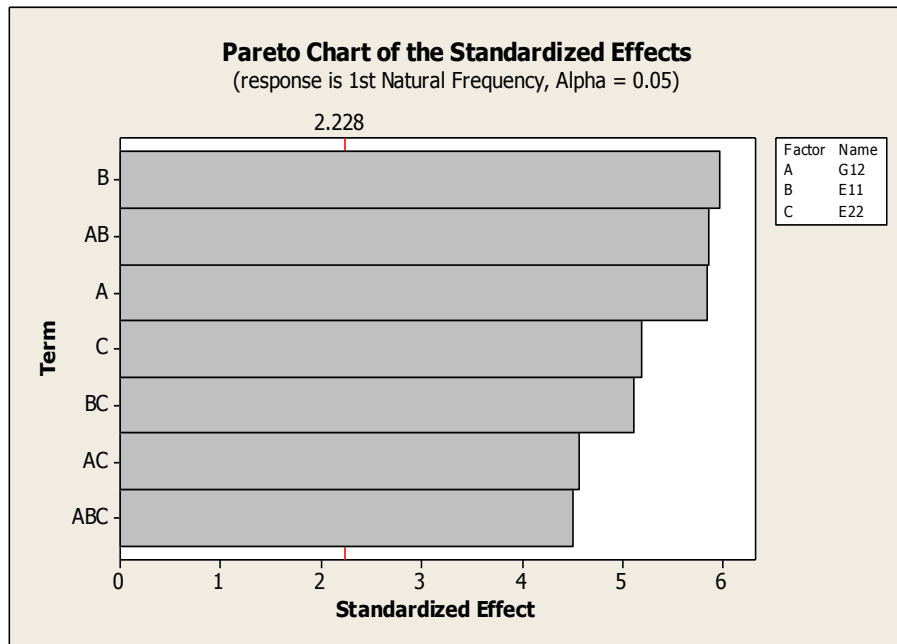
Figure 4.9: Sensitivity analysis of effective stiffness properties

The natural frequencies also should give an indication of where there will be dips in the sound transmission loss. This concept is tested and will be discussed in later sections. Based on the results seen in the natural frequency, it is predicted that the models with greater internal cell angles (and greater shear moduli) should have sound transmission loss dips that are spaced farther apart from each other.

4.2.4   Natural Frequencies for 2 x 80 Models

It is important to point out that, while the equations for effective material properties are generally accurate, there are situations where they are not exact. When the number of cell rows is small, as is the case in these simulations, the results can be changed by the boundary effects of the core structure. The resulting effect is that two different models can have identical calculated effective stiffness properties, but still

exhibit differing responses. To view this effect, the natural frequency is also run on two row sandwich plates for some of the angle models. These models have the exact same effective properties as their single row counterparts, but the unit cell size is scaled down so that more rows can be included. The natural frequency results for the 15° increment double row models are shown in Table 4.5.

Table 4.5: Natural frequencies for selected double row core sandwich plates

Mode #	-45°	-30°	-15°	15°	30°	45°
1	10.3	17.4	25.8	45.5	59.3	81.9
2	20.9	35.0	51.9	91.8	121.2	177.7
3	32.0	53.4	79.9	143.0	191.2	288.6
4	43.9	72.38	108.6	194.6	261.4	403.9
5	56.6	92.1	138.3	247.0	331.9	520.6
6	70.4	112.7	169.1	300.1	402.1	636.7
7	85.4	134.3	200.8	354.3	472.5	752.2
8	101.6	157.0	233.6	409.4	543.1	767.7
9	119.3	180.8	267.4	465.4	614.0	866.8
10	138.3	205.8	302.0	522.4	685.2	980.7

It can be observed that the natural frequencies differ from the frequencies of the single row models with identical effective stiffness properties. This further highlights the fact that, while CMT provides a good reference point for comparing models, it does not completely account for the effect that the connection points of the faces sheets may have on the core properties and some further interpretation is necessary. The trends of the 2 x 80 models are consistent with the 1 x 40 models though. The models with the greater internal cell angles have first natural frequencies that are higher. In addition the models with the higher natural frequencies also have a greater spacing between modes.

4.3   Sound Transmission Loss Results

All of the steady state simulations are run and the STL for each of the panels is calculated. As predicted, the dips in the transmission curve correspond with the natural frequencies. Specifically, they align with the odd mode numbers from the natural frequencies as shown in Figure 4.10. At these frequencies, the structure vibrates at higher rates and thus more acoustic energy is transmitted.
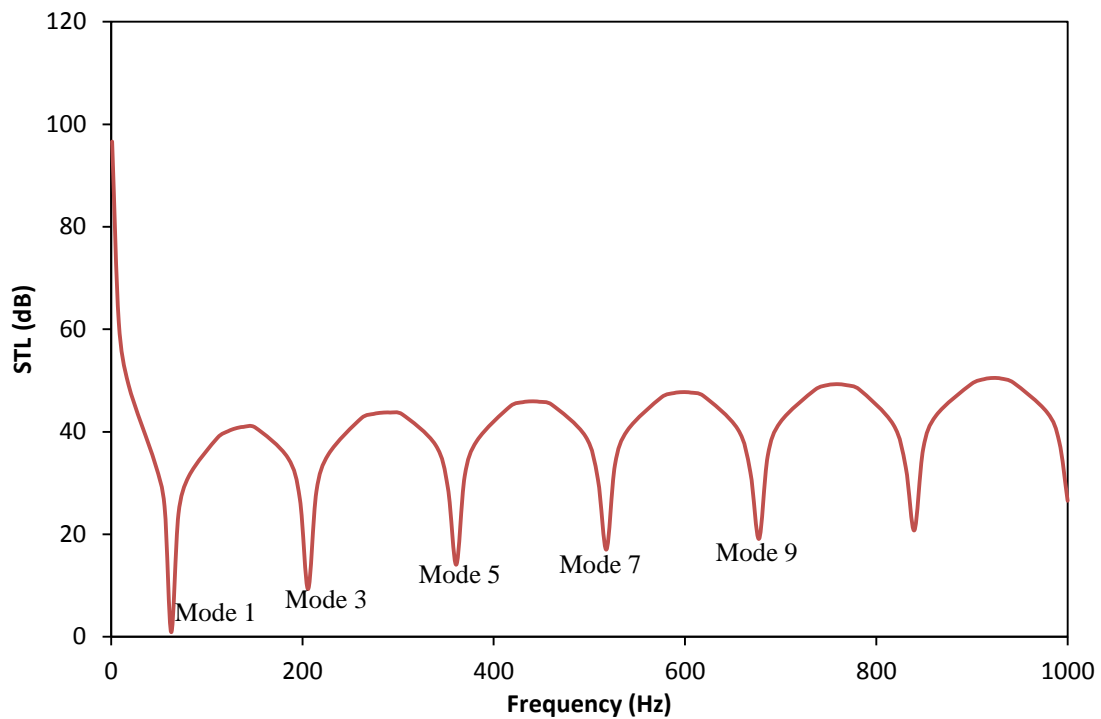
Figure 4.10: Positive 30° panel with vibration mode numbers shown

The results for some, but not all, of the panels are shown below. Some of the results are omitted for clarity and brevity purposes, but the general trends can be seen with the results shown here. Figure 4.11 shows the results for 15° increments of the positive angle cores. The results from the other panels are shown in the Appendix. For

the positive angle models, the behavior of the sound transmission loss follows similarly with the trends of the natural frequencies. The first dip occurs at higher frequencies for the models with greater internal cell angle (more positive), thus shifting up the resonance controlled region and causing greater spacing between dips as predicted.
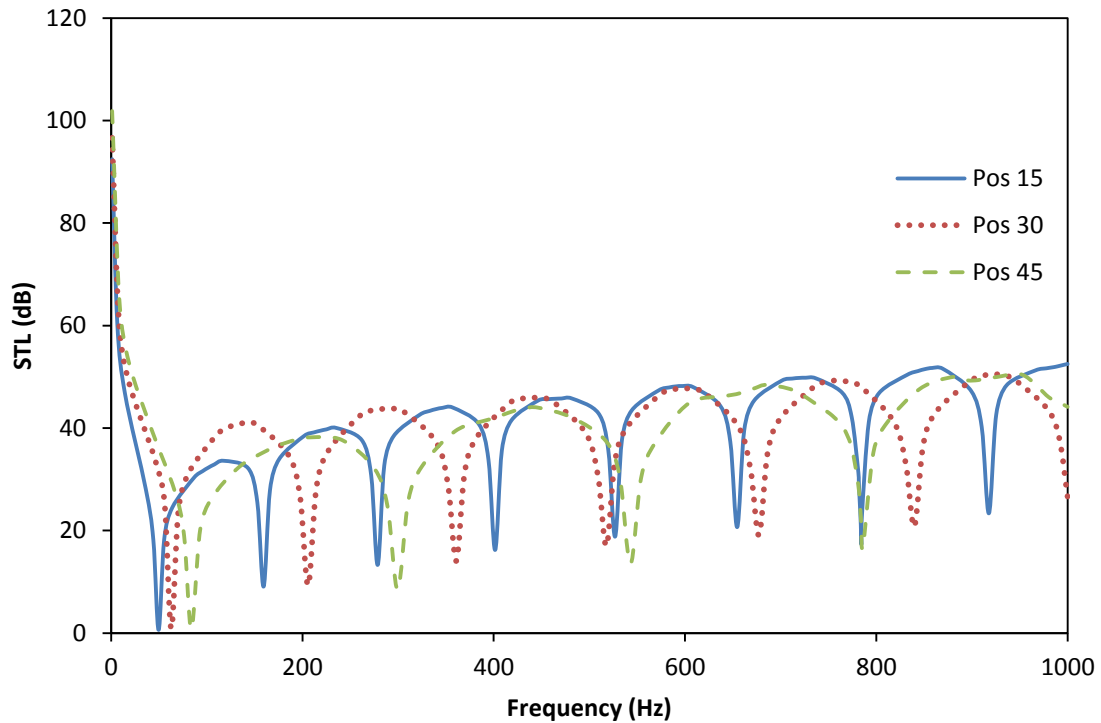
Figure 4.11: Sound transmission loss of panels with positive angle cores

The results of the negative angle cores (Figure 4.12) exhibit the same behavior. As the angle increases (becomes less negative), the dips in the STL become fewer and less frequent. The -45° exhibits the lowest first frequency dip and consequently the smallest dip spacing (more occurrences in the specified range) and smallest stiffness controlled region of any of the models tested. For the negative angles, it can also be observed that some abnormal dips start occurring at the higher frequencies. These

correspond to the anti-symmetric vibration modes, which start occurring at earlier frequencies for models with smaller internal cell angles. This is especially obvious for the -45° model starting at 500 Hz.
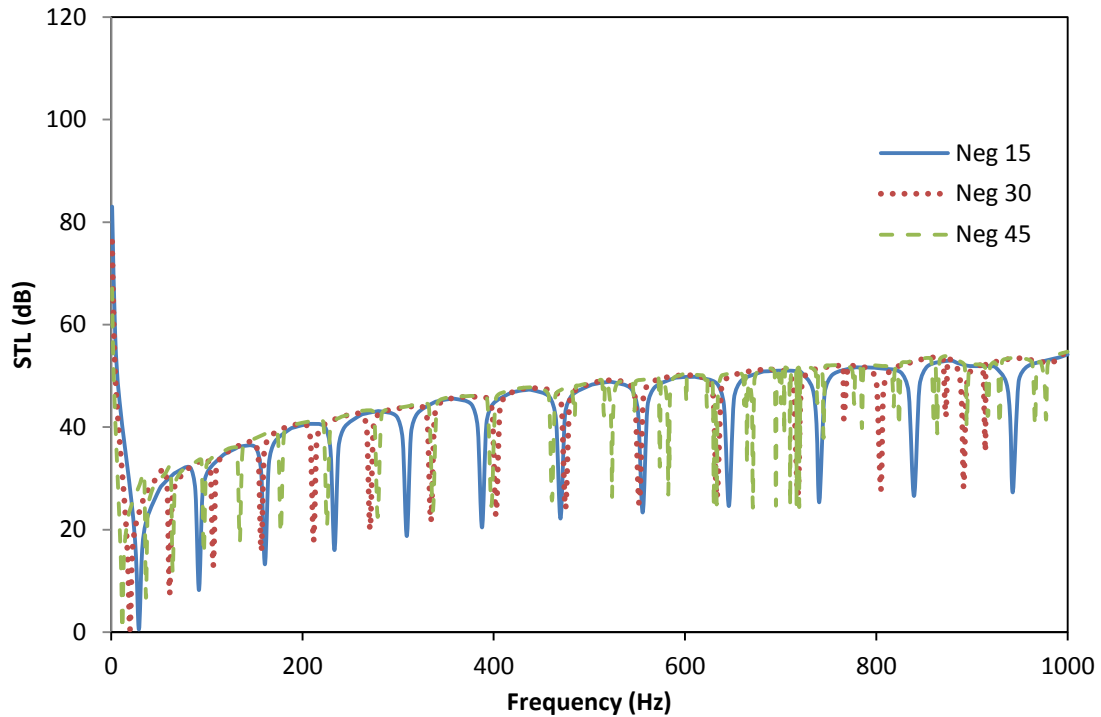
Figure 4.12: Sound transmission loss of panels with negative angle cores

As predicted, the mass does appear to be the governing factor in determining the magnitude of the sound transmission loss. It can be observed in both the regular honeycombs and the auxetics that, while the dips occur in varying locations, the magnitude of the curve remains relatively constant between all the models. This is due to the fact that the mass is kept constant and this concept will be further verified in later sections of this report that describe the simulations with varying mass.

4.3.1 Comparison/Discussion

As previously discussed, the models with increased cellular angles (and higher shear modulus) have both higher first natural frequencies and larger spacing between dips. To further highlight this and give a general idea of the range of dip spacing, plots quantifying the spacing are shown in Figure 4.13. For each of the same mass models, the spacing between the first and second sound transmission loss dips is measured. The spacing ranges from 24.7 Hz in the -45° model to 215.7 Hz in the +45° model. If the designer wants to isolate a particular frequency and have a large tolerance around that frequency, then the models with larger spacing would be more desirable. This large spacing range even with models of the same mass begins to show the flexibility that these honeycomb panels offer. The spacing between the other dips would be approximately the same as the first spacing.
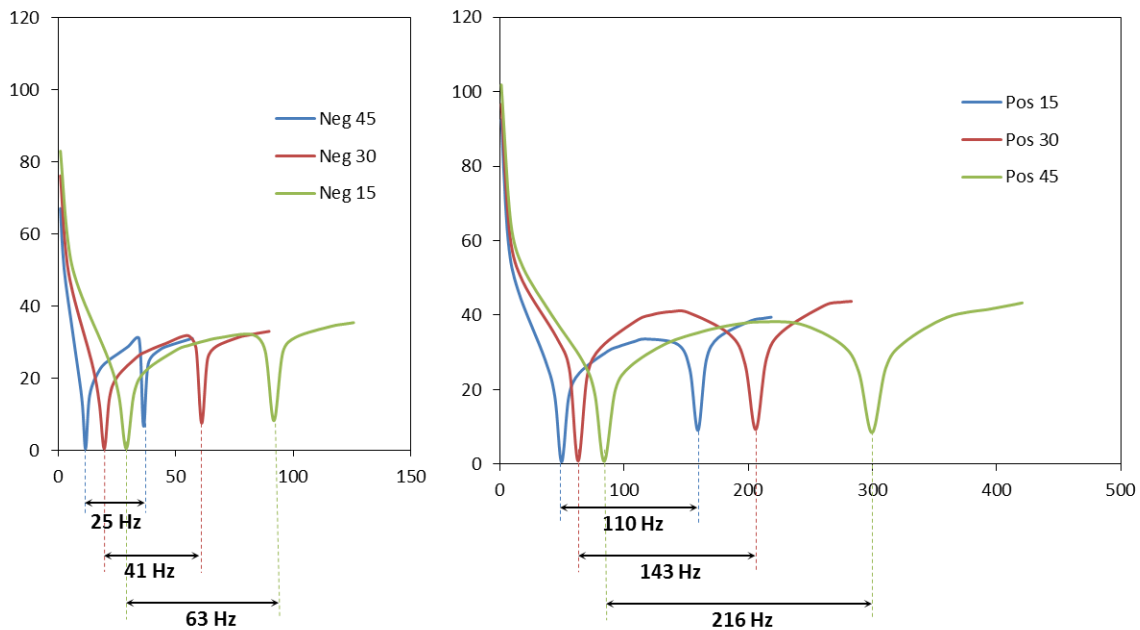
Figure 4.13: Varying spacing between dips in the sound transmission loss curve

For the 2 x 80 model steady-state simulations, not all of the results are presented here in this report (see Appendix for all results), but some comparisons are made between their 1 x 40 counterparts. Figure 4.14 shows the results from the +30° single row model and the +30° double row model. These two panels are identical in all of the effective stiffness properties studied in this work. However, while having similar sound transmission loss curves, they do deviate from each other after the first dip. The general shape of the dips is the same, but the spacing is different being 143.1 Hz for the 1 x 40 model and 131.9 Hz for the 2 x 80 model. A similar observation can be made by looking at the results comparison for the 1 x 40 and 2 x 80 models in the -30° configuration.
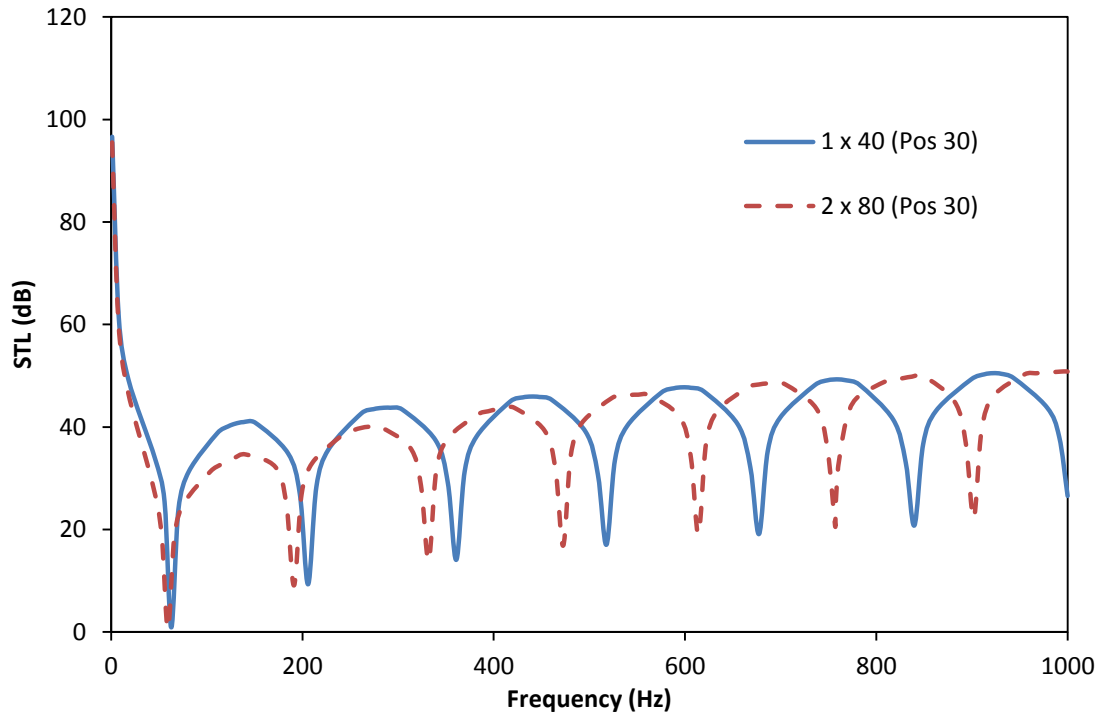
Figure 4.14: Comparison for 1 x 40 and 2 x 80 models in the +30° configuration
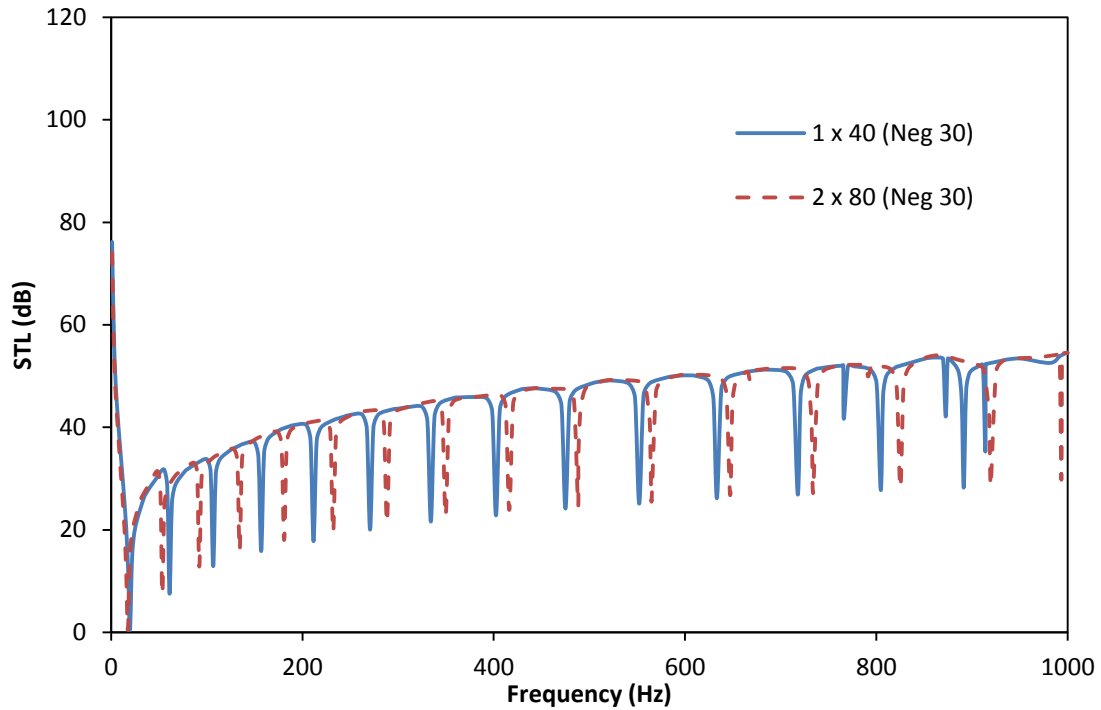
Figure 4.15: Comparison for the 1 x 40 and 2 x 80 models in the -30° configuration

Again, as pointed out in the natural frequency sections, the acoustic behavior cannot fully be defined by the effective stiffness property equations. This is due to the effect that the face sheet connections at the boundary have on the behavior. However, it is observed that these effectively identical structures are similar, while not exact, in their behavior.

Another observation made from the sound transmission loss is the shape of the dips in the sound transmission loss curve. The negative angle models, while having more dips (high modal density), appear to have dips that are narrower. This could reduce the likelihood of hitting one of these dip frequencies even though they are more frequent meaning overall better performance across all frequencies, which may be desirable to the

designer. In order to take into consideration both the number of dips and the width of the dips, the area under the curve is calculated as a metric to compare all of the panels. Those results are shown in Table 4.6 and split up as stiffness region, resonance region, and total values.

Table 4.6: Values for area under the sound transmission loss curve for the constant mass panels

Model	Area Under Curve (dB·Hz)		
	Stiffness Region	Resonance Region	Total
-45°	346.7	44081.8	44428.5
-40°	441.6	44841.6	45283.0
-35°	543.4	44526.5	45070.0
-30°	646.3	43574.1	44220.4
-25°	768.9	44092.9	44862.0
-20°	892.7	43606.3	44499.0
-15°	1019.1	42331.5	43350.5
-10°	1196.6	42738.5	43935.0
-5°	1337.1	41602.1	42939.0
5°	1626.5	40401.8	42028.0
10°	1762.3	39342.1	41104.0
15°	1891.2	39044.3	40935.5
20°	2090.1	36859.2	38949.0
25°	2286.3	35355.8	37642.0
30°	2649.4	37642.9	40292.3
35°	2774.8	35874.7	38650.0
40°	3095.6	37227.9	40324.0
45°	3434.3	36218.3	39652.6

It can be seen in the results that, while the positive angle models perform better in the stiffness region and have fewer sound transmission loss dips in the resonance region, their total values for area under the curve are consistently less than the negative angle

models. This tradeoff should be further explored in future works. However, currently, it is up to the designer to determine which property is more desirable.

4.3.2 Acoustic Field Pressure Distributions

In addition to studying the amount of transmitted acoustic energy, the transmitted pressure distribution in the acoustic field is also studied graphically. The direction and pattern of the transmitted pressure is of particular interest. Since the pressure levels vary several magnitudes between models, a logarithmic scaled value is needed to compare the pressure distributions similar to the sound transmission calculation in previous sections. The value used here is the sound pressure level (SPL), which is calculated by Eq. [4.1]. The SPL describes an effective sound pressure relative to a reference value and the units are in decibels (dB). The sound pressure level is typically the value used to describe the magnitude level of a sound.

$$SPL = 20\log_{10}\left(\frac{p}{p_{ref}}\right) \qquad \textbf{[4.1]}$$

In the equation, p_{ref} is the standard reference pressure, which is 20 µPa for air [41]. This value is generally considered to be the minimum threshold magnitude for human hearing. The value p refers to the acoustic pressure in Pascals. For reference purposes, the incident sound load is 1 Pa amplitude, which corresponds to an SPL value of 94 dB.

The acoustic field steady state SPL distributions for select models are calculated. The pressure values at all of the nodes in the air domain for select frequencies are

exported and Matlab 7.10 (R2010a) is used to calculate and plot the sound pressure level. The SPL distributions for the positive 30° model and the negative 30° models at frequencies of approximately 200 Hz, 500 Hz, and 900 Hz are shown below in Figure 4.16 and Figure 4.17 respectively. The frequencies in the figure are selected because they corresponded to dips in the sound transmission loss curve to illustrate the higher levels of sound transmission.

~200 Hz

~500 Hz

~900 Hz
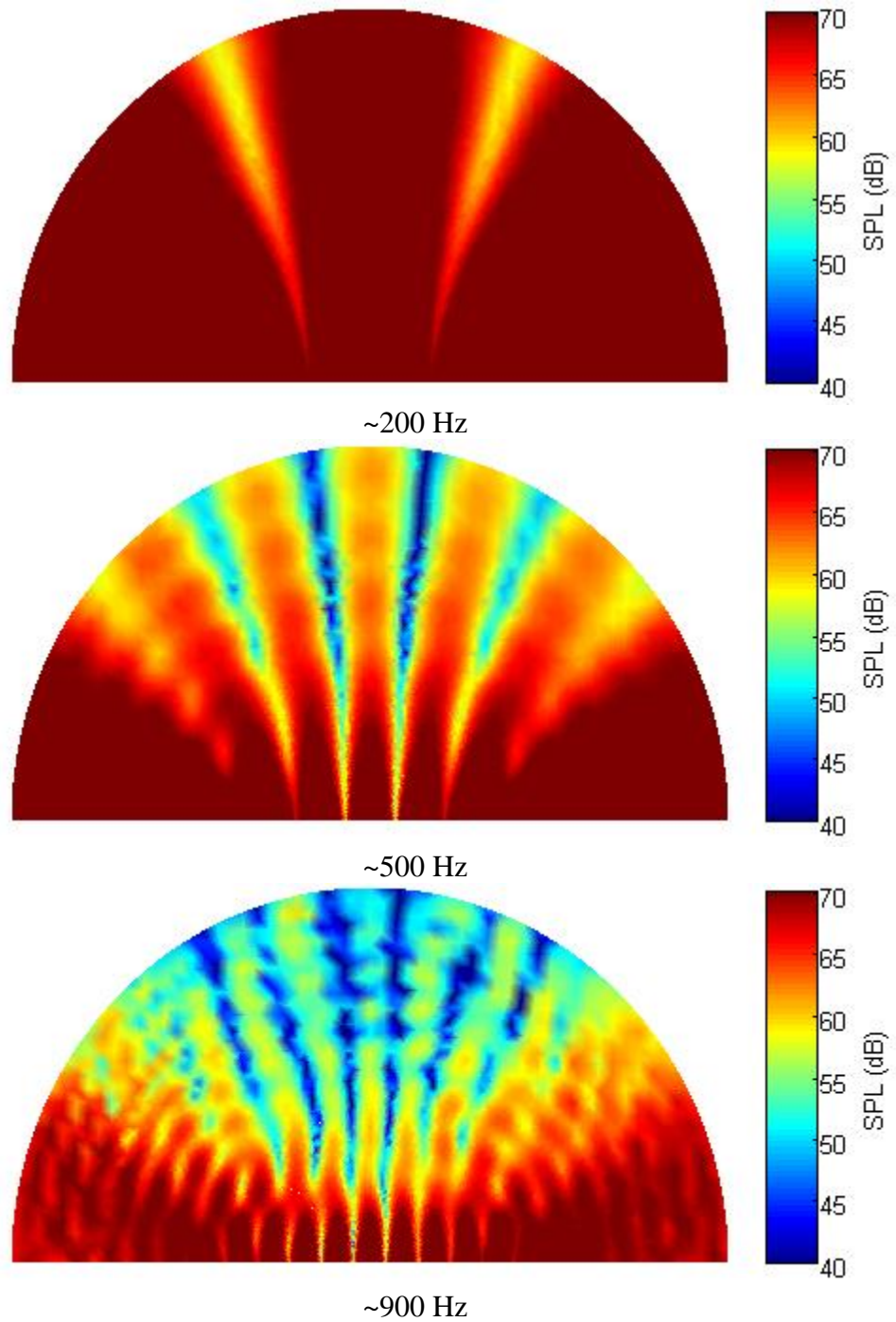
Figure 4.16: Pressure distribution of positive 30° panel at varying frequencies
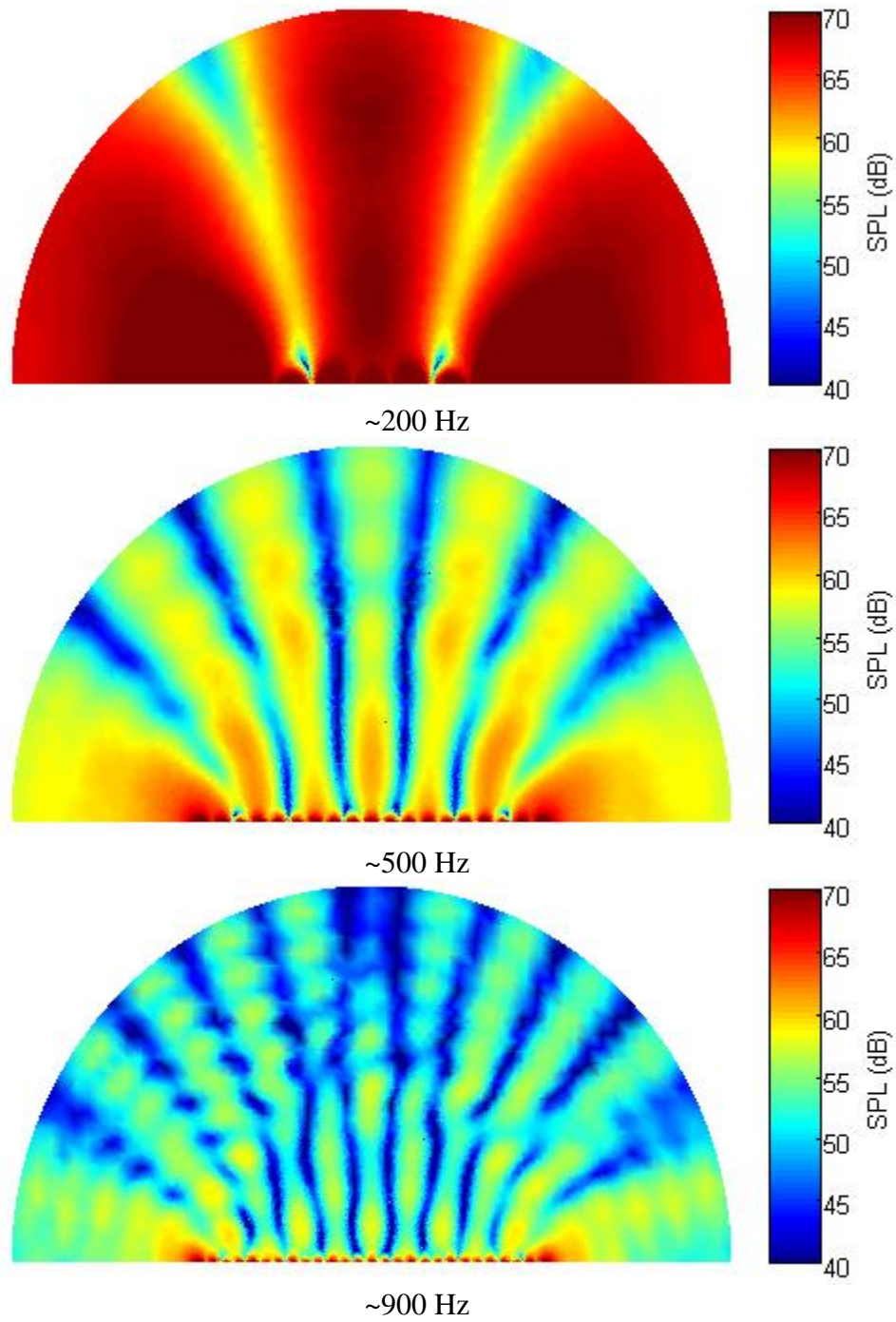
Figure 4.17: Pressure distribution of negative 30° panel at varying frequencies

One trend observed between both of the models is that the SPL attenuates as frequency increases. For both models, at the low frequency range (~100 Hz), high sound pressure levels of greater than 70 dB can be seen up to the extent of the air domain. At the higher frequency range (~900 Hz) for both models, the SPL remains below 50 dB at the far end of the air domain. At this frequency, the high SPL regions are only present in close proximity to the transmitted face of the honeycomb panel, with the positive 30° panel having a larger high SPL region. Another observation made is that the negative 30° model attenuates the sound pressure level more than the positive 30° model. This can be seen at all three frequencies shown in the figure. For the negative 30° model, the distribution patterns are similar to the positive 30° model, but at lower magnitude levels. Both models at higher frequencies show a tendency to direct larger magnitudes of acoustic pressure to the sides than straight back to the end of the air domain.

Sound pressure level distributions are also shown for some non-dip frequencies as well in Figure 4.18 to give general view of what the magnitudes look like. These frequencies exhibit similar frequencies to the higher magnitude frequencies in that the sound pressure level attenuates at higher frequencies and the negative 30° model attenuates more than the positive 30° model.

Positive 30°   Negative 30°

~300 Hz

~600 Hz

~920 Hz
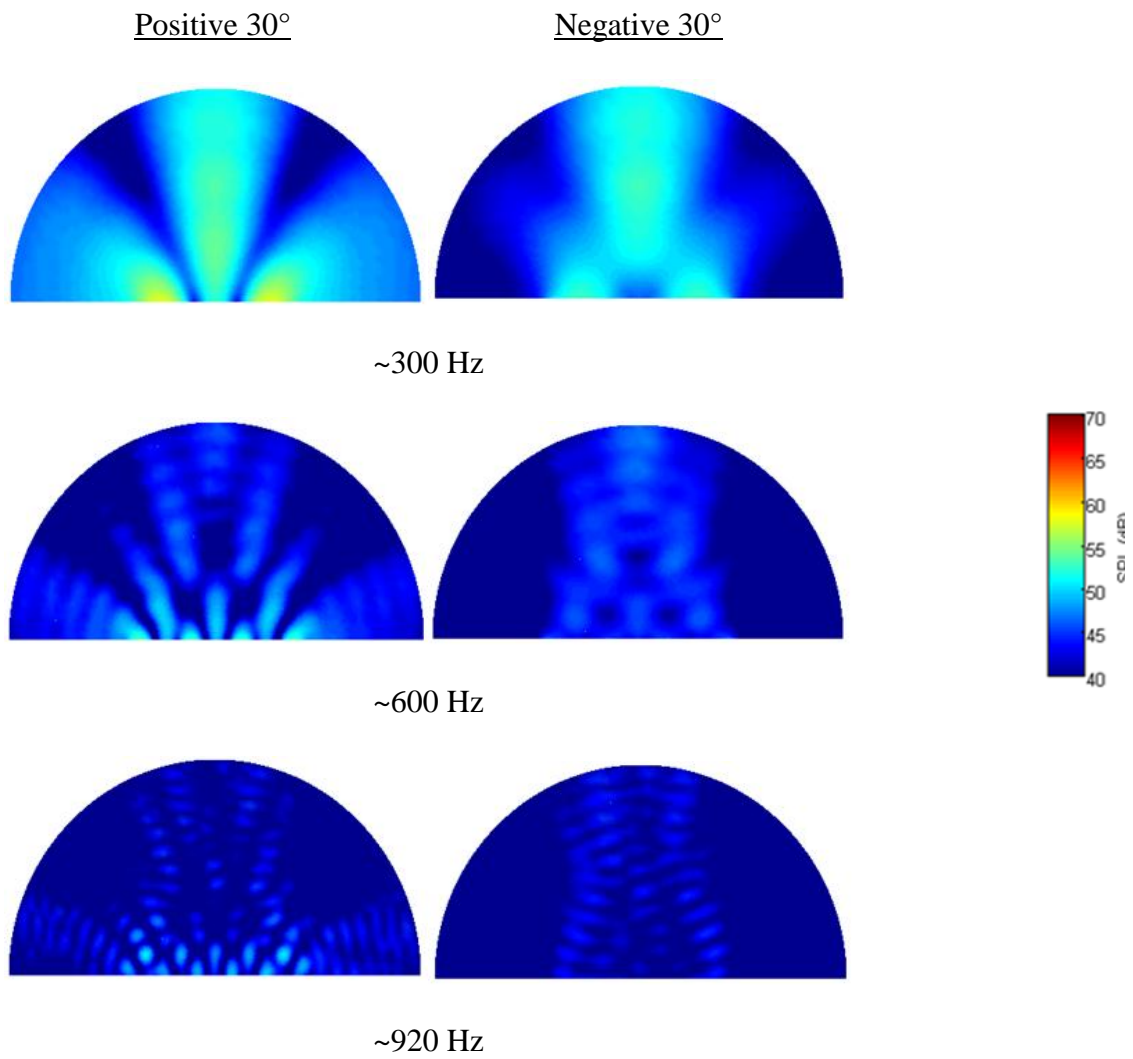
Figure 4.18: Transmitted sound pressure level distributions non-dip regions of STL curve (constant mass panels)

CHAPTER 5: SOUND TRANSMISSION LOSS FOR CONSTANT SHEAR
MODULUS AND STRUCTURE SIZE PANELS WITH VARYING CORE
GEOMETRY
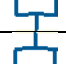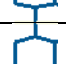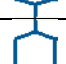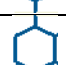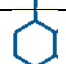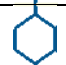
The second scenario studied includes panels of constant shear modulus and size.

This is not to say that shear modulus is the only significant property because all of the

stiffness properties play a role in the response. However, only one effective property can

be kept constant at a time. Further, shear modulus is held constant because, as in the

previous simulations, it appears that shear modulus has a large effect on the trend of the

natural frequencies and spacing of the sound transmission loss dips. In addition, it has

been identified by previous researchers that the shear of the panel has one of the largest

effects on the sound transmission loss [35]. The geometries of the core, including the

thickness, in this study are allowed to vary resulting in varying masses and elastic

moduli.

5.1   Model Geometries

As was the case with the constant mass panels, the overall structure dimensions

are kept constant. Also, the models again vary in 5° increments and have the same l and

h specifications in order to maintain the structure dimensions. The thickness is adjusted

to keep a constant shear modulus of 2.00 MPa. For this study, only the 1 x 40 models are

analyzed. The parameters and effective properties of each model are summarized in

Table 5.1. Figures 5.1, 5.2, and 5.3 are shown to illustrate how each of the geometric

parameters changes in relation to changes in internal cell angle under the constant unit

cell size constraints. The thickness figure illustrates that the thickness decreases with

70

increasing cell in order to maintain the constant shear modulus of the structure. This means that negative angle models allow for thicker cell walls if constant shear modulus is required. The h and l parameters are identical to the constant mass study as these parameters depend only on the unit cell size requirements, which are not changed in this study.

Table 5.1: Geometric and effective properties of 1 x 40 constant shear modulus honeycomb cores

Cell Angle		Unit Cells	l (mm)	h (mm)	t (mm)	$G_{12}*$ (MPa)	$\rho*$ (kg/m^3)	$E_{11}*$ (MPa)	$E_{22}*$ (MPa)
-45°		1 x 40	35.36	68.30	2.35	2.00	408.1	24.2	72.6
-40°		1 x 40	32.64	64.28	2.21	2.00	357.5	30.9	65.3
-35°		1 x 40	30.52	60.81	2.09	2.00	317.8	40.1	59.0
-30°		1 x 40	28.87	57.73	1.99	2.00	285.9	53.3	53.3
-25°		1 x 40	27.58	54.97	1.89	2.00	259.6	73.9	48.2
-20°		1 x 40	26.60	52.40	1.80	2.00	237.6	109	43.4
-15°		1 x 40	25.88	50.00	1.72	2.00	218.7	181	38.9
-10°		1 x 40	25.39	47.71	1.65	2.00	202.3	372	34.7
-5°		1 x 40	25.10	45.49	1.57	2.00	187.9	1330	30.6
5°		1 x 40	25.10	41.11	1.43	2.00	163.3	1010	23.1
10°		1 x 40	25.39	38.89	1.36	2.00	152.5	211	19.7
15°		1 x 40	25.88	36.60	1.29	2.00	142.4	76.2	16.4
20°		1 x 40	26.60	34.20	1.22	2.00	132.8	33.6	13.4
25°		1 x 40	27.58	31.64	1.14	2.00	123.4	16.2	10.6
30°		1 x 40	28.87	28.87	1.05	2.00	113.9	8.00	8.00
35°		1 x 40	30.52	25.80	0.96	2.00	104.1	3.90	5.73
40°		1 x 40	32.64	22.32	0.86	2.00	93.46	1.79	3.78
45°		1 x 40	35.36	18.30	0.73	2.00	81.24	0.73	2.18
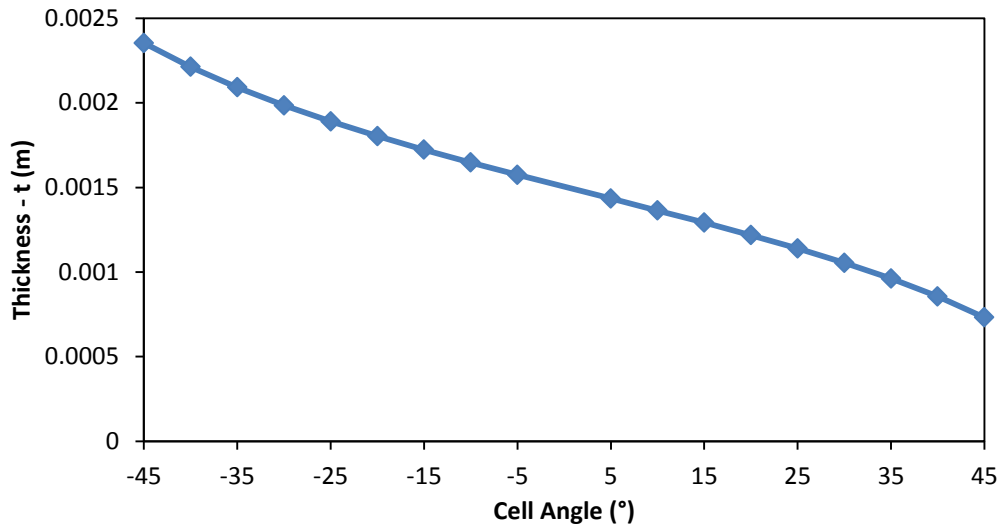
Figure 5.1: Cell wall thickness at varying cell angles for constant shear modulus
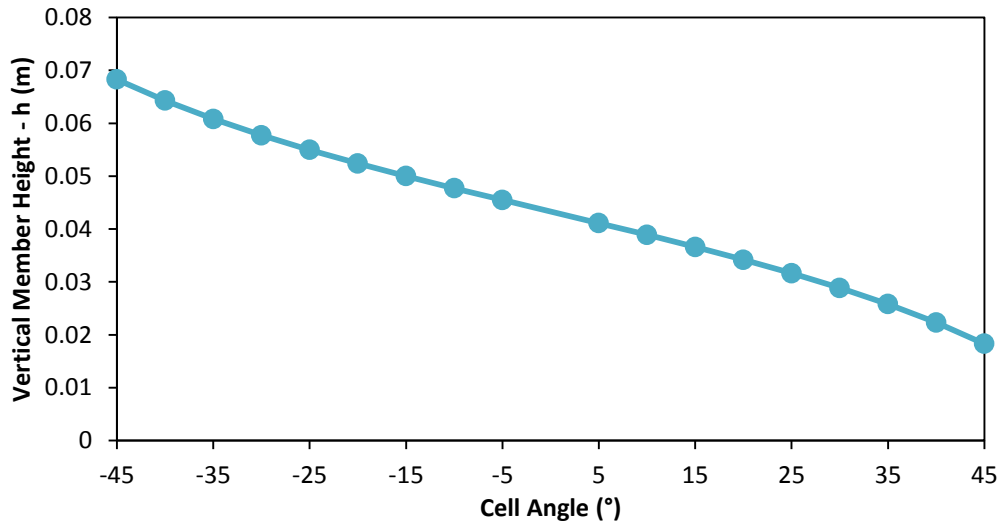
Figure 5.2: Vertical member height at varying cell angles for constant shear modulus
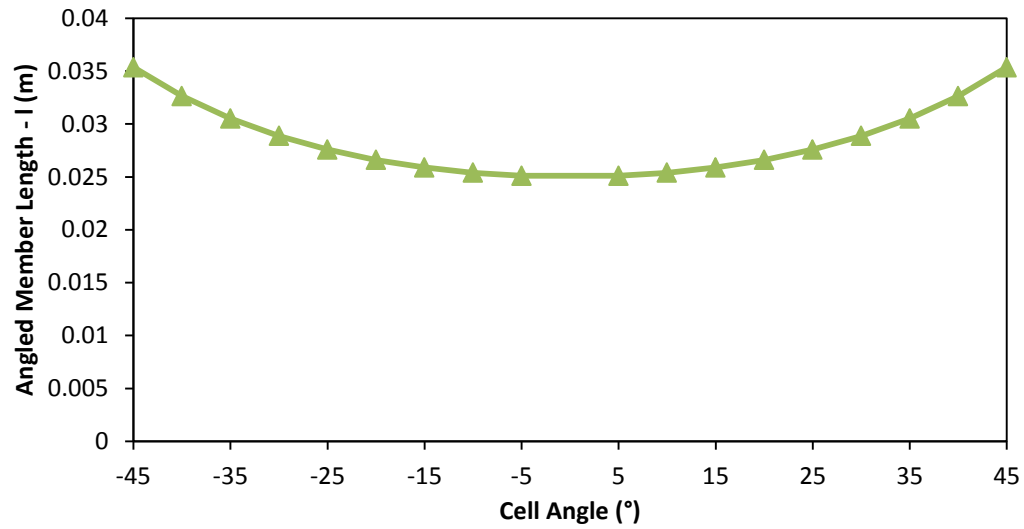
Figure 5.3: Angled member length at varying cell angles for constant shear modulus

5.2   Natural Frequencies

The natural frequencies are extracted for all models and recorded. All value frequencies are recorded, but again only the first ten are used here for analysis for the same reasons specified in the constant mass section. The results of the positive angle panels are shown in Table 5.2 and those of the negative angle panels are shown in Table 5.3.

Table 5.2: Natural frequencies of positive angle constant shear modulus core sandwich panels
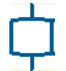
Mode #	5°	10°	15°	20°	25°	30°	35°	40°	45°
1	27.2	26.6	26.4	26.4	26.6	26.9	27.2	27.6	28.2
2	55.4	54.2	53.5	53.3	53.5	54.0	54.6	55.4	56.4
3	85.6	83.9	82.5	81.9	81.9	82.4	83.2	84.3	85.8
4	116.7	114.6	112.6	111.3	111.0	111.3	112.1	113.4	115.3
5	148.4	146.4	143.9	142.0	141.1	141.0	141.8	143.2	145.3
6	180.7	179.0	176.3	173.8	172.3	171.8	172.3	173.7	175.9
7	213.5	212.4	209.7	206.8	204.7	203.7	203.8	205.0	207.3
8	247.1	246.6	244.1	240.9	238.3	236.7	236.4	237.3	239.5
9	281.6	281.7	279.5	276.3	273.2	271.0	270.2	270.8	272.7
10	317.0	317.7	315.9	312.7	309.4	306.7	305.3	305.3	306.9

Table 5.3: Natural frequencies of negative angle (auxetic) constant shear modulus core sandwich panels

Mode #	-45°	-40°	-35°	-30°	-25°	-20°	-15°	-10°	-5°
1	18.2	19.2	20.1	20.9	21.7	22.4	23.4	24.4	26.0
2	36.6	38.6	40.4	42.1	43.9	45.6	47.6	50.0	53.0
3	56.1	59.2	62.1	64.8	67.6	70.5	73.9	77.8	82.3
4	76.1	80.4	84.4	88.4	92.4	96.6	101.5	106.8	112.4
5	96.8	102.5	107.8	113.1	118.5	124.0	130.2	136.7	143.2
6	118.5	125.5	132.3	138.9	145.6	152.5	159.9	167.4	174.4
7	141.1	149.6	157.8	165.8	173.9	182.0	190.5	198.8	206.3
8	164.7	174.8	184.4	193.9	203.2	212.5	221.9	230.9	238.8
9	189.4	201.1	212.2	223.0	233.5	243.9	254.1	263.8	272.2
10	215.1	228.4	241.0	253.1	264.9	276.3	287.3	297.6	306.5

Between all of the models, the range of the first natural frequency values is small compared to the constant mass panels. The lowest natural frequency is observed for the -45° model at 18.2 Hz and the highest natural frequency is observed for the +45° model at 28.2 Hz, a range of only 10 Hz. There is an even smaller range for just the positive angle modes varying only 1.6 Hz between the model with the lowest first natural frequency

(15°) and the model with the highest first natural frequency (45°). This holds for the subsequent natural frequencies as well in that there is little variation between the models. Even at the tenth mode, the models only differ by 12.4 Hz at most. The negative angle models vary more, but are still similar at the first natural frequency varying at most by 7.8 Hz. They begin to separate more as the mode number increases.

The mode shapes are similar to the first ten constant mass panel mode shapes and do not need to be shown again. Refer to the natural frequency extraction in Chapter 4 if necessary.

5.3   Sound Transmission Loss Results

Steady state analyses are then performed for the constant shear modulus panels using the natural frequencies as input points. The same previously stated parameters are used including six to seven points between each natural frequency and a bias parameter of two towards the natural frequency points. As was the case with the constant mass panels, the odd number nodes align with the dips in the sound transmission loss curve. This excludes the dilatational modes at the later frequencies, which begin occurring at earliest around 700-800 Hz for most of the models. For clarity, only the results for the panels in 15° increments are shown in Figure 5.4 for the positive angle models and Figure 5.5 for the negative angle models. The results for all of the other panels can be found in the Appendix.
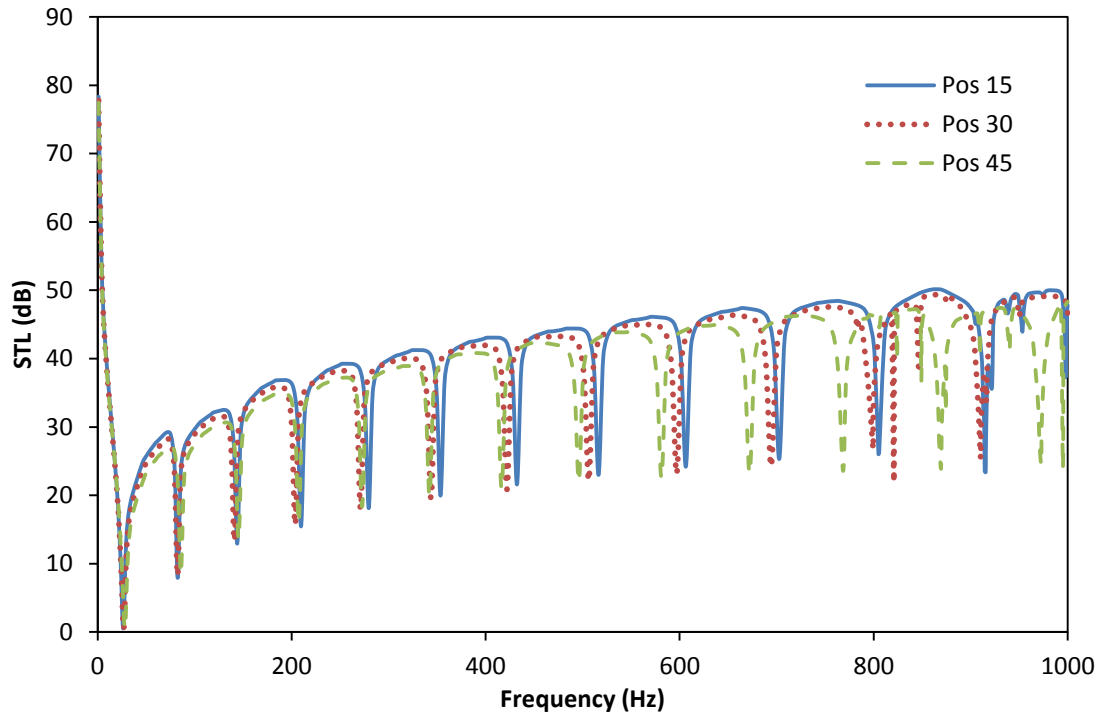
Figure 5.4: Sound transmission loss for positive angle constant shear modulus panels

It can be observed with the positive angle panels that, like the natural frequencies, the first dip aligns identically between the models resulting in a stiffness region that is also identical. The dips in the STL curve continue to be similar for approximately the first five resonant frequencies. After that, they begin to deviate from each other. There are also noticeable differences in the magnitude of the curve that are not present in the constant mass study. For the positive angle models, the lower angle models have higher STL magnitudes due to the fact that the lower angle models have more mass. This coincides with what was previously predicted by the mass law in that increased mass

should result in higher magnitudes of sound transmission loss. The difference is subtle for the positive angle models, but is more apparent in the negative angle models.
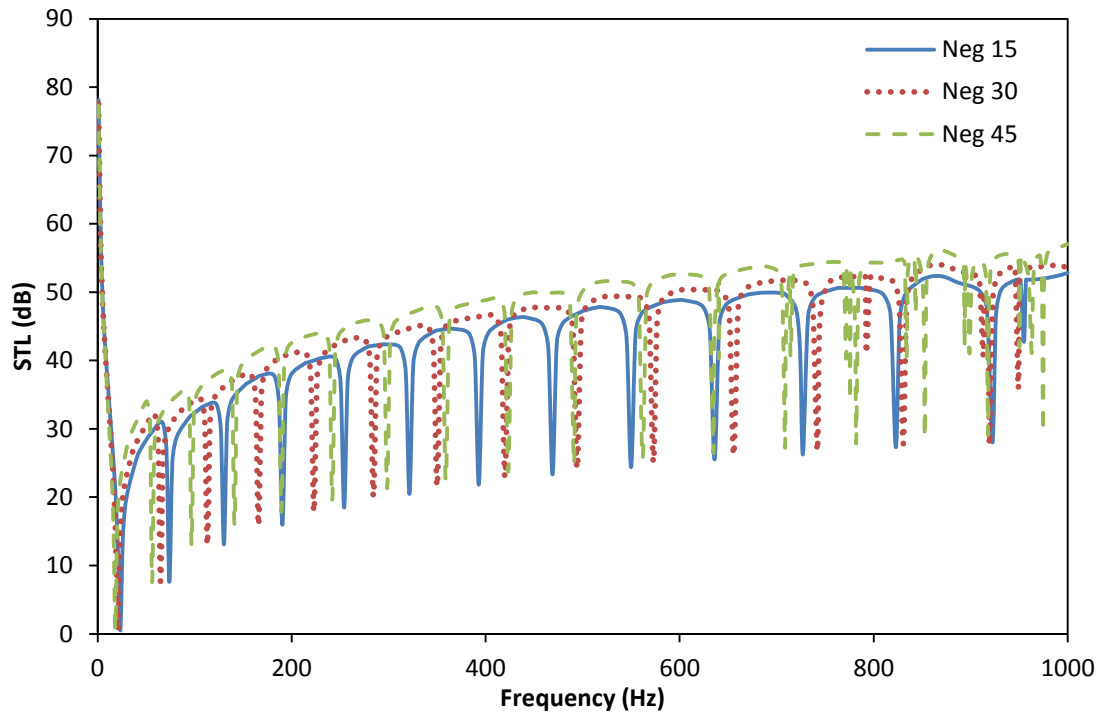
Figure 5.5: Sound transmission loss for negative angle constant shear modulus panels

The negative angle panels exhibit the same behavior with the first sound transmission loss dip and stiffness controlled region. Each of the panels aligns closely in this aspect. However, after the first sound transmission loss dip, the subsequent dips in the curve do not align as closely as the positive angle models. The difference in magnitude between the curves of the models is also more apparent with these models. The lower angle (more negative) models exhibit noticeably larger magnitudes due to their higher overall masses. The larger difference in magnitude is due to the fact that there are

greater mass differences between the panels than the positive angle models. Similar to the constant mass panels, the dilatational vibration dips appear at earlier frequencies with the negative angle model, specifically with the lower angle models. The first dilatational mode is visible in the -45° model at approximately the 700 Hz model.

5.4   Comparison/Discussion

Since there are noticeable changes in the magnitude of the sound transmission loss in response to the changing mass, this relationship is further illustrated and quantified. For each of the models, a logarithmic trend line is fit through the top points along the transmission loss curve, excluding the dips in the curve. This logarithmic curve illustrates the magnitude of the curve and represents the approximate maximum potential sound transmission loss at each frequency. The curve fit process is shown in Figure 5.6.
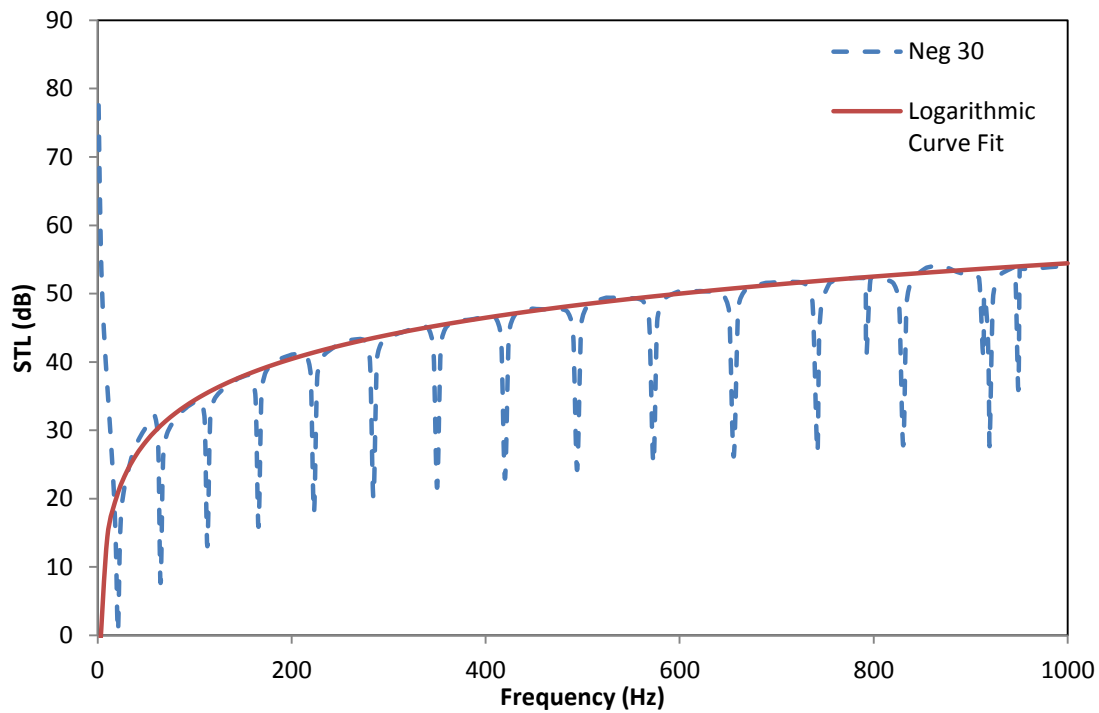
Figure 5.6: Example of logarithmic curve fit for the magnitude of -30° panel results

This curve fit is performed on all of the models and the results for the 15° increments of both the positive and negative models are shown below in Figure 5.7. The masses of each panel are also shown in the plot for reference. It can further be seen that sound transmission loss magnitude increases with increasing mass. In the plot, the magnitude increases with each model starting with the positive 45° model (14.0 kg) up to the negative 45° model (70.7 kg).
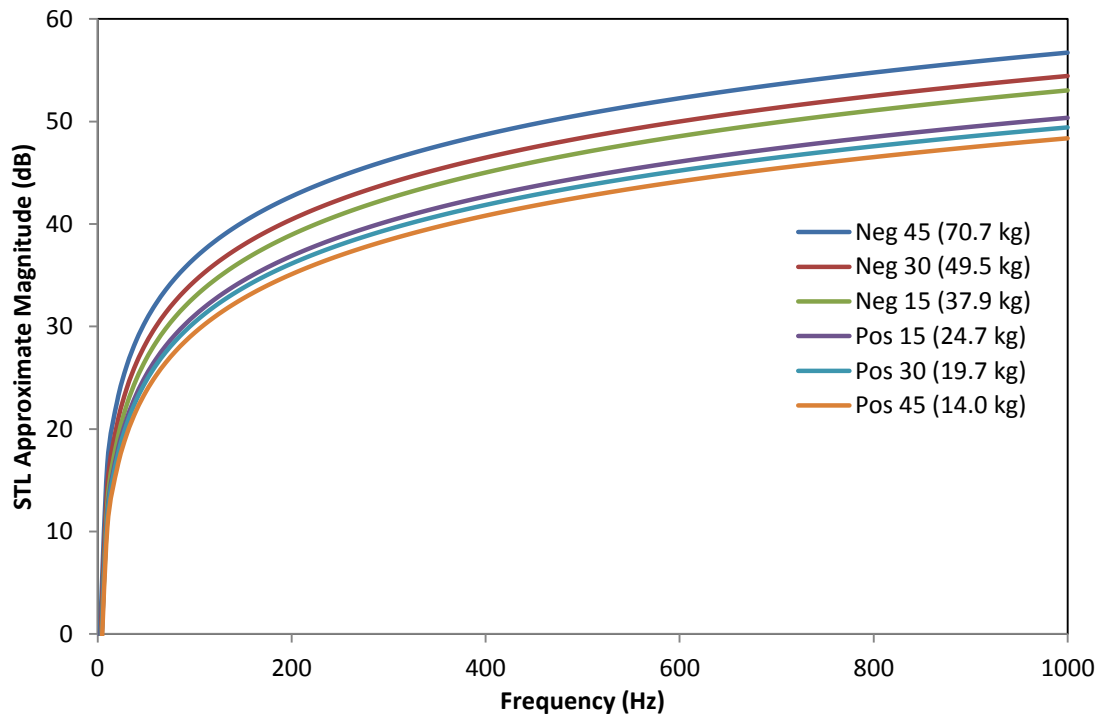
Figure 5.7: Logarithmic approximate STL magnitudes for -45°, -30°, -15°, 15°, 30°, and 30° panels

The effects of increasing mass on the STL are compared to the mass law. Since the STL presented in this report is on a different scale than the mass law equation, the increases in STL are compared relatively between panels to determine if they trend the same. As stated in Chapter 1, the mass law states that the STL of a panel is:

$$STL_1 = 20\log(fm_1) - 42dB \qquad \textbf{[5.1]}$$

From this equation, it can be seen that a change of mass (m_1) to mass (m_2) will result in a new sound transmission loss at any frequency of:

$$STL_2 = STL_1 + 20\log\left(\frac{m_2}{m_1}\right) \qquad \textbf{[5.2]}$$

Thus, the relative sound transmission loss difference between two panels of differing mass should be:

$$STL_{difference} = 20\log\left(\frac{m_2}{m_1}\right) \qquad \textbf{[5.3]}$$

This difference value is calculated for all of the panels using the STL values at 1000 Hz. It should be noted that the difference at any frequency should be the same and any variation may be due to the degree of inaccuracy in the curve fitting. The sound transmission loss of the positive 45° panel is used as the point of reference since it is the lowest mass panel. The mass law predicted differences and observed differences are shown below in Table 5.4.

Table 5.4: Mass law predictions for STL difference and observed values

Panel	Mass (kg)	Mass Law Difference (dB)	Observed Difference (dB)	% Error
+45°	41.070	-	-	-
+30°	46.731	1.122	1.050	6.42
+15°	51.669	1.994	1.905	4.46
-15°	64.880	3.972	4.318	8.71
-30°	76.515	5.404	5.764	6.66
-45°	97.684	7.526	8.028	6.67

The observed values are similar to and exhibit the same trend as the mass law predicted values for the relative difference in STL. At most, the values differed by 8.71%. This agreement with the mass law has been shown previously for panels in the

mass controlled region but was only just predicted to also be accurate as a general magnitude gauge for the resonance region. These results show this agreement and also show that, for honeycomb panels using this model, the relative change in magnitude of the STL curve can be accurately predicted by Eq. 5.3 as long as the STL for a reference panel has been determined. For future simulations and forward design with this model, the same reference panel (+45°) will be used.

The area under the curve of the sound transmission results is also calculated as was done for the constant mass panels. This is to capture the effects that both the number of dips and width of the dips have on the total sound transmission capability of the panel. This represents the performance across all frequencies studied. It should be noted however though that these panels are varying in mass, unlike in the previous study, so direct comparison may not be as directly applicable. The results are summarized in Table 5.5 and split into results for the stiffness region, resonance region, and total values.

Table 5.5: Values for area under the sound transmission loss curve for the constant shear modulus panels

Model	Area Under Curve (dB·Hz)		
	Stiffness Region	Resonance Region	Total
-45°	633.0	45962.4	46595.4
-40°	657.4	45029.5	45686.9
-35°	679.7	44314.4	44994.1
-30°	700.6	43672.6	44373.2
-25°	721.2	42981.4	43702.6
-20°	741.1	42445.3	43186.4
-15°	767.8	41987.1	42754.9
-10°	800.6	41292.0	42092.6
-5°	849.1	40353.2	41202.3
5°	882.5	39604.0	40486.6
10°	851.7	39700.7	40552.5
15°	836.6	39480.7	40287.7
20°	831.0	39129.0	39960.0
25°	830.4	38836.9	39667.3
30°	832.5	38642.5	39442.1
35°	836.5	38230.1	39066.6
40°	842.0	37867.1	38709.0
45°	849.1	37414.3	38216.6

As was shown by the sound transmission loss curves (and natural frequencies), the area under the curve values in the stiffness region are all comparable to each other, especially for the positive angle models. Also, the values in the resonance region and total values are highest for the -45° and gradually decrease from model to model down to the +45°. This is most likely due to the increased mass of the negative models and higher overall magnitude. Based on visual observations of the shape of curves and their dips, it is believed that the effects of the dip width are not as prevalent for the constant shear modulus panels.

5.5   Transmitted Acoustic Pressure Distributions

The transmitted pressure distribution in the acoustic field is also studied graphically as was done in the constant mass study. Observations are made about the direction and pattern of the transmitted pressure. The logarithmic value of sound pressure level (SPL) is used to compare different panels at varying frequencies. The pressure values at all of the nodes in the air domain for select frequencies are exported and Matlab 7.10 (R2010a) is used to calculate and plot the sound pressure level. The SPL distributions for the positive 30° model and the negative 30° models at frequencies of approximately 200 Hz, 500 Hz, and 900 Hz are shown below in Figure 5.8 and Figure 5.9 respectively. Again the specific frequencies chosen correspond to dips in the sound transmission loss curve, which are points of high sound transmission.
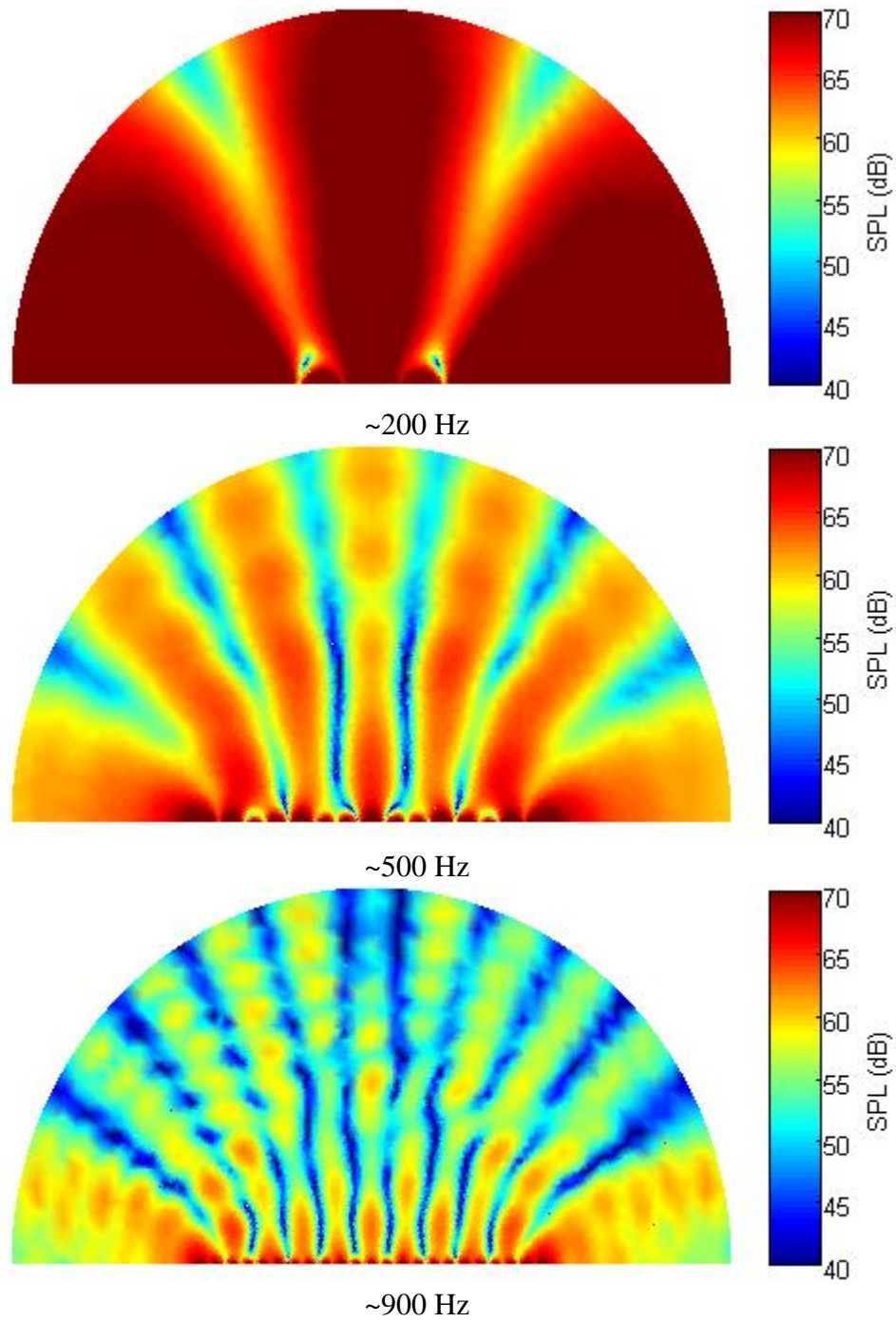
Figure 5.8: Transmitted sound pressure level distributions for positive 30° constant shear modulus panel

~200 Hz

~500 Hz

~900 Hz
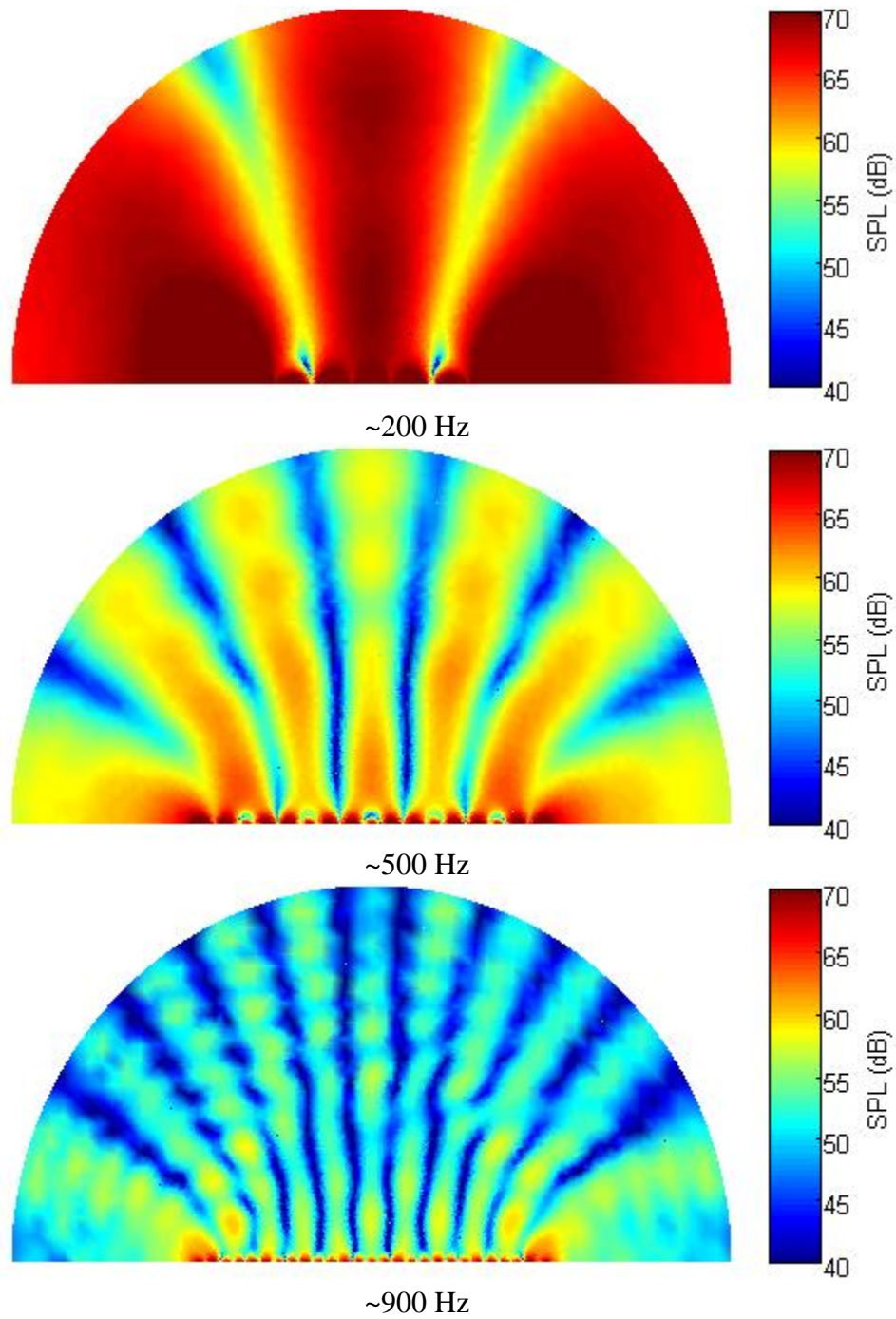
Figure 5.9: Transmitted sound pressure level distributions for negative 30° constant shear modulus panels

As was observed in the previous study, the sound pressure levels attenuate more as the frequency increases for both models. At 200 Hz, the SPL was 70 dB throughout most of the air domain the models. At 900 Hz, the SPL level drops to 40-55 dB at the outer boundary of the air domain. Unlike the constant mass panels, there is not as noticeable a difference in attenuation between the positive and negative 30° panels. The magnitude of sound pressure level is comparable between the two at each frequency, with the positive 30° model having slightly higher levels most likely due to the lower mass of the panel.

The SPL distributions at non-dip frequencies are also shown in Figure 5.10 for reference to illustrate what the distribution looks like at lower transmission levels. Again, the lower magnitude transmission frequencies exhibit similar behavior to the higher magnitude ones.

Positive 30°   Negative 30°

~300 Hz

~600 Hz

~920 Hz
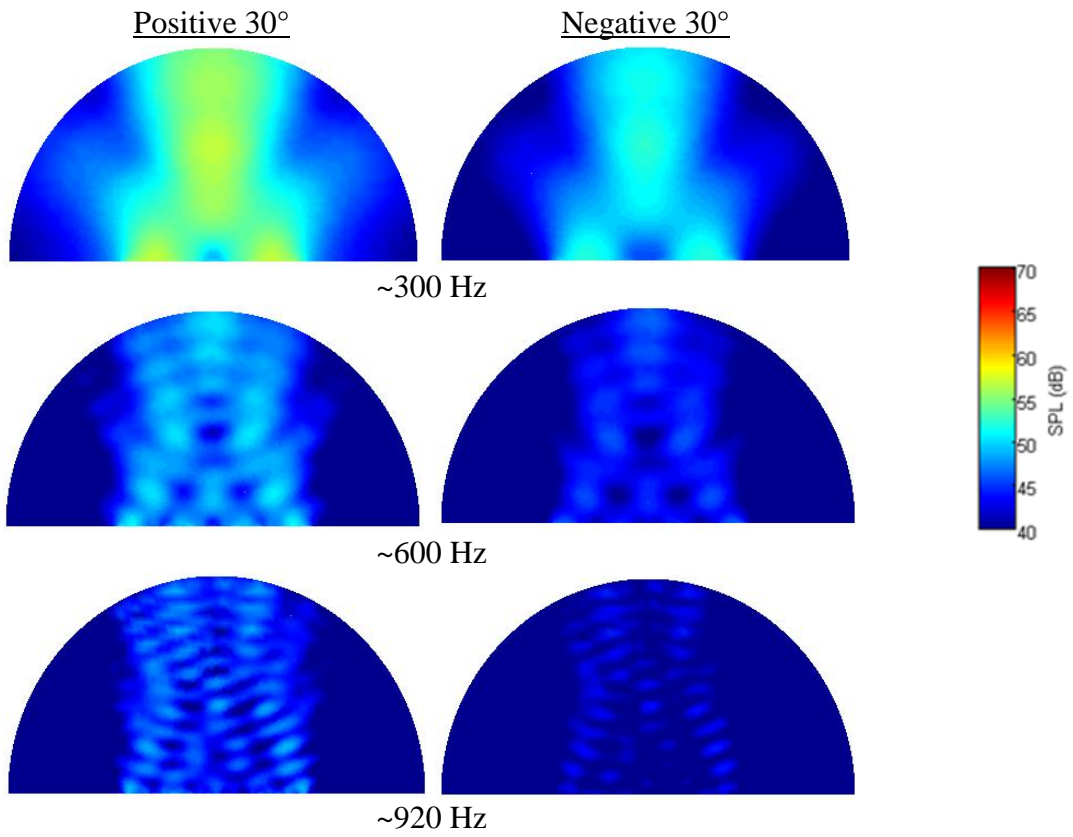
Figure 5.10: Transmitted sound pressure level distributions for non-dip regions in the sound transmission loss curve (constant shear modulus panels)

CHAPTER 6: HONEYCOMB PANEL DESIGN METHOD TO TARGET ACOUSTIC
PROPERTIES

In order to aid the design process for future applications, a design method using the model and preliminary results discussed is formalized and detailed in this chapter. A hypothetical test example of an application to a design problem is also presented to show how the method can be used to isolate problematic frequencies for a solid aluminum sheet in terms of vibro-acoustic properties.

The design method is summarized by the flow chart in Figure 6.1. It is grounded in the requirement that the two main acoustic responses that can be controlled from this work are the magnitude of the sound transmission loss curve at varying frequencies and the location of the dips in the sound transmission loss curve, which correspond to high levels of sound transmission. The general algorithm consists of converting design requirements to metamaterial parametric requirements, generating honeycomb model configurations from those requirements, and then testing those configurations to satisfy the additional acoustic requirements. The end result is a set of designs that satisfy all requirements for the application.
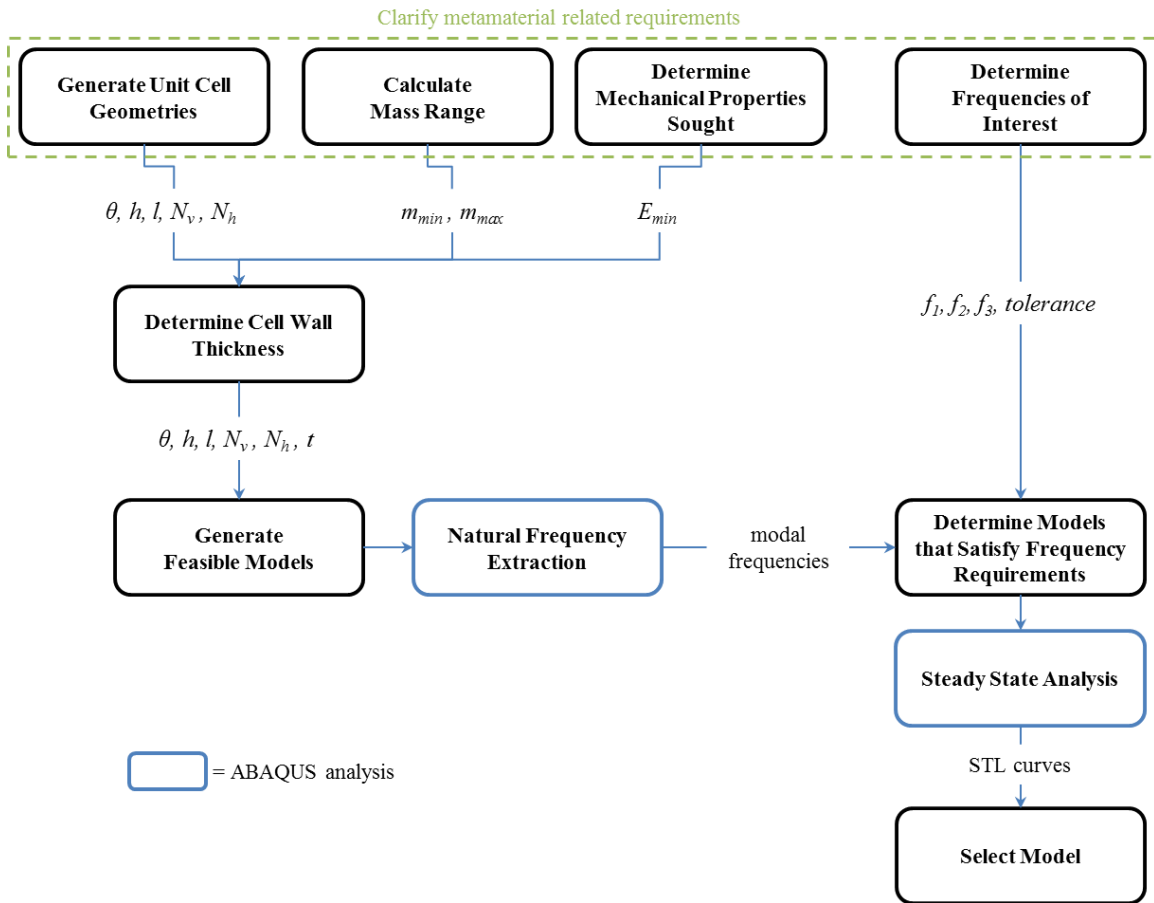
Figure 6.1: Flowchart of design method for the design of acoustic honeycomb panels

In this example, a design is sought to replace a 13 mm aluminum panel. This panel is used as a partition for applications in which the primary driving frequencies are around 370 Hz and 610 Hz. This causes high levels of sound transmission due to the fact that these coincide with the modal frequencies in the panel, causing relatively little sound transmission loss by the panel. The new panel design must also be made of aluminum and must have a comparable general magnitude of STL as the original panel while also performing better around these specific frequencies within ±25 Hz. A lightweight

solution is also desired (< 75.5 kg) even as the panel structurally must still retain an elastic modulus of 40 MPa in the y-direction. These requirements are summarized below:

Frequencies of interest: 369 Hz & 609 Hz

Tolerance = ±25 Hz

Approximate STL Magnitude: ≥ 47.3 dB (at 500 Hz) *General trend*

$\mathbf{m} \leq 75.5 \text{ kg}$

$E_{22}* \geq 40 \text{ MPa}$

6.1   Generate Unit Cell Geometries

It is important to first translate the given requirements into localized metamaterial requirements. This can first be done with the geometric parameters of the unit cell (excluding thickness), which can all be determined based on the size requirements of the structure. The number of cells in the x and y directions must first be determined. For the sake of consistency, this example uses the 1 x 40 configuration that was used in previous chapters, but any configurations may be used. The L_x and L_y unit cell dimensions can then be calculated from the length ($L_{structure}$) and height ($H_{structure}$) as follows:

$$Lx = \frac{L_{structure}}{N_h} \tag{6.1}$$

$$L_y = \frac{H_{structure}}{N_v} \tag{6.2}$$

For this example, the L_x dimension is 0.05 m and the L_y dimension is 0.0866 m. With these known values, the unit cell parameters h and l can be calculated for each of

internal cell angle (θ) increments using Equations 2.1 and 2.2. This example uses 15° incremented models, but this method is not limited to those increment sizes. Smaller increments of 5° would provide more design choices and if this tool were automated, then this method would not be constrained to preset increments. For illustrative purposes, though, 15° increments are adequate. The calculated configurations and their parameters are shown in Table 6.1.

Table 6.1: Sizing parameters to fit structure size requirements

Cell Angle		Unit Cells	l (mm)	h (mm)
-45°		1 x 40	35.36	68.30
-30°		1 x 40	28.87	57.73
-15°		1 x 40	25.88	50.00
15°		1 x 40	25.88	36.60
30°		1 x 40	28.87	28.87
45°		1 x 40	35.36	18.30

6.2   Calculate Mass Range

The next step in the design algorithm is to determine the upper and lower bounds of the panel mass. The upper bound mass limit can be directly extracted from the given requirements. Typically, since it is desirable to keep the panel lightweight, which is a desirable property of many honeycomb structures, a constraint on the weight is given for the design problem. This example requires that the mass be no greater than 75.5 kg, or an effective core density of 280 kg/m^3 without the face sheets. The lower bound mass limit

is extracted from the minimum sound transmission loss specified in the requirements. This mass can be calculated by deriving from Equation [5.2]:

$$m_2 = m_1 10^{\frac{1}{20}(STL_2 - STL_1)} \qquad \textbf{[6.3]}$$

Using the same reference mass (41.070 kg), the reference STL at the specified frequency, and the minimum STL stated by the requirements at that frequency, the minimum mass of the structure can be calculated:

$$m_2 = (41.070) * 10^{\frac{1}{20}(47.3 - 42.647)}$$

$$m_2 = 70.174$$

This mass, after subtracting out the mass of the face sheets, is 43.174 kg, corresponding to an approximate effective core density of 250 kg/m^3.

6.3   Determine Feasible Models

The last local metamaterial requirement to be determined is the cell wall thickness. For each of the model configurations, the upper and lower bounds for mass can be translated to wall thickness values using the equation for effective density (Equation 2.6) and provide a starting point for the thickness bounds. These thickness bounds, shown in Table 6.2, can be further refined using the structural requirements stated.

$$t = \frac{\rho *}{\rho} \frac{2l \cos\theta \left(\frac{h}{l} + \sin\theta \right)}{\left(\frac{h}{l} + 2 \right)} \qquad \textbf{[6.4]}$$

Table 6.2: Cell wall thickness ranges for each configuration

Cell Angle		Cell Wall Thickness Range (mm)
-45°		$1.44 < t < 1.80$
-30°		$1.74 < t < 1.94$
-15°		$1.97 < t < 2.21$
15°		$2.27 < t < 2.54$
30°		$2.32 < t < 2.59$
45°		$2.25 < t < 2.52$

The structural requirement could be any of the effective stiffness properties such as E_{11}^*, E_{22}^*, or G_{12}^*. It could also include properties such as the Poisson's ratios (v_{12}^* and v_{21}^*). In this example, the structural constraint is on the elastic modulus in the y-direction (E_{22}^*). Again, using the CMT equations for effective modulus, the lower thickness bound can be further refined, eliminating more potential designs. The results of this refinement are shown in Table 6.3. For the -15°, +15°, +30°, and +45° models, this does not affect the thickness range as all of these in the mass range satisfy the E_{22}^* constraint. However, there are no configurations of cell wall thickness for the -45° model that satisfied the constraint and the lower bound for the -30° model must be adjusted.

Table 6.3: Refined thickness ranges based on elastic modulus requirement

Cell Angle		Cell Wall Thickness Range (mm)
-45°		No feasible designs
-30°		$1.85 < t < 1.94$
-15°		$1.97 < t < 2.21$
15°		$2.27 < t < 2.54$
30°		$2.32 < t < 2.59$
45°		$2.25 < t < 2.52$

After this refinement, the full set of feasible designs that satisfy the initial metamaterials requirements has been determined. Each of designs consists of a set of honeycomb unit cell parameters in 15° increments along with a thickness range that allows the models to satisfy the mass and structural constraints. Thickness increments of 0.05 mm are used in this example, but like the internal cellular angle increments, this method need not be limited to these increments if this algorithm were automated. Thirty designs in total are analyzed here. The next step after this is to perform a natural frequency extraction using ABAQUS 6.10.

6.4 Natural Frequency Extraction

Using the finite element model laid out in Chapter 3, a natural frequency analysis is performed on all thirty of the designs. The range for the natural frequency extraction only needs to be large enough to ensure that all of the frequencies of interest plus their

tolerances are captured. The frequency range in this example is 1-750 Hz. The results from all of the models analyzed are shown in the Appendix. However, only the models that satisfy the requirements are discussed in the following sections.

6.5   Determine Models that Satisfy Tolerances

The particular frequencies of concern are the odd numbered modes. It needs to be determined which models have odd numbered modes that are spaced at least the specified tolerance (± 25 Hz) distance away from the frequencies of interest, 309 Hz and 609 Hz. All models that have odd numbered modes inside this frequency plus tolerance range are eliminated from consideration. This is done using the natural frequency results for all thirty designs, eliminating all but twelve. This approach is illustrated in Figure 6.2 and the properties of the final twelve designs are shown in Table 6.4.
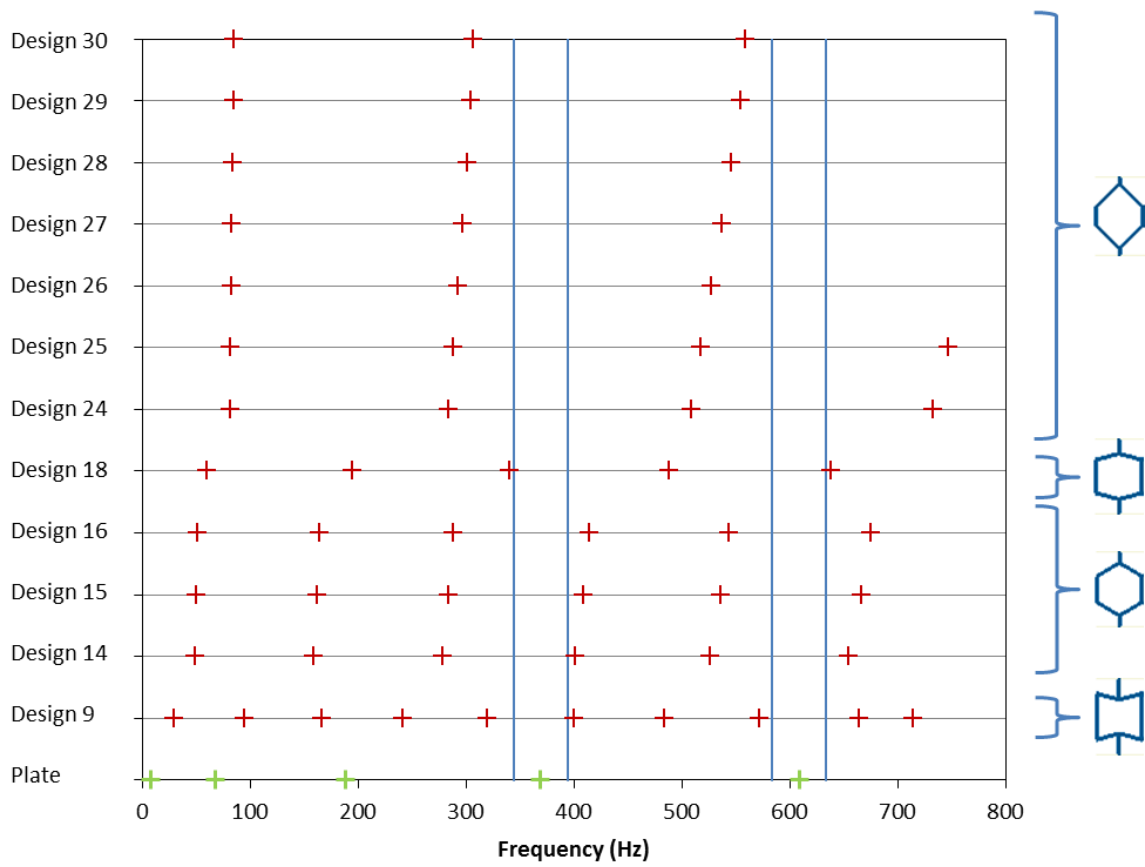
Figure 6.2: Odd numbered modes for designs that satisfy the frequency tolerances

Table 6.4: Final twelve design solutions and their geometric and effective properties

ID	Cell Angle	l (mm)	h (mm)	t (mm)	$G_{12}*$ (MPa)	$\rho*$ (kg/m³)	$E_{11}*$ (MPa)	$E_{22}*$ (MPa)
9	-15°	25.88	50.00	2.206	4.20	280.00	379.1	81.7
14	15°	25.88	36.60	2.450	13.6	269.99	519.1	111.8
15	15°	25.88	36.60	2.500	14.5	275.50	551.5	118.8
16	15°	25.88	36.60	2.541	15.2	280.00	579.0	124.7
18	30°	28.87	28.87	2.350	22.1	253.80	88.5	88.5
24	45°	35.36	18.30	2.252	58.3	250.00	21.2	63.6
25	45°	35.36	18.30	2.300	62.1	255.31	22.6	67.7
26	45°	35.36	18.30	2.350	66.2	260.86	24.1	72.2
27	45°	35.36	18.30	2.400	70.5	266.41	25.6	76.9
28	45°	35.36	18.30	2.450	75.0	271.96	27.3	81.8
29	45°	35.36	18.30	2.500	79.7	277.51	29.0	87.0
30	45°	35.36	18.30	2.522	81.9	280.00	29.8	89.3

None of the -30° models satisfy the frequency and tolerance requirements and thus are eliminated from consideration and design #9 (θ = -15°, t = 2.206 mm) is the only negative cell angle model to satisfy the requirements. All of the +45° models satisfy the requirements. These models have the largest spacing between odd modes and the highest shear moduli, consistent with the previous studies.

6.6   Steady State Analysis

The next step, after the models that satisfy all the requirements have been determined, is to perform the steady state analysis. This validates the magnitude and frequency results and shows what the shape of the sound transmission loss curve looks like to aid in the selection of a model. The same steady state procedure outlined in Chapter 3 is used. The steady state results for some of the final design solutions

previously discussed are shown below in Figure 6.3. The other designs are located in the

Appendix.
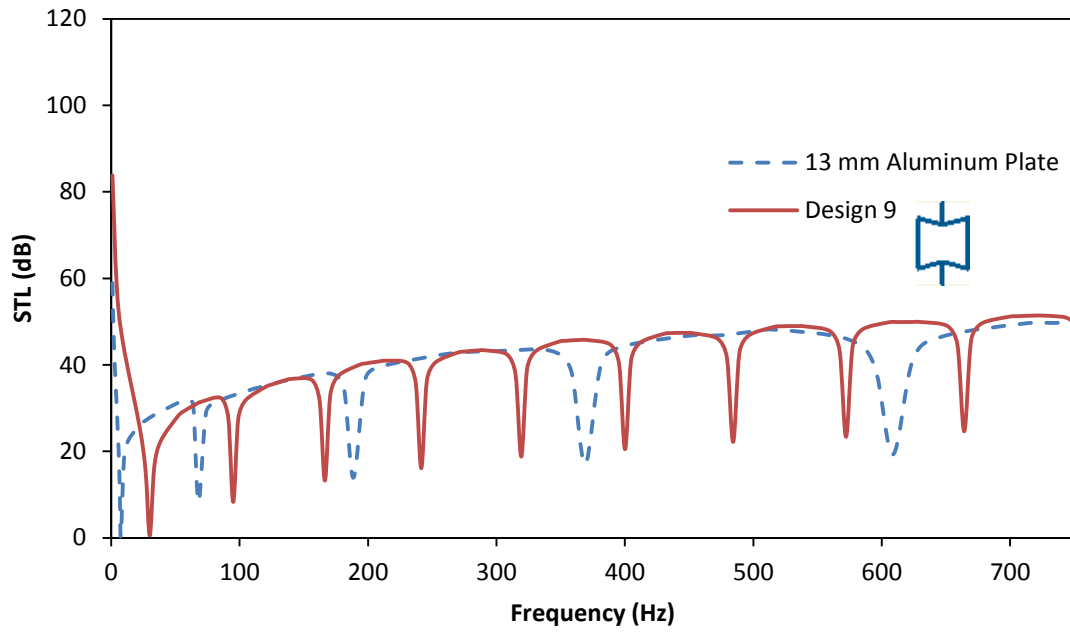
Figure 6.3: STL comparison for design 9 vs. aluminum plate
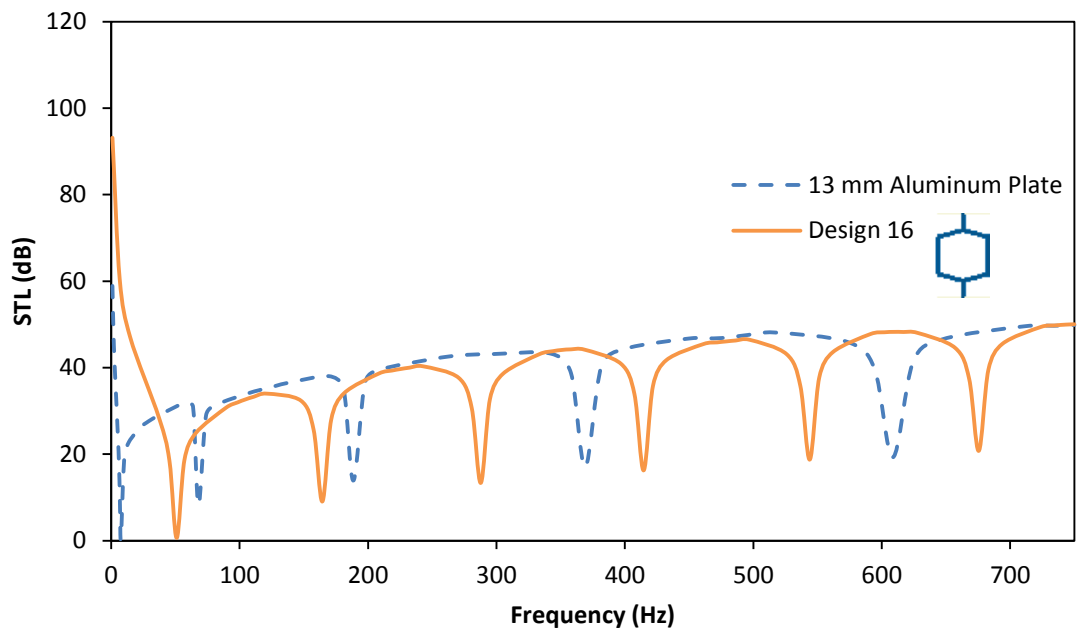
Figure 6.4: STL comparison for design 16 vs. aluminum plate
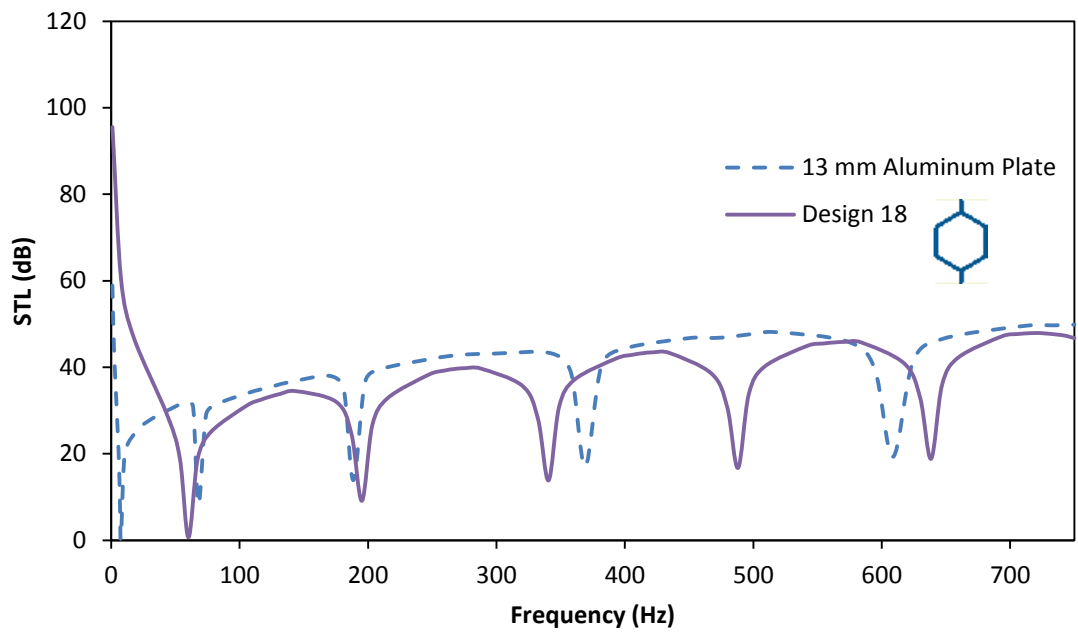
Figure 6.5: STL comparison for design 18 vs. aluminum plate

101
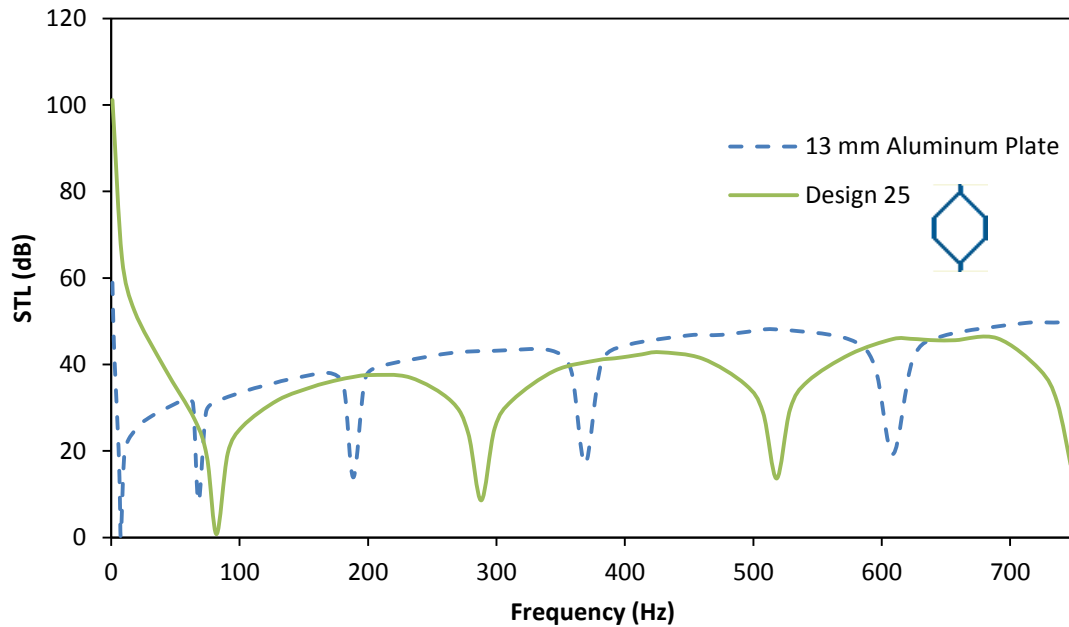
Figure 6.6: STL Comparison for design 25 vs. aluminum plate

It should be noted that some of these designs do not exactly meet the magnitude requirement due to the fact that the method is an approximation. The main emphasis is just to estimate a general trend of what the magnitude should be.

6.7   Select Final Design

At this point in the design algorithm, several designs have already been determined to satisfy all of the provided requirements. All of these are valid design solutions, but now the designer determines which model is the preferred solution depending on the application and additional desirable properties. Some of the properties that should potentially be considered, in no particular order, are:

- Mass – Of the valid design solutions, higher mass means even higher levels of sound transmission loss which would be desirable if the application called for the highest STL possible. On the contrary, the application may call for lighter panels and so the lower mass pass panels would be more desirable at the expense of higher transmission loss.

- Manufacturability – While the solution may satisfy the specified requirements, it may not be feasible to actually produce the design. Most metal honeycombs are made by pressing sheet metal into a half-hexagonal profile and then gluing the corrugated sheets together as shown Figure 6.7 [5]. The available sheet thicknesses, which correspond to cellular wall thickness, can further limit the feasible design solutions
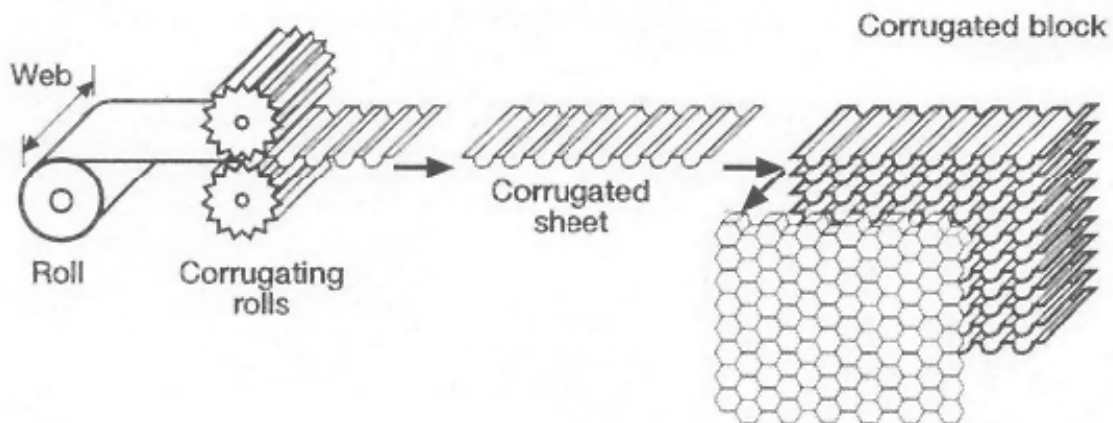
Figure 6.7: Manufacturing process for metal honeycombs using glued together corrugated sheets [42]

- Shape of STL Curve – As seen in the Chapter 4, the shape of the curves and specifically the dips changes from model to model. One curve may have a larger spacing between dips but may not have as consistently high of a sound transmission loss level between those dips as a model with smaller dip spacing. The area under the curve metric can be used to evaluate this. An example is shown Figure 6.8, where design 9 has a smaller spacing, but performs better between that spacing than design 16.
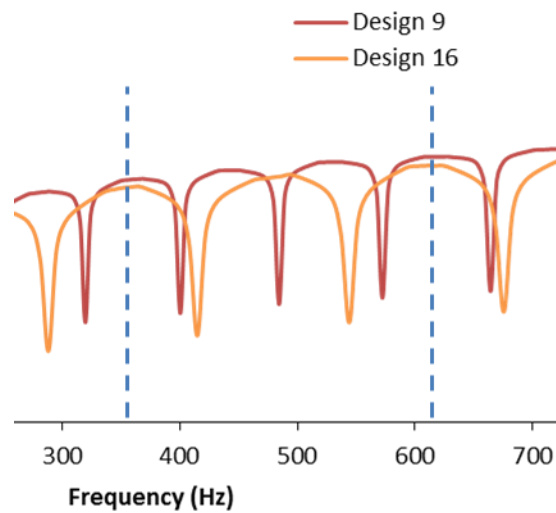
Figure 6.8: Differing STL curve shapes between designs

- Additional Structural Properties – In this example, the elastic modulus in the y-direction was the prime structural constraint. However, the other effective structural properties ($E_{11}*$, $G_{12}*$, $v_{12}*$, or $v_{21}*$) could be used to justify the selection of one of the panels over the others.

These are just a few possible characteristics that could be used in the final design selection process. Other factors could be considered such as thermal, fatigue, or even

dynamic properties of the panel. The design method presented in this report only provides the possible designs that satisfy the requirements provided to it. It is up to the discretion of the designer to make the selection of the appropriate solution as seen fit.

This method should be used as a tool to effectively generate multiple solutions to meet requirements for acoustic applications. It takes a set of design requirements, translates them in to parametric metamaterials requirements, and analyzes potential configurations to test for satisfaction of the original requirements. If this algorithm were automated, then it could generate solutions quickly and efficiently with minimal input from the designer.

CHAPTER 7: CONCLUSIONS AND FUTURE WORK

In this work, the acoustic properties of in-plane honeycomb sandwich panels were studied. A finite element model on ABAQUS 6.10 was developed and is documented in detail in Chapter 3. This same model was used for the analysis of honeycomb panels to determine significant properties in regards to sound transmission. Varying honeycomb cellular geometries were tested for the core layer in the sandwich panel to study the geometric effects on the acoustic response so that they can be better used in forward design. From this work, several major conclusions can be drawn to aid the designer and will be the focus of future work.

The results from the constant panel mass study are discussed in Chapter 4. Eighteen aluminum sandwich panels, with varying honeycomb core configurations of internal cell angles ranging from -45° to +45°, were studied. The natural frequencies were extracted from these panels, analyzed for trends, and then correlated to the steady state analyses that followed. From the natural frequency results, the shear modulus of the core had the most prevalent trend with the effect on where the first natural frequency occurs and how far the natural frequencies are spaced apart. The steady state analyses then presented the results in the form of sound transmission loss. It was observed that increasing the internal cell angle, and thus increasing the effective shear modulus of the core, caused the dips in the sound transmission loss curve (odd numbered natural frequencies) to occur later in the frequency range and be spaced further apart as predicted by the natural frequency extraction. The sound pressure levels were also studied and it was seen that larger frequency incident sounds displayed more attenuation. Also, in

general, the negative 30° model displayed more attenuation of SPL magnitude than the positive 30° at varying comparable driving frequencies.

The results from the constant shear modulus panel study are discussed in Chapter 5. The same procedure as the constant mass study was used, only this time holding the shear modulus of the core constant between honeycomb configurations that varied in cell angle between -45° and +45°. Based on the previous study, it was predicted that the different panels would have similar natural frequencies and consequently similar dips in the sound transmission loss curve due to their constant shear modulus. In general, this was true in that there was less variation from model to model than in the constant mass case, especially for the negative angle cores. However, there was still some variation, with more evident variation in the positive angle cores. This illustrates that while the shear properties of the panel play a large role, there are other interrelated stiffness properties that affect the response. Also observed was that the general magnitude, which was a logarithmic trend, varied between models due to the changing mass of the panels. This variation was quantified and was consistent with mass law. The SPL distribution was also studied and the same trends were seen as in the constant mass case. Higher frequencies attenuate more and the negative 30° model attenuated sound pressure more than the positive 30° model, although not as noticeable as in the constant mass study.

A systematic design method that employs the model from Chapter 3 and the results from Chapter 4 and 5 is presented in Chapter 6. The method is capable of taking a set of size, acoustic, and structural requirements and generating multiple solutions that satisfy these requirements. The method was demonstrated on a hypothetical test design

example and was successfully able to generate twelve different models that isolated the frequencies of interest, 369 Hz and 609 Hz, at the desired STL level while still satisfying constraints for mass and elastic modulus. The method shows the flexibility of honeycomb metamaterials in that they can be adjusted to create many different acoustic responses.

7.1   Other Geometric Parameters

While this work studies the effects of several geometric parameters such as vertical member height, angle member length, and internal cell angle, there are additional parameters that can be further studied. Cellular parameters such as number of cells in the x and y directions, as opposed to simply scaling like was done in this work, and unit cell orientations should be tested. With the unit cell, only one orientation is presented out of several different ways to orient the honeycomb unit cell studied in other works (Figure 7.1). These should be tested to determine if they exhibit significantly different properties than the unit cell in this work.

This Work   **Ruzzene [25]**   **Ju et al. [5-7]**
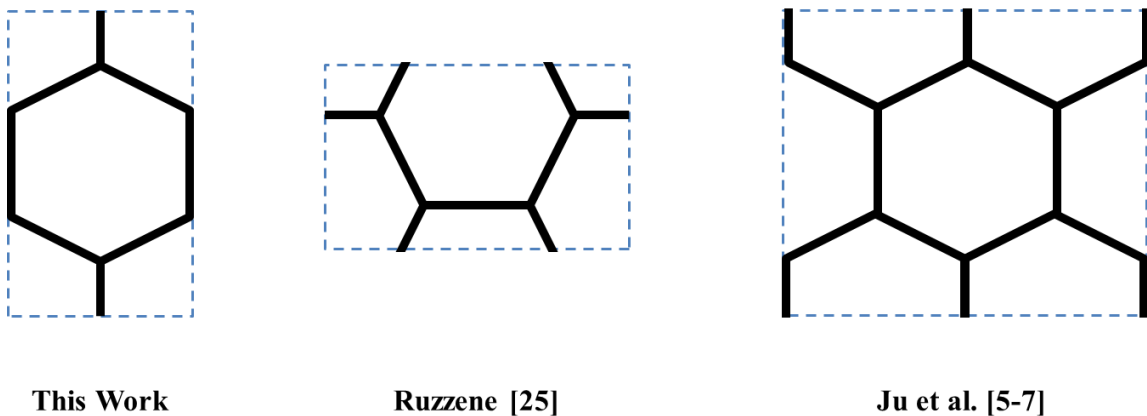
Figure 7.1: Varying types of honeycomb unit cell orientations

7.2 Experimental Validation

The finite model presented in this thesis was validated by showing consistent results with previously published work. However, as with any analysis model, the results need to be verified experimentally to show that the computer model accurately predicts what will be seen in real use case scenarios. Experimental testing can help to show that the results are consistent and can also determine to what degree the finite element model results should be scaled. Since a specific definition of sound transmission loss was given for this model due to the discrete nature of output results, it is necessary to translate the results of this work into the real world definition of sound transmission loss through some type of scaling factor. Students within CEDAR (Clemson Engineering Design Applications & Research) are currently working to develop experimental testing equipment to test the acoustic performance of different honeycomb models.

The setup of the acoustic testing apparatus is similar to layout of other works by Ford et al. [21] and Smolenski & Krokosky [22], only scaled down due to test sample size limitations. The layout is shown in Figure 7.2 and the major components include a speaker box and an enclosed anechoic space with a rigid wall separating the two spaces. The honeycomb sandwich panel is secured in the middle of the rigid wall and microphones are placed on both the incident and transmitted sides of the panel. The speakers are driven by a control source that is capable of producing and sustaining an acoustic signal at a specific frequency.
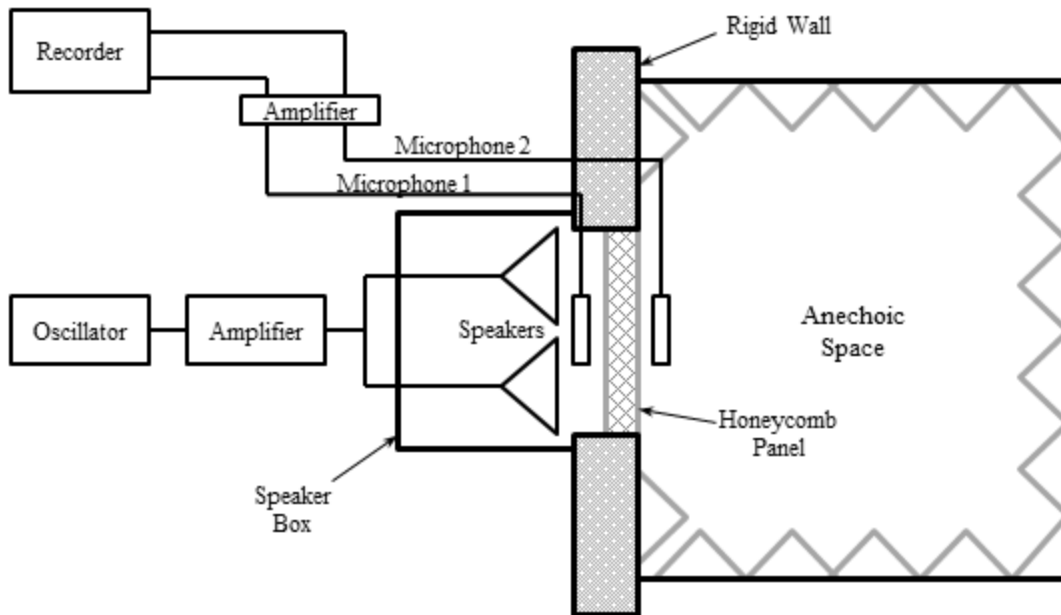
Figure 7.2: Layout of acoustic testing equipment

A graphic of the actual built setup is also shown for reference below in Figure 7.3. The apparatus is still in development at the moment and subject to modifications. The overall construction of the enclosure is made out of 1/2" medium density fiberboard and the entire interior space is lined with 3" acoustic foam. The source sound is generated by a wide frequency range 3" TB speaker and 25W amplifier. The transmitted sound is recorded by a Dayton EMM-6 microphone. The driving frequency signal is controlled by a Matlab based code, which also process the signal from the microphone.
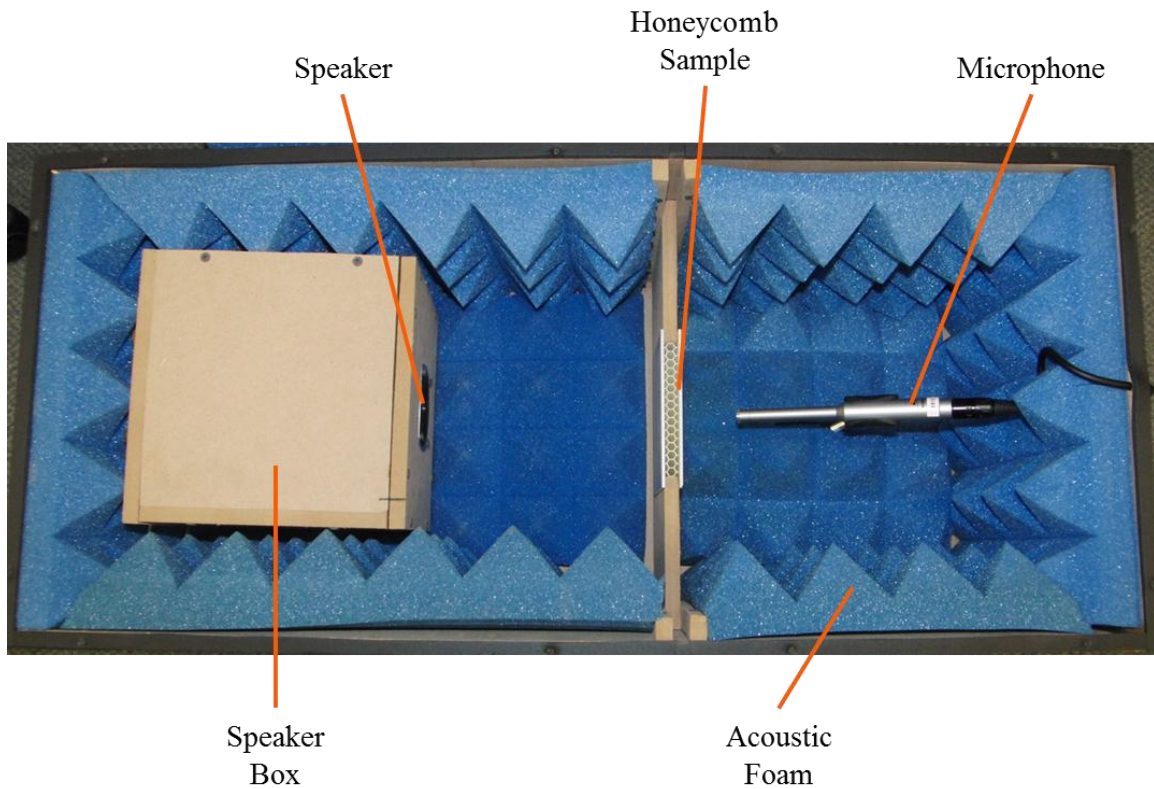
Figure 7.3: Experimental test apparatus developed for testing honeycomb samples

Some issues will have to be addressed with this specific setup. First, the setup is a scaled down version of the model presented in this report. Care must be taken to ensure that the experimental setup is accurately scaled in order to compare results. Second, the sample is printed on an Objet 3D printer due to limitations on manufacturing custom honeycomb panels. The printer produces plastic models (Figure 7.4) and plastic is not a linear material. It will exhibit damping characteristics not present in the finite element model. The FEM must be properly adjusted to account for these nonlinear material properties. Finally, the boundary conditions may have to be adjusted in the FEM to match those in the experimental setup. Currently, the model uses pinned boundary

conditions for the honeycomb panel but the experimental setup more closely resembles simply supported conditions.
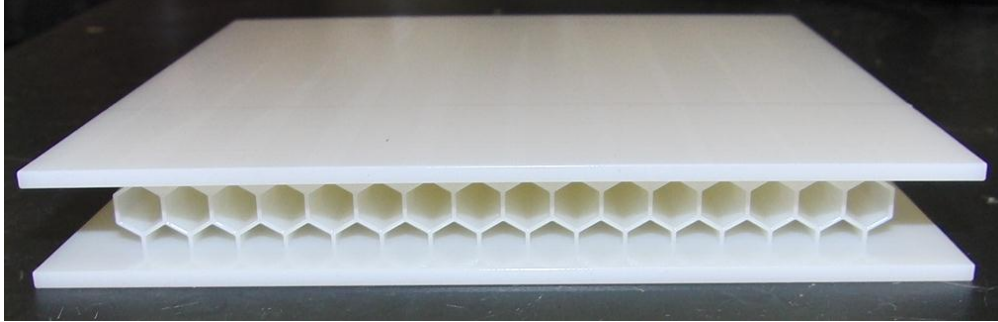
Figure 7.4: Plastic honeycomb sandwich panel sample used for testing

7.3   Automated Design Tool

In this thesis work, a design method is presented along with a general process for how it can be used in forward design. Automation of this process was out of the scope of this work and therefore was not done. However, this process could be potentially automated to be an even more powerful tool, which has been done in previous works [3,4]. Due to the changing mesh size and the need to specify loading surfaces and output sets, it was difficult in this work to automate the analysis. However, the honeycomb geometric parameters, part model sketches, and general analysis setup could be automated. After that, only a small amount of manual input would be required to specify the remaining analysis parameters. This automation would help to save time in future works with the model.

7.4   Alternative Core Topologies

The core topologies studied in this work include standard honeycomb and auxetic configurations. These structures were chosen due to familiarity from previous work and

due to predefined effective mechanical properties as laid out by Gibson and Ashby [5]. However, this same analysis model and procedure could be applied to alternative core topologies such as chiral honeycombs [6], hybrid and accordion honeycombs [43], and bristle structures [3,44]. Examples of a tetrachiral and accordion core are shown in Figure 7.5.
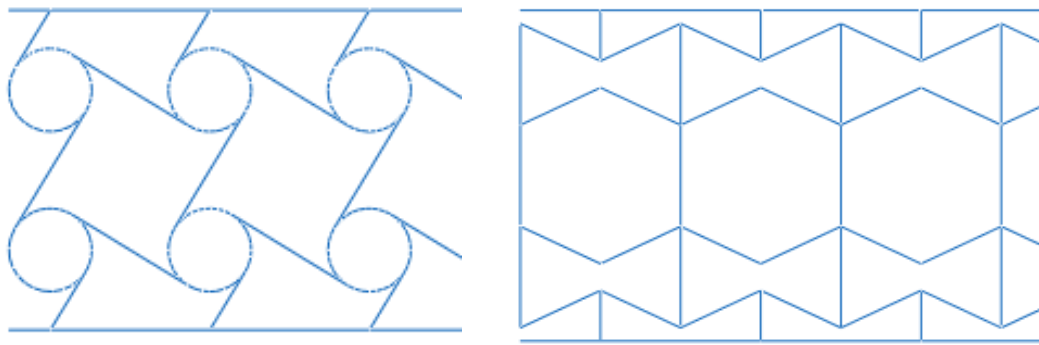
Figure 7.5: Examples of a chiral honeycomb panel (left) and a zero Poisson's ratio honeycomb panel (right)

One of the major differences with using different topologies is that certain effective properties may need to be determined ahead of time either computationally or experimentally. There may not be a pre-existing set of equations that describe these properties such as the CMT equations for honeycomb effective density, shear modulus, and elastic modulus. These core configurations could be an area of exploration for future works.

7.5   Induced Frequencies

Another area for future work is to study the induced frequencies that are generated by honeycomb panels. This is property that would be useful for the designing panels that change or transform the incident sound. Specifically, the panel could emit a sound different from the driving sound frequency by inducing another frequency that masks the original sound. This work begins to explore some properties related to these potential induced frequencies with the natural frequency extraction. By definition, these natural frequencies are the frequencies at which the structure will tend to vibrate at when set into motion. The natural frequencies that would be more prevalent in an emitted sound would be the ones corresponding to the STL dips. Analysis of the induced frequency could be performed using a dynamic model as opposed to the steady-state procedure described in this thesis report. The output sound results could be processed using a fast Fourier transform as shown below in Figure 7.6.
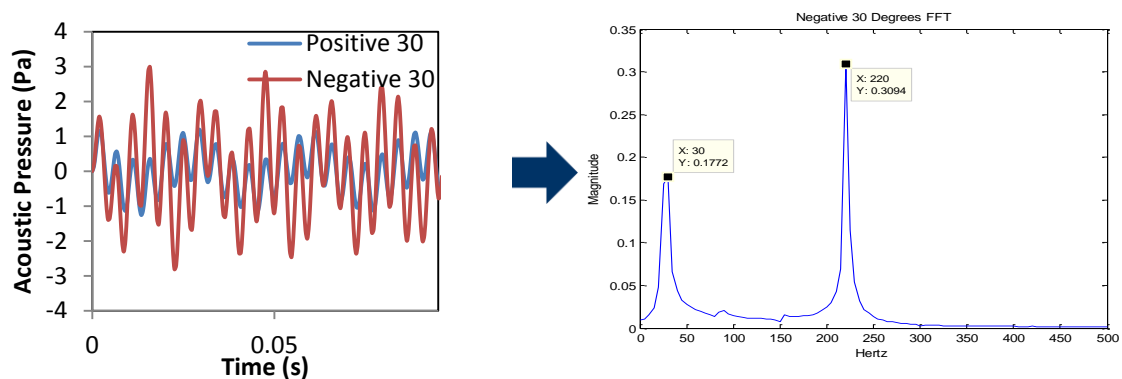
Figure 7.6: Sample dynamic induced frequency results with fft

WORKS CITED

[1] G. Pahl and W. Beitz, *Engineering Design: A Systematic Approach*, 3rd ed. London: Springer-Verlag, 2007.

[2] J. Ju, J. Summers, J. Ziegert, and G. Fadel, "Design of Honeycombs for Shear Stiffness and Maximum Shear Strain," *Journal of Engineering Materials and Technology*, accepted February 2011.

[3] Luke Berglind, "Design Tool for Cellular Structure Synthesis to Achieve Desired Properties," Clemson University, Clemson, Master's Thesis 2010.

[4] Jesse Schultz, "Modeling and Finite Element Analysis Methods for the Dynamic Crushing of Honeycomb Cellular Meso-Structures," Clemson University, Clemson, Master's Thesis 2011.

[5] Lorna J. Gibson and Michael F. Ashby, *Cellular Solids: Structure and Properties*, 2nd ed. Cambridge, UK: Cambridge University Press, 1997.

[6] A. Kolla, J. Ju, J. Summers, G. Fadel, and J. Ziegert, "Design of Chiral Honeycomb Meso-Structures for High Shear Flexure," in *ASME International Design Engineering Technical Conferences & Computers and Information in Engineering Conference*, Montreal, Quebec, Canada, 2010.

[7] Z. Zou, S. Reid, P. Tan, S. Li, and J. Harrigan, "Dynamic Curshing of Honeycombs and Features of Shock Fronts," *International Journal of Impact Engineering*, vol. 36, pp. 165-176, 2009.

[8] M. Ruzzene, "Vibration and Sound Radiation of Sandwich Beams with Honeycomb Truss Core," *Journal of Sound and Vibration*, vol. 277, pp. 741-763, 2004.

[9] Hans-Peter Degischer and Brigitte Kriszt, Eds., *Handbook of Cellular Materials: Production, Processing, Applications*. Weinheim, Germany: WILEY-VCH, 2002.

[10] J. Schultz et al., "Design of Honeycomb Meso-Structures for Crushing Energy Absorption," *Journal of Mechanical Design*, accepted February 2012.

[11] J. Ju, J. Summers, J. Ziegert, and G. Fadel, "Design of Honeycomb Meta-Materials for High Shear Flexure," in *ASME International Design Engineering Technical Conferences & Computers and Information in Engineering Conference*, San Diego, California, 2009.

[12] J. Ju, J. Summers, J. Ziegert, and G. Fadel, "Cyclic Energy Loss of Honeycombs Under In-Plane Shear Loading," in *ASME International Mechanical Engineering Congress and Exposition*, Buena Vista, Florida, 2009.

[13] B.M. Dempsey, S. Eisele, and D.L. McDowell, "Heat Sink Applications of Extruded Metal Honeycombs," *International Journal of Heat and Mass Transfer*, vol. 48, no. 3-4, pp. 527-535, 2005.

[14] Francesco Franco, Kenneth A. Cunefare, and Massimo Ruzzene, "Structural-Acoustic Optimization of Sandwich Panels," *Journal of Vibration and Acoustics*, vol. 129, pp. 330-340, June 2007.

[15] S. Joshi et al., "Experimental Damage Characterization of Hexagonal Honeycombs Subjected to In-Plane Shear Loading," in *ASME International Design Engineering Technical Conferences and Computers and Information in Engineering Conference*, Montreal, Quebec, Canada, 2010, pp. 35-41.

[16] Thomas D. Rossing, Ed., *Springer Handbook of Acoustics*. New York, USA: Springer Science, 2007.

[17] M. Moser, *Engineering Acoustics: An Introduciton to Noise Control*. Berlin, Germany: Springer Science, 2004.

[18] C.F. Ng and C.K. Hui, "Low Frequency Sound Insulation using Stiffness Control with Honeycomb Panels," *Applied Acoustics*, vol. 69, pp. 231-301, 2008.

[19] Daniel R. Raichel, *The Science and Applications of Acoustics*, 2nd ed. New York, USA: Springer Science, 2006.

[20] G. Kurtze and B.G. Watters, "New Wall Design for High Transmisison Loss or High Damping," *The Journal of the Acoustical Society of America*, vol. 31, no. 6, pp. 739-748, 1959.

[21] R.D. Ford, P. Lord, and A.W. Walker, "Sound Transmission through Sandwich Construction," *J. Sound Vib.*, vol. 5, no. 1, pp. 9-21, 1967.

[22] C.P. Smolenski and E.M. Krokosky, "Dilational-Mode Sound Transmission in Sandwich Panels," *The Journal of the Acoustical Society of America*, vol. 54, pp. 1449-1457, 1973.

[23] C.L. Dym and M.A. Lang, "Transmission of Sound through Sandwich Panels," *Journal of the Acoustical Society of America*, vol. 56, pp. 1523-1532, 1974.

[24] Tongan Wang, Shan Li, Shankar Rajaram, and Steven R. Nutt, "Predicting the Sound Transmission Loss of Sandwich Panels by Statistical Energy Analysis Approach," *Journal of Vibration and Acoustics*, vol. 132, February 2010.

[25] Tongan Wang, Vladimir Sokolinsky, Shankar Rajaram, and Steven Nutt, "Assessment of Sandwich Models for the Prediction of Sound Transmission Loss in Unidirectional Sandwich Panels," *Applied Acoustics*, vol. 66, pp. 245-262, 2005.

[26] J.A. Moore and R.H. Lyon, "Sound Transmission Loss Characteristics of Sandwich Panel Constructions," *Journal of the Acoustical Society of America*, vol. 89, no. 2, pp. 777-791, 1991.

[27] C.L. Dym and D.C. Lang, "Transmission Loss of Damped Asymmetric Sandwich Panels with Orthotropic Cores," *Journal of Sound and Vibration*, vol. 88, no. 3, pp. 299-319, 1983.

[28] Priya Thamburaj and J.Q. Sun, "Effect of Material and Geometry on the Sound and Vibration Transmisison across a Sandwich Beam," *Journal of Vibration and Acoustics*, vol. 123, pp. 205-212, April 2001.

[29] P. Thamburaj and J.Q. Sun, "Effect of Material Anisotropy on the Sound and Vibration Transmission Loss of Sandiwch Aircraft Structures," *Journal of Sandwich Structures and Materials*, vol. 1, pp. 76-92, 1999.

[30] H. Denli and J.Q. Sun, "Structural-Acoustic Optimization of Sandwich Structures with Cellular Cores for Minimum Sound Radiation," *Journal of Sound and Vibration*, vol. 301, pp. 93-105, 2007.

[31] F. Scarpa and G. Tomlinson, "Theoretical Characteristics of the Vibration of Sandwich Plates with In-Plane negative Poisson's Ration Values," *Journal of Sound and Vibration*, vol. 230, no. 1, pp. 45-67, 2000.

[32] Michael El-Raheb and Paul Wagner, "Transmission of Sound Across a Trusslike Periodic Panel," *J. Acoust. Soc. Am.*, vol. 102, no. 4, pp. 2176-2183, October 1997.

[33] T.S. Lok and Q.H. Cheng, "Free Vibration of Clamped Orthotropic Sandwich Panel," *Journal of Sound and Vibration*, vol. 229, no. 2, pp. 311-327, 2000.

[34] Usik Lee, "Equivalent Continuum Representation of Lattice Beams: Spectral Element Approach," *Engineering Strudctures*, vol. 20, no. 7, pp. 587-592, 1998.

[35] S. Narayanan and R.L. Shanbhag, "Sound Transmission through a Damped Sandwich Panel," *Journal of Sound and Vibration*, vol. 80, no. 3, pp. 315-327, 1982.

[36] Hiroaki Nakamoto, Tadaharu Adachi, and Wakako Araki, "In-plan Impact Behavior of Honeycomb Structures Filled with Linearly Arranged Inclusions," *International Journal of Impact Engineering*, vol. 36, pp. 1019-1026, 2009.

[37] Nikhil Seera, "Viscoelastic Damping of Hexagonal Honeycomb Sandwich Panels," Clemson University, Clemson, Master's Thesis 2011.

[38] *ABAQUS 6.8 Documentation*.

[39] C. Jackman and M. Zampino, "Estimating Acoustic Performance of a Cell Phone Speaker Using Abaqus," Simulia,.

[40] "Shock Response and Acoustic Radiation Analysis," ABAQUS, Inc., ABAQUS Technology Brief 2004.

[41] "Acoustical Terminology," American National Standards Institute, ANSI S1.1-1994 (R2004),.

[42] (2012) Paneltech International. [Online]. www.paneltech.biz

[43] K. Olympio and F. Gandhi, "Zero-v Cellular Honeycomb Flexible Skins for One-Dimensional Wing Morphing," in *AIAA/ASME/ASCE/AHS/ASC Structures, Structural Dynamics, and Materials Conference*, Honolulu, Hawaii, 2007.

[44] L. Berglind, J. Ju, and J. Summers, "Aluminum Taper Bristle Shaped Shear Band for a Non-pneumatic Tire," in *The Tire Society*, Akron, OH, 2010.

APPENDICES

Appendix A. ABAQUS Details for Finite Element Model

This section describes all of the necessary modeling parameters needed to recreate the finite element model described in Chapter 3 and used in the subsequent chapters. Each of models are generated and analyzed in ABAQUS 6.10. All simulations are run on a Dell Precision T7400 computer with dual quad core 2.00 GHz Intel Xeon processors, allotting 6 of the cores for use. Table A- 1 describes the parameters for the natural frequency extraction and Table A- 2 describes the setup for the steady state analysis.

Table A- 1: Analysis/Modeling details for natural frequency extraction

Simulation Type	Frequency
Part Type	**Honeycomb** 2D, deformable (wire)
Section Details	Beam Section Integration During Analysis Material: *Aluminum*, Section Poisson's ratio: 0.33 Temperature Variation Linear by Gradients All other default settings
Profiles	*Boundary Profile*: a = 1, b = 0.0025 *Core Profile*: a = 1, b = 0.0025 (for +30°, changes between models)
Material Properties	*Aluminum*, $\rho = 2700$ kg/m^3, E = 71 GPa, $\nu = 0.33$, Elastic
Element Type	B22: Standard, Quadratic Geometric Order, All other default settings
Sets created	*Honeycomb Ends* (geometry): the nodes along the sides of the honeycomb panel
Boundary Conditions	Displacement/Rotation: Applied to *Honeycomb Ends*, U1=U2= 0
Step Details	Frequency Extraction: Lanczos, 1-1000 Hz, All other default settings
Field Output Request	F-Output-1: All default outputs for frequency step

Table A- 2: Analysis/Modeling details for steady state analysis

Simulation Type	Steady-state dynamics, Direct
Part Type	**Honeycomb** 2D, deformable (wire) **Air Fluid** 2D, deformable (shell)
Section Details	**Honeycomb** Beam Section Integration During Analysis Material: *Aluminum*, Section Poisson's ratio: 0.33 Temperature Variation Linear by Gradients All other default settings **Air Fluid** Solid, Homogenous Material: *Air*, Plane Stress/Strain Thickness = 1
Profiles	*Boundary Profile*: a = 1, b = 0.0025 *Core Profile*: a = 1, b = 0.0025 (for +30°, changes between models)
Material Properties	**Honeycomb** *Aluminum*, ρ = 2700 kg/m^3, E = 71 GPa, ν = 0.33, Elastic **Air Fluid** *Air*, ρ = 1.2 kg/m^3, κ = 1.01E5, Acoustic Medium
Element Type	**Honeycomb** B22: Standard, Quadratic Geometric Order, All other default settings **Air Fluid** AC2D3: Standard, Acoustic, Linear Geometric Order, All other default settings
Partitions	**Air Fluid** Vertically through the middle of the air domain
Sets created	*Honeycomb Ends* (geometry): the nodes along the sides of the honeycomb panel *Air Bottom Interface* (nodes): The nodes along the bottom of the air fluid in contact with the honeycomb structure

Surfaces	**Honeycomb** *Bottom*: Bottom side of bottom honeycomb panel face sheet *Top*: Top side of top honeycomb panel face sheet **Air Fluid** *Bottom*: Bottom side of air domain
Boundary Conditions	*Pinned*: Displacement/Rotation - Applied to *Honeycomb Ends*, U1=U2= 0
Loads	Pressure Load: Applied to surface Honeycomb *Bottom* Distribution: Uniform Magnitude: 1 + 0i Amplitude: Instantaneous
Constraints	*Tie:* Master Surface = Honeycomb *Top* Slave Surface = Air Fluid *Bottom*
Step Details	*Steady State*: Compute complex response, Linear Input modal frequencies into data, 6 Points, Bias =2 All other default settings
History Output Request	*H-Output-1:* POR, on set *Air Bottom Interface,* Interval: 200
Field Output Request	F-Output-1: POR, on Whole Model, Interval: 20
Interactions	**Absorbing Boundary:** Type: Acoustic Impedance Step: Steady State Surface: Back of air domain Nonreflecting Definition Circular (r = 2) Nonreflecting Type

Appendix B. Extended Results from Simulations

In the report, only the results of the 15° incremented models were discussed. This section shows the results from all other models that were tested in Chapters 4, 5, and 6.

B.1. Vibration Modes

This section presents the vibrations modes for the negative 30° panel, which is not discussed in the main body this report, which only includes the positive 30° model figures. The overall macro behavior between the two panels is this same, which is why the negative 30° panel is excluded in the main body. However, the results are shown here for visualization purposes so that the deformation behavior of the core can be observed for an auxetics model. The first ten modes are shown in Figure B- 1.
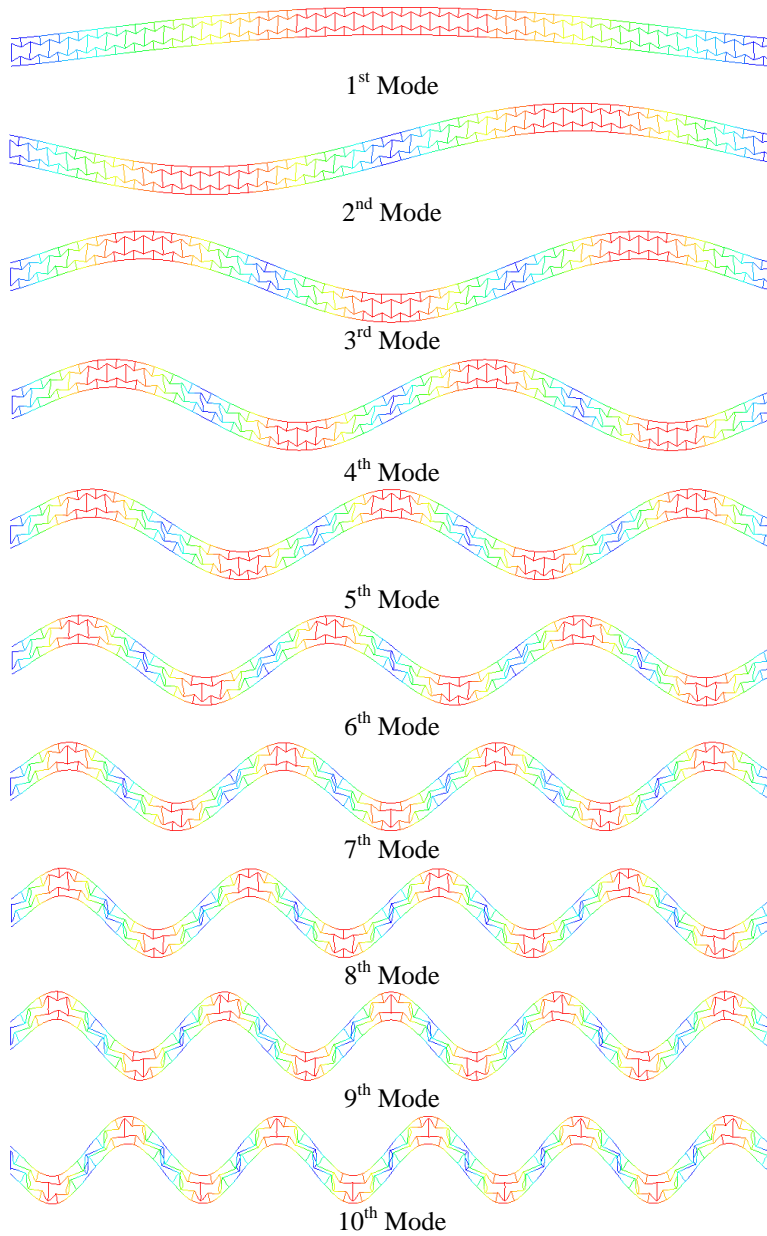
1st Mode

2nd Mode

3rd Mode

4th Mode

5th Mode

6th Mode

7th Mode

8th Mode

9th Mode

10th Mode

Figure B- 1: First ten vibration modes of Negative 30° Model

B.2. Constant Mass Results

The results for the negative angle constant mass panels not discussed in the reported are shown below in this section of the appendix. The negative 40° and 45°

models are shown in Figure B- 2, the negative 25° and 20° models are shown in Figure

B- 2, and the negative 10° and 5° models are shown in Figure B- 4.
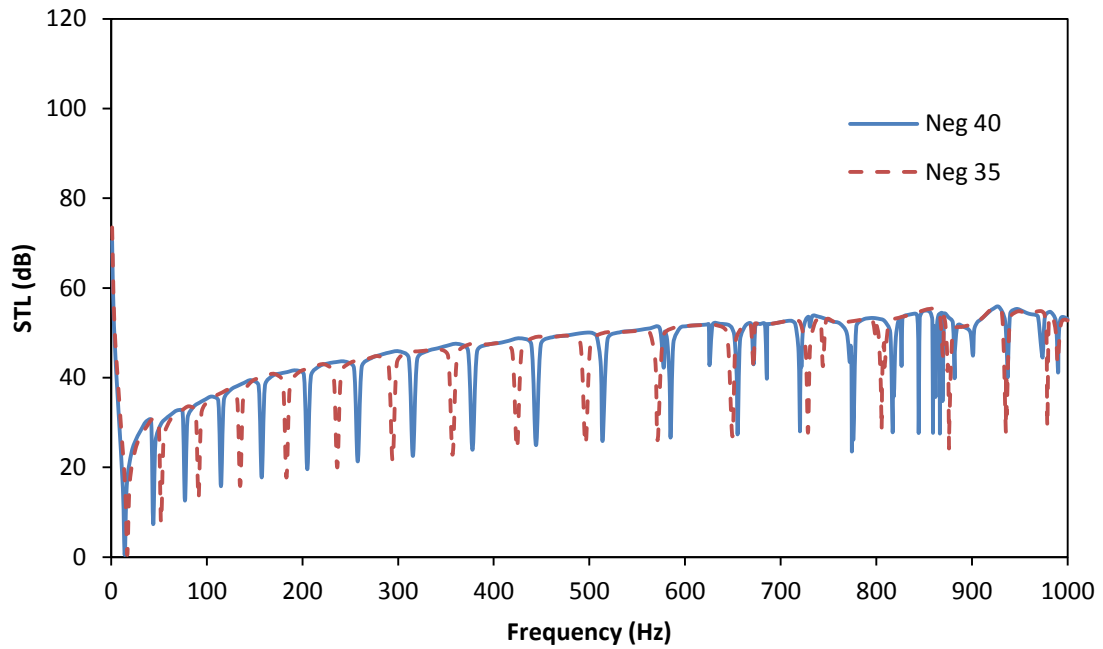

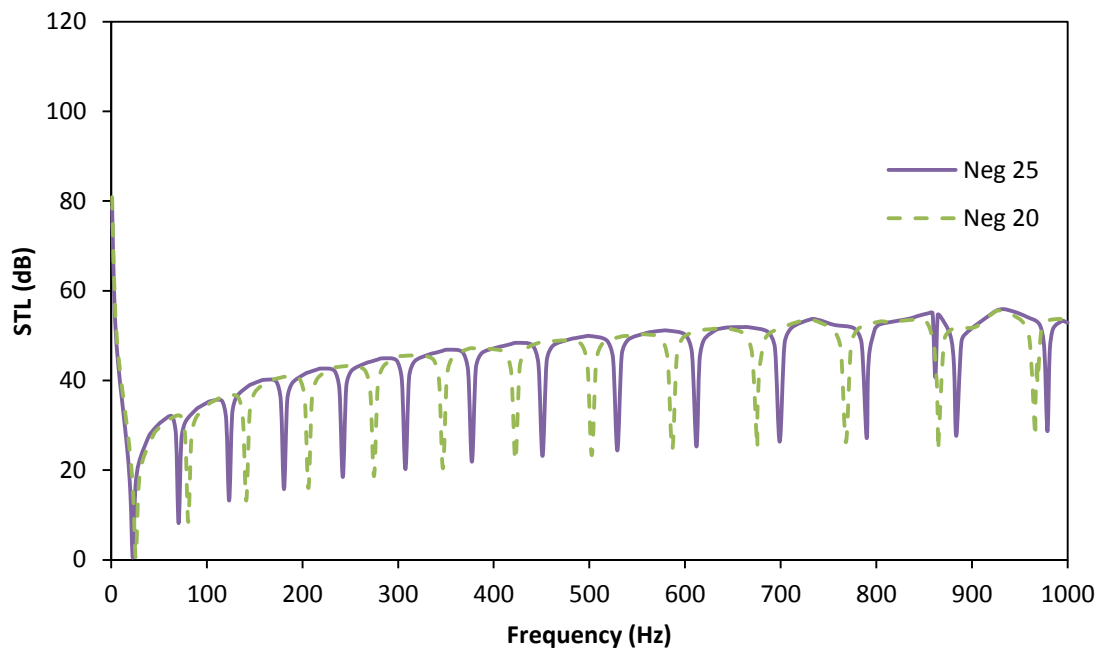**Figure B- 2: STL results for the -40° and -35° constant mass panels**

Figure B- 3: STL results for the -25° and -20° constant mass panels

Figure B- 4: STL results for the -10° and -5° constant mass panels

The results for the positive angle constant mass panels not discussed in the reported are shown below in this section of the appendix. The positive 5° and 10° models are shown in Figure B- 5, the positive 20° and 25° models are shown in Figure B- 6, and the positive 35° and 40° models are shown in Figure B- 7.

Figure B- 5: STL results for the +5° and +10° constant mass panels

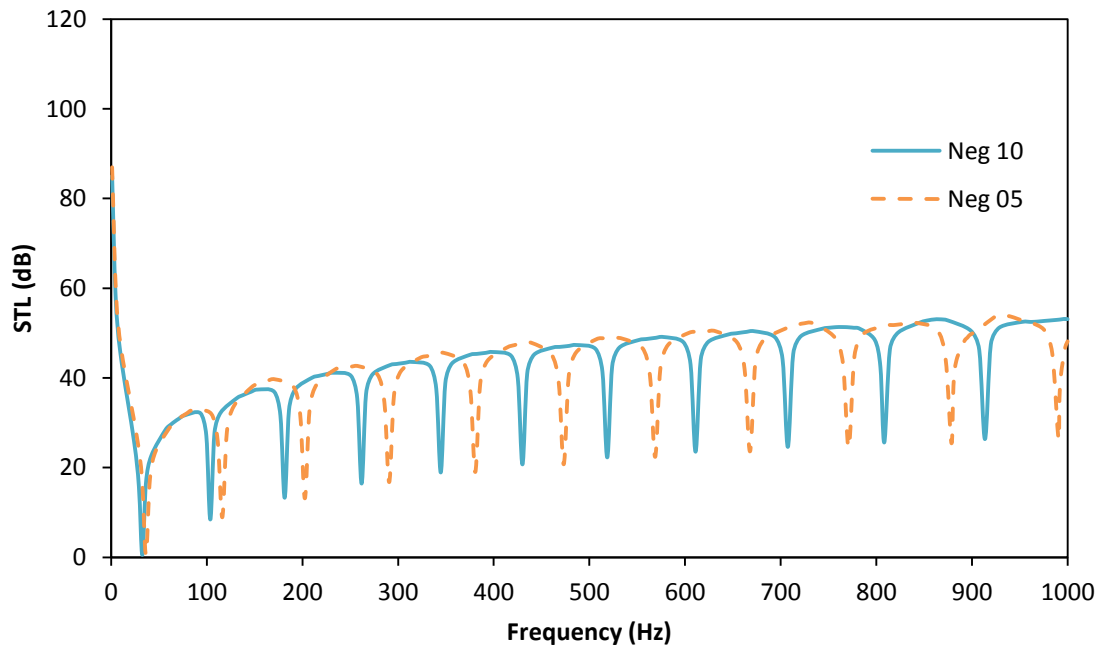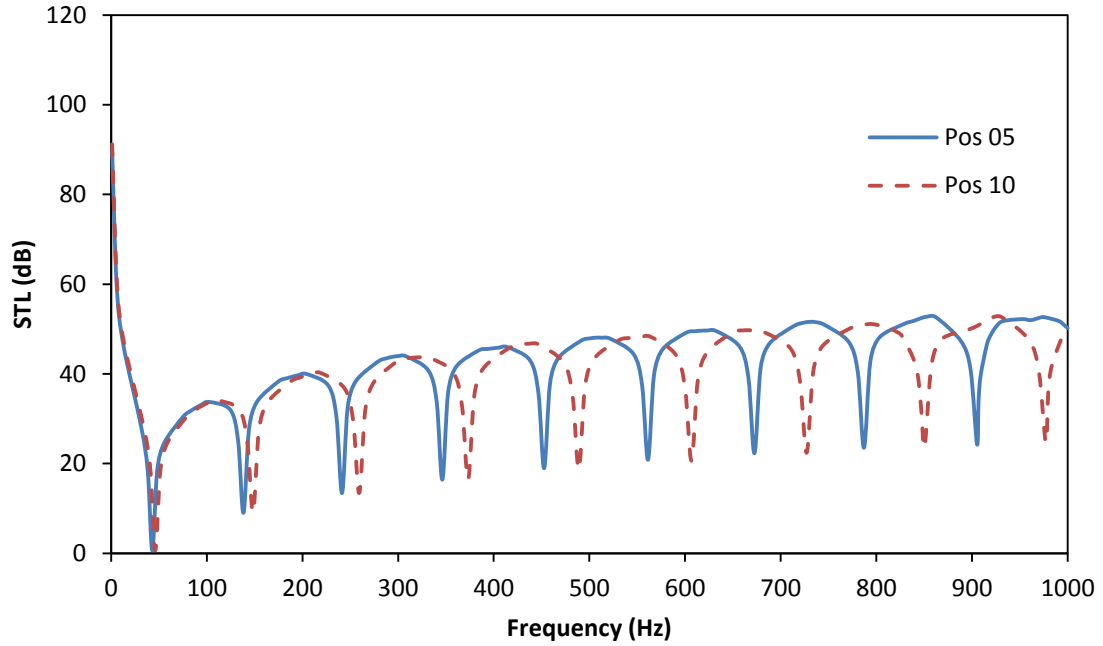**Figure B- 6: STL results for the +20° and +25° constant mass panels**
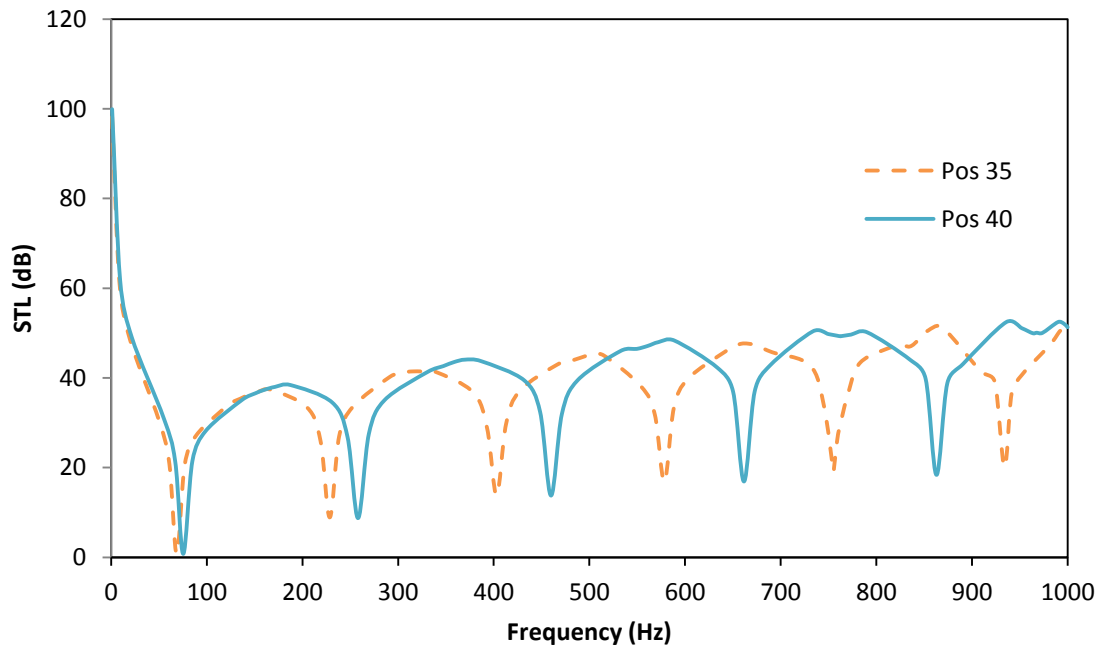
Figure B- 7: STL results for the +35° and +40° constant mass panels

B.3. Constant Shear Modulus Results

The results for the negative angle constant shear modulus panels not discussed in the reported are shown below in this section of the appendix. The negative 40° and 45° models are shown in Figure B- 8, the negative 25° and 20° models are shown in Figure B- 9, and the negative 10° and 5° models are shown in Figure B- 10.

Figure B- 8: STL results for the -40° and -35° constant shear modulus panels

Figure B- 9: STL results for the -25° and -20° constant shear modulus panels
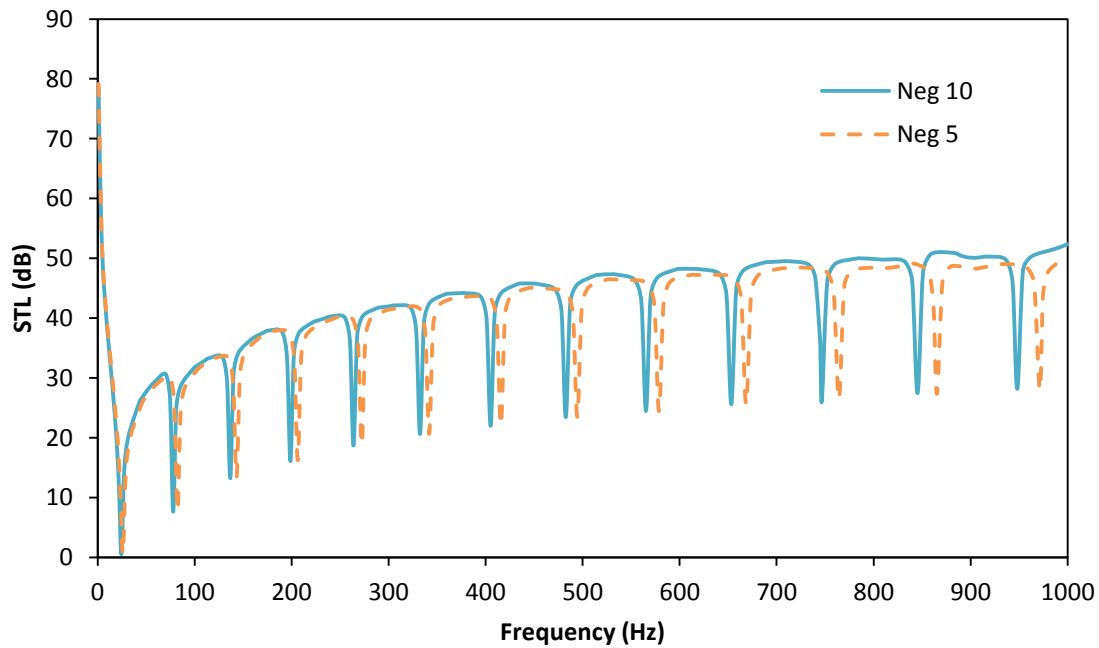
Figure B- 10: STL results for the -10° and -5° constant shear modulus panels

The results for the positive angle constant shear modulus panels not discussed in the reported are shown below in this section of the appendix. The positive 5° and 10° models are shown in Figure B- 11, the positive 20° and 25° models are shown in Figure B- 12, and the positive 35° and 40° models are shown in Figure B- 13.
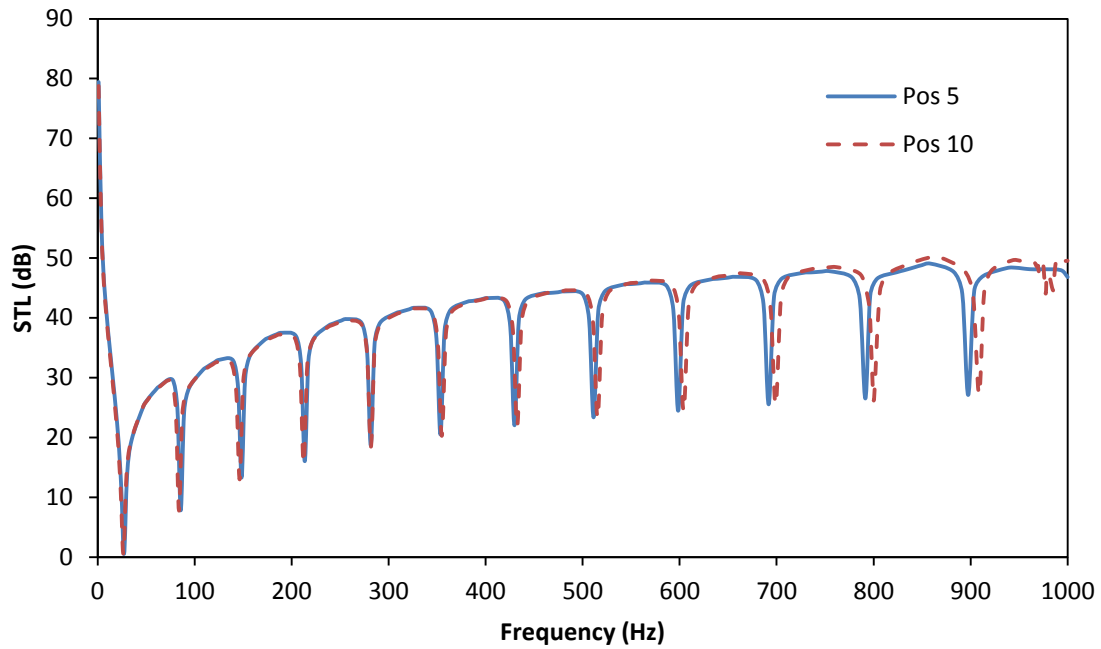
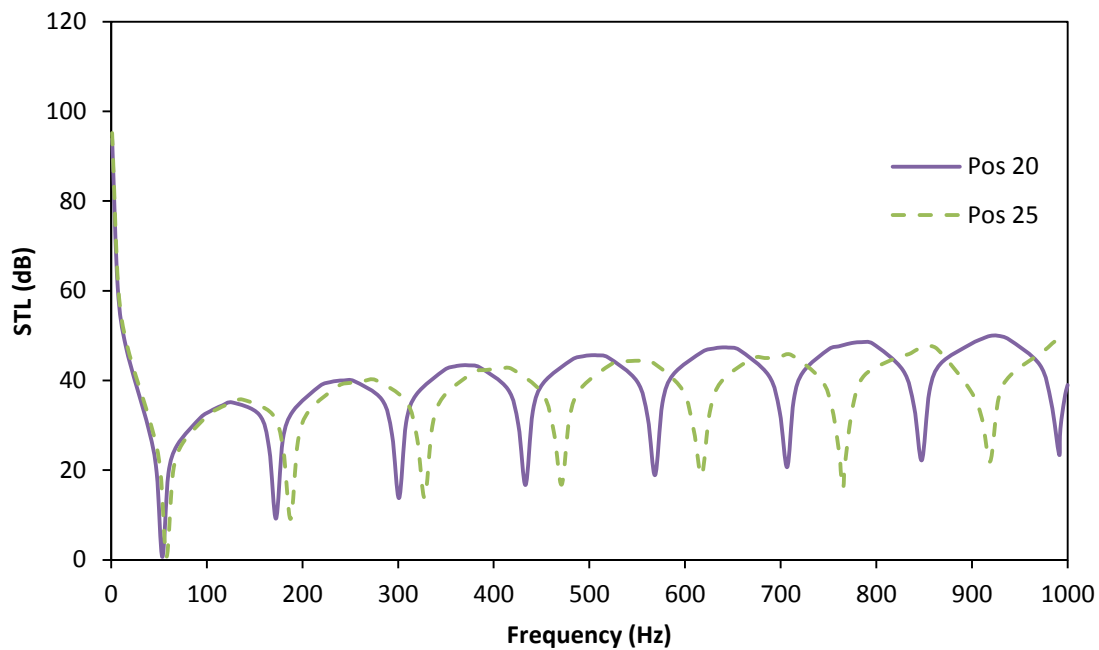**Figure B- 11: STL results for the +5° and +10° constant shear modulus panels**

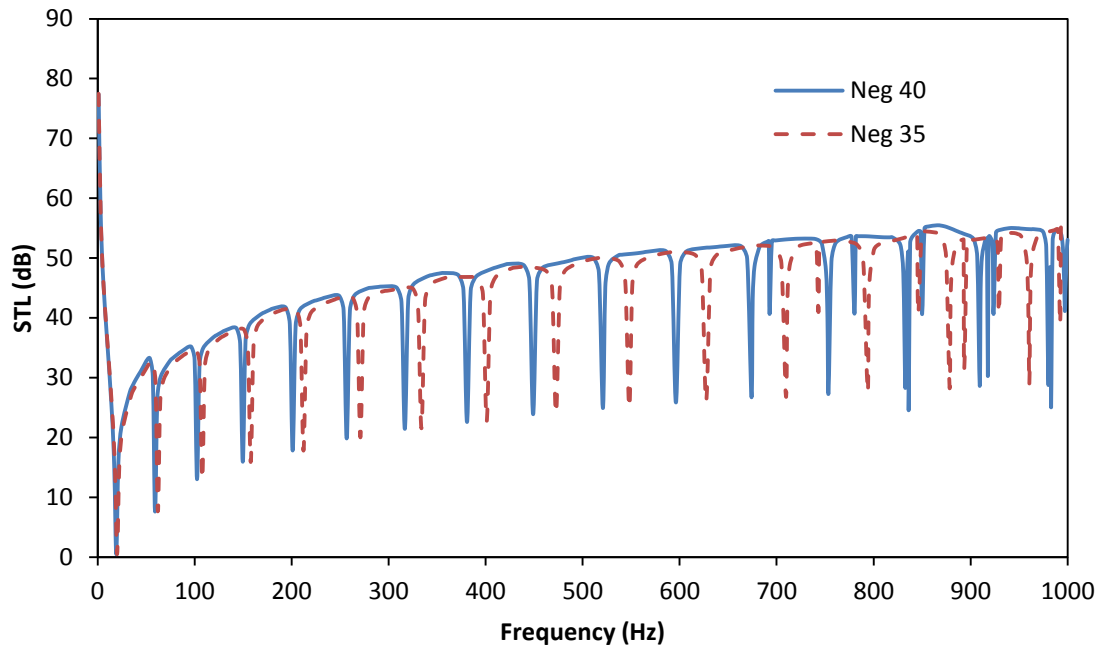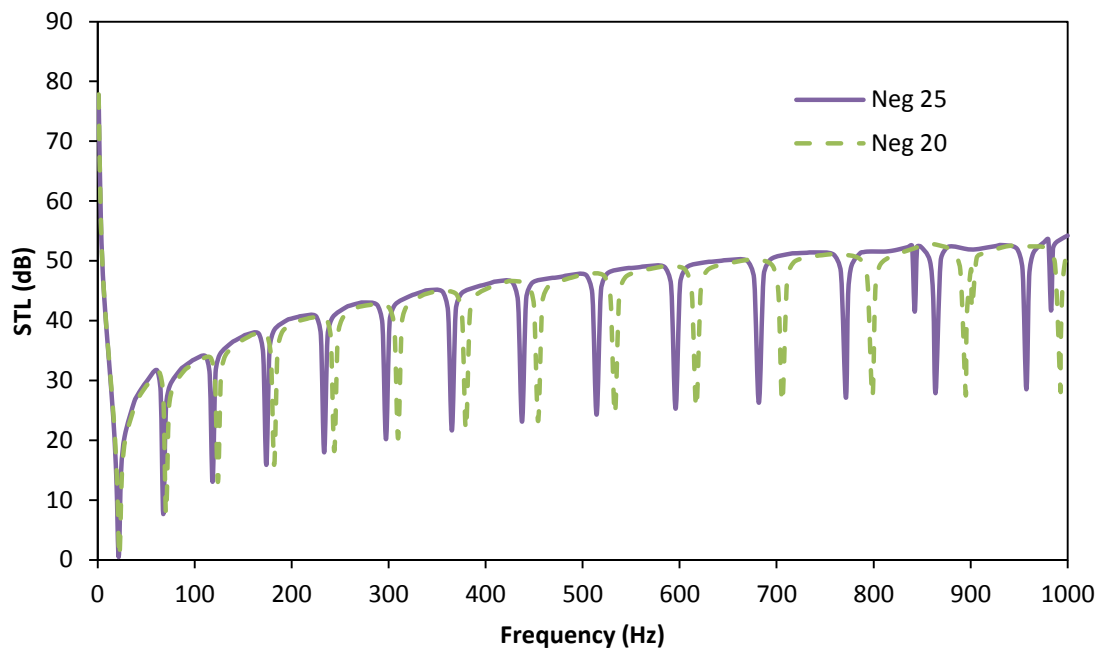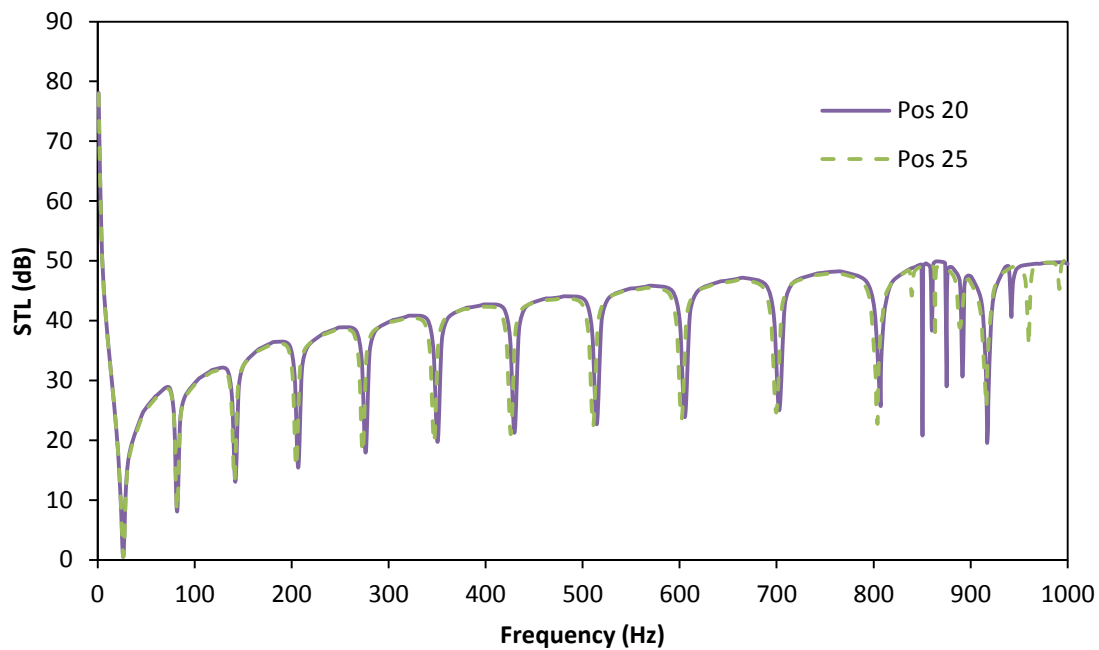**Figure B- 12: STL results for the +20° and +25° constant shear modulus panels**
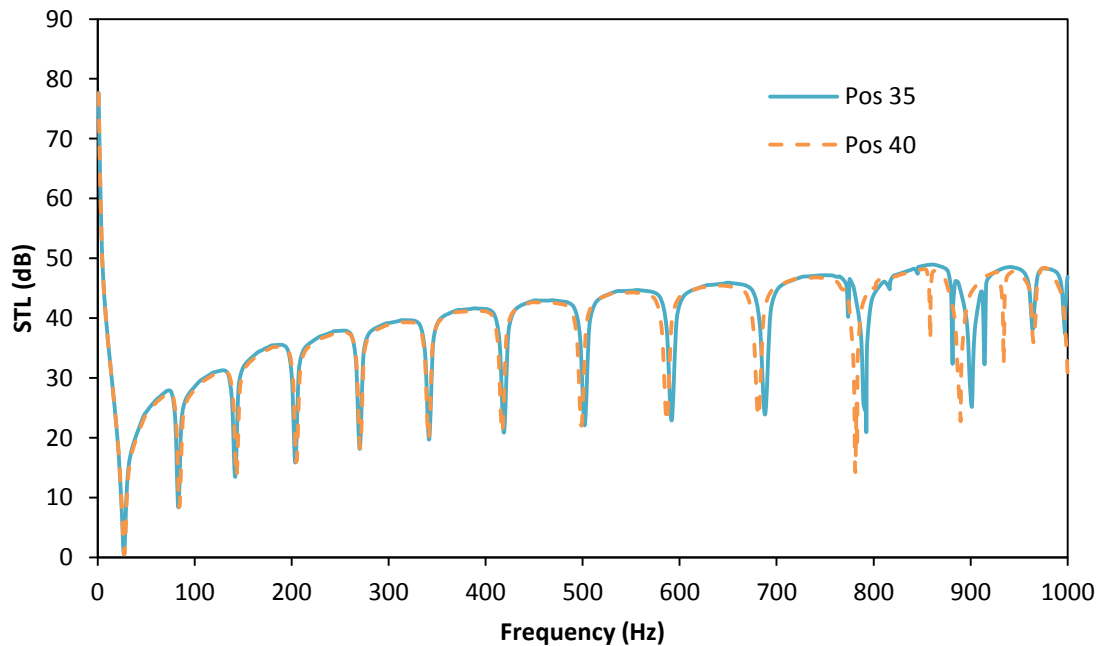
Figure B- 13: STL results for the +35° and +40° constant shear modulus panels

B.4. Design Example Results

The odd mode results for all designs in the design chapter are presented here in Figure B- 14. In the figure, the designs which do not meet the given requirements can be observed. These designs show an odd mode within the specified frequency tolerance range. In the main body of the report, only the designs that satisfy the requirements are shown.
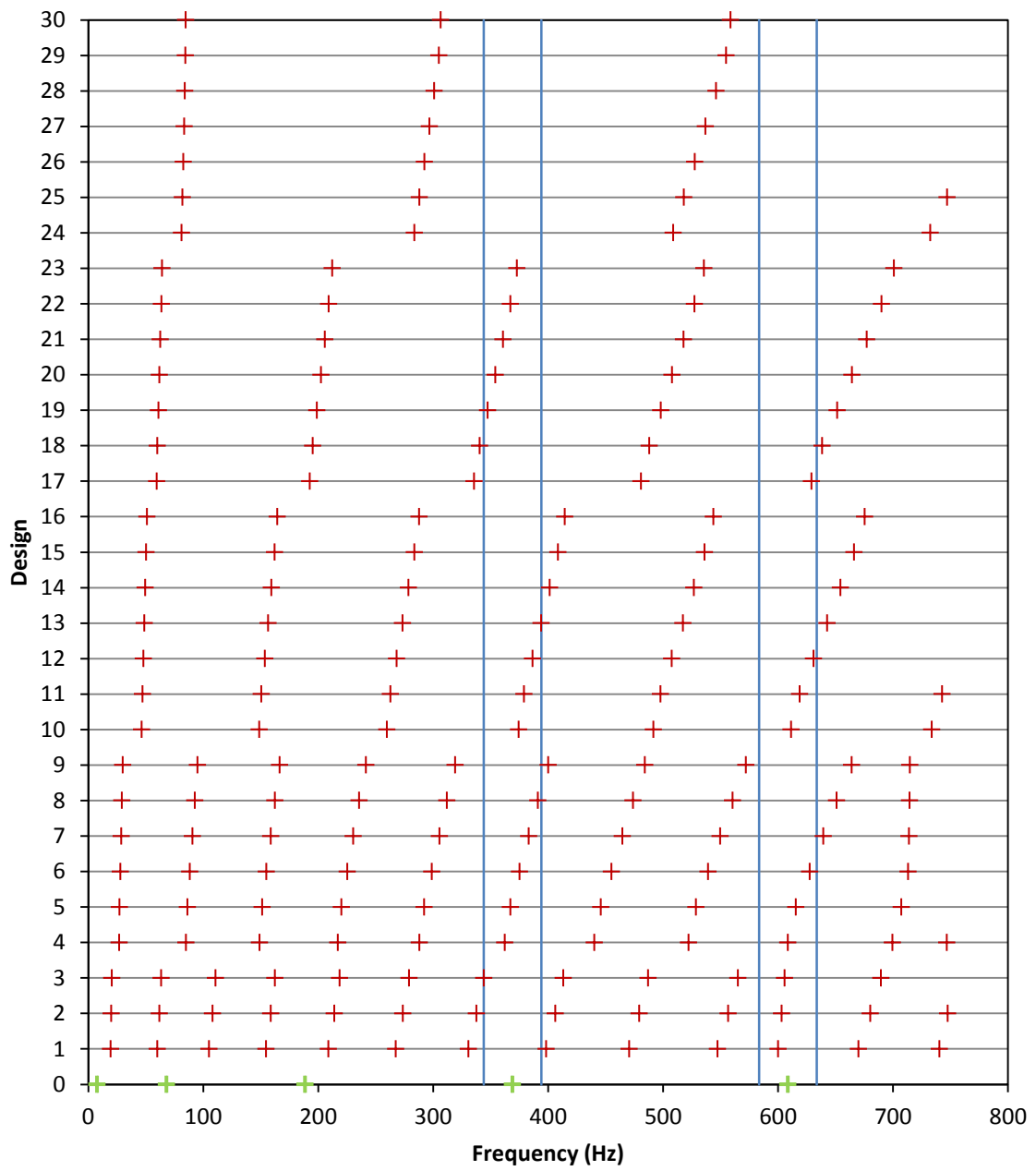
Figure B- 14: Odd modes for all designs

This chapter of the Appendix presents the various input files and script codes that were used throughout the analysis procedure in ABAQUS as well as the post-processing that was done in Matlab.

C.1. ABAQUS Input Files

This section shows the ABAQUS input file that was used for the natural frequency extraction procedure. The specific file being shown is for the positive 30° model, but the same structure was used for all models. Specific node and element selects have been omitted for length purposes.

```
*Heading
** Job name: pos30_Modal Model name: Model-1
** Generated by: Abaqus/CAE 6.10-EF1
*Preprint, echo=NO, model=NO, history=NO, contact=NO
**
** PARTS
**
*Part, name="Positive 30 - 1 Row"
*Node
      [all nodes for honeycomb specified here, omitted for space]
*Element, type=B22
      [all elements for honeycomb specified here, omitted for space]
*Nset, nset=_PickedSet11, internal, generate
      [picked nodes specified, omitted for space]
*Elset, elset=_PickedSet11, internal, generate
      [picked elements specified, omitted for space]
*Nset, nset=Ends
      ["Ends" set nodes specified here, omitted for space]
*Elset, elset=Ends
      ["Ends" set elements specified here, omitted for space]
*Nset, nset=Core
      ["Core" set nodes specified here, omitted for space]
*Elset, elset=Core
      ["Core" set elements specified here, omitted for space]
*Nset, nset=Boundary
      ["Boundary" set nodes specified here, omitted for space]
*Elset, elset=Boundary
      ["Boundary" set nodes specified here, omitted for space]
** Section: Boundary Section  Profile: Boundary Profile
```

```
*Beam Section, elset=Boundary, material=Aluminum, poisson = 0.33,
temperature=GRADIENTS, section=RECT
1., 0.0025
0.,0.,-1.
** Section: Core Section  Profile: Core Profile
*Beam Section, elset=Core, material=Aluminum, poisson = 0.33,
temperature=GRADIENTS, section=RECT
1., 0.0025
0.,0.,-1.
*End Part
**
**
** ASSEMBLY
**
*Assembly, name=Assembly
**
*Instance, name="Positive 30 - 1 Row-1", part="Positive 30 - 1 Row"
*End Instance
**
*End Assembly
**
** MATERIALS
**
*Material, name=Aluminum
*Density
2700.,
*Elastic
 7.1e+10, 0.3
**
** PHYSICAL CONSTANTS
**
*Acoustic Wave Formulation
** ----------------------------------------------------------------
**
** STEP: Frequency Extraction
**
*Step, name="Frequency Extraction", perturbation
*Frequency, eigensolver=Lanczos, acoustic coupling=on,
normalization=displacement
, 1., 750., , ,
**
** BOUNDARY CONDITIONS
**
** Name: BC-1 Type: Displacement/Rotation
*Boundary
"Positive 30 - 1 Row-1".Ends, 1, 1
"Positive 30 - 1 Row-1".Ends, 2, 2
**
** OUTPUT REQUESTS
**
*Restart, write, frequency=0
**
** FIELD OUTPUT: F-Output-1
**
```

```
*Output, field, variable=PRESELECT
*End Step
```

This section shows the ABAQUS input file that was used for the steady state analysis procedure. The specific file being shown is for the positive 30° model, but the same structure was used for all models. Specific node and element selects have been omitted for length purposes.

```
*Heading
** Job name: p30 Model name: Model-1
** Generated by: Abaqus/CAE 6.10-EF1
*Preprint, echo=NO, model=NO, history=NO, contact=NO
**
** PARTS
**
*Part, name=Air
*Node
      [all nodes for air specified here, omitted for space]
*Element, type=AC2D3
      [all elements for air specified here, omitted for space]
*Nset, nset=_PickedSet10, internal, generate
      [picked nodes specified, omitted for space]
*Elset, elset=_PickedSet10, internal, generate
      [picked elements specified, omitted for space]
*Nset, nset="Air Bottom Interface"
      ["Air Bottom Interface" set nodes specified here, omitted for
space]
*Elset, elset="Air Bottom Interface"
      ["Air Bottom Interface" set elements specified here, omitted for
space]
*Elset, elset=_Bottom_S2, internal
      [internal element set related to surface, omitted for space]
*Elset, elset=_Bottom_S1, internal
      [internal element set related to surface, omitted for space]
*Elset, elset=_Bottom_S3, internal
      [internal element set related to surface, omitted for space]
*Surface, type=ELEMENT, name=Bottom
_Bottom_S2, S2
_Bottom_S1, S1
_Bottom_S3, S3
** Section: Air
*Solid Section, elset=_PickedSet10, material=Air
1.,
*End Part
**
*Part, name="Positive 30 - 1 Row"
*Node
      [all nodes for honeycomb specified here, omitted for space]
```

```
*Element, type=B22
      [all elements for honeycomb specified here, omitted for space]
*Nset, nset=_PickedSet11, internal, generate
      [picked nodes specified, omitted for space]
*Elset, elset=_PickedSet11, internal, generate
      [picked elements specified, omitted for space]
*Nset, nset=Ends
      ["Ends" set nodes specified here, omitted for space]
*Elset, elset=Ends
      ["Ends" set elements specified here, omitted for space]
*Nset, nset=Core
      ["Core" set nodes specified here, omitted for space]
*Elset, elset=Core
      ["Core" set elements specified here, omitted for space]
*Nset, nset=Boundary
      ["Boundary" set nodes specified here, omitted for space]
*Elset, elset=Boundary
      ["Boundary" set elements specified here, omitted for space]
*Elset, elset=_Top_SPOS, internal
      [internal element set related to surface, omitted for space]
*Surface, type=ELEMENT, name=Top
_Top_SPOS, SPOS
*Elset, elset=_Bottom_SNEG, internal, generate

*Surface, type=ELEMENT, name=Bottom
_Bottom_SNEG, SNEG
** Section: Boundary Section  Profile: Boundary Profile
*Beam Section, elset=Boundary, material=Aluminum, poisson = 0.33,
temperature=GRADIENTS, section=RECT
1., 0.0025
0.,0.,-1.
** Section: Core Section  Profile: Core Profile
*Beam Section, elset=Core, material=Aluminum, poisson = 0.33,
temperature=GRADIENTS, section=RECT
1., 0.0025
0.,0.,-1.
*End Part
**
**
** ASSEMBLY
**
*Assembly, name=Assembly
**
*Instance, name=Air-1, part=Air
          0.,     0.086603,             0.
*End Instance
**
*Instance, name="Positive 30 - 1 Row-1", part="Positive 30 - 1 Row"
*End Instance
**
*Elset, elset=__PickedSurf84_S1, internal, instance=Air-1
      [internal element set related to surface, omitted for space]
*Elset, elset=__PickedSurf84_S3, internal, instance=Air-1
      [internal element set related to surface, omitted for space]
```

```
*Elset, elset=__PickedSurf84_S2, internal, instance=Air-1
       [internal element set related to surface, omitted for space]
*Surface, type=ELEMENT, name=_PickedSurf84, internal
__PickedSurf84_S1, S1
__PickedSurf84_S3, S3
__PickedSurf84_S2, S2
** Constraint: Tie Air to Honeycomb
*Tie, name="Tie Air to Honeycomb", adjust=yes
Air-1.Bottom, "Positive 30 - 1 Row-1".Top
*End Assembly
**
** MATERIALS
**
*Material, name=Air
*Acoustic Medium
141179.,
*Density
 1.2,
*Material, name=Aluminum
*Density
2700.,
*Elastic
 7.1e+10, 0.3
**
** PHYSICAL CONSTANTS
**
*Acoustic Wave Formulation
** ----------------------------------------------------------------
**
** STEP: Steady State
**
*Step, name="Steady State", perturbation
*Steady State Dynamics, direct, frequency scale=LINEAR, friction
damping=NO
1., 62.7895, 6, 2.
62.7895, 129.747, 6, 2.
129.747, 205.871, 6, 2.
205.871, 282.965, 6, 2.
282.965, 360.806, 6, 2.
360.806, 438.976, 6, 2.
438.976, 517.776, 6, 2.
517.776, 597.185, 6, 2.
597.185, 677.321, 6, 2.
677.321, 758.155, 6, 2.
758.155, 760.195, 6, 2.
760.195, 839.719, 6, 2.
839.719, 921.979, 6, 2.
921.979, 1000., 6, 2.
**
** BOUNDARY CONDITIONS
**
** Name: Pin Type: Displacement/Rotation
*Boundary, real
"Positive 30 - 1 Row-1".Ends, 1, 1
```

```
"Positive 30 - 1 Row-1".Ends, 2, 2
*Boundary, imaginary
"Positive 30 - 1 Row-1".Ends, 1, 1
"Positive 30 - 1 Row-1".Ends, 2, 2
**
** LOADS
**
** Name: Pressure Load   Type: Pressure
*Dsload, real
"Positive 30 - 1 Row-1".Bottom, P, 1.
**
** INTERACTIONS
**
** Interaction: Absorbing Boundary
*Simpedance, nonreflecting=CIRCULAR
_PickedSurf84, 2.
**
** OUTPUT REQUESTS
**
**
** FIELD OUTPUT: F-Output-2
**
*Output, field
*Node Output
A, CF, POR, RF, U, V
*Element Output, directions=YES
LE, S
**
** HISTORY OUTPUT: H-Output-1
**
*Output, history
*Node Output, nset=Air-1."Air Bottom Interface"
POR,
*End Step
```

C.2. Matlab SPL Distribution Generation Code

This section presents the Matlab code that was used to generate the sound pressure level distributions that were seen in Chapters 4 and 5. The code pulls from data text files of the pressure results that were manually generated in a report from ABAQUS.

```
load Pressure_G_neg30_920Hz.dat
load Nodes.dat

X = Nodes(:,2);
Y = Nodes(:,3);
P = Pressure_G_neg30_920Hz(:,2);

SPL = 20 *log10(P/20E-6);
```

```matlab
tri = delaunay (X,Y);
[r,c] = size(tri);

figure('units','inches','position',[5 5 6 2.5])
trisurf ( tri, X, Y,SPL, 'FaceColor', 'interp', ...
          'EdgeColor', 'interp' )

view([0 90])
axis off
caxis([40,70])
h = colorbar;
ylabel(h, 'SPL (dB)');
whitebg('w')
```